DESIGN AND CHARACTERIZATION OF TUNABLE HYDROGELS TO EXAMINE MICROENVIRONMENTAL REGULATION OF BREAST CANCER RECURRENCE

by

Lisa A. Sawicki

A dissertation submitted to the Faculty of the University of Delaware in partial fulfillment of the requirements for the degree of Doctor of Philosophy in Chemical Engineering

Winter 2017

DESIGN AND CHARACTERIZATION OF TUNABLE HYDROGELS TO EXAMINE MICROENVIRONMENTAL REGULATION OF BREAST CANCER RECURRENCE

by

Lisa A. Sawicki

Approved: _____
Abraham M. Lenhoff, Ph.D.
Chair of the Department of Chemical and Biomolecular Engineering

Approved: _____
Babatunde A. Ogunnaike, Ph.D.
Dean of the College of Engineering

Approved: _____
Ann L. Ardis, Ph.D.
Senior Vice Provost for Graduate and Professional Education

I certify that I have read this dissertation and that in my opinion it meets the academic and professional standard required by the University as a dissertation for the degree of Doctor of Philosophy.

Signed: _____

April M. Kloxin, Ph.D.
Professor in charge of dissertation

I certify that I have read this dissertation and that in my opinion it meets the academic and professional standard required by the University as a dissertation for the degree of Doctor of Philosophy.

Signed: _____

Kelvin H. Lee, Ph.D.
Member of dissertation committee

I certify that I have read this dissertation and that in my opinion it meets the academic and professional standard required by the University as a dissertation for the degree of Doctor of Philosophy.

Signed: _____

Wilfred Chen, Ph.D.
Member of dissertation committee

I certify that I have read this dissertation and that in my opinion it meets the academic and professional standard required by the University as a dissertation for the degree of Doctor of Philosophy.

Signed: _____

Kenneth L. van Golen, Ph.D.
Member of dissertation committee

I certify that I have read this dissertation and that in my opinion it meets the academic and professional standard required by the University as a dissertation for the degree of Doctor of Philosophy.

Signed: _____

Millicent O. Sullivan, Ph.D.
Member of dissertation committee

ACKNOWLEDGMENTS

Thank you to all who have made my dissertation possible and provided support during my studies at the University of Delaware. First, I would like to thank my advisor, Dr. April Kloxin, for providing invaluable mentorship and guidance, without which the project would not have been possible. I would also like to thank the members of my committee Dr. Kelvin Lee, Dr. Wilfred Chen, Dr. Millicent Sullivan, and Dr. Kenneth van Golen for all of their helpful discussions and insight as the project progressed. I have also had the opportunity to work with a number of wonderful researchers during my time at Delaware. Thank you to all of my labmates, collaborators, and undergraduate researchers for assistance with the various projects in this work. Finally, I would like to thank all of my friends and family for their love and support, and especially my parents Sharon and Mark Sawicki for all of their encouragement from the beginning.

TABLE OF CONTENTS

LIST OF TABLES

LIST OF FIGURES

ABSTRACT

Late recurrence of breast cancer within distant metastatic tissue sites is often difficult to diagnose and treat, resulting in poor prognosis for patients. It is hypothesized that cells may go dormant by interactions with or lack of adhesion to the extracellular matrix (ECM) within these tissues, which differs from native breast tissue. The metastatic ECM is a complex microenvironment, containing a mixture of mechanical and chemical cues to which cells respond. To investigate how the ECM regulates cancer recurrence, two-dimensional (2D, plates) and three-dimensional (3D, naturally-derived scaffolds) *in vitro* culture models have been used. However, lack of complexity (2D), mechanical property control (2D, 3D), and chemical property control (3D) makes it challenging to identify key factors involved in regulating dormancy or activation in these systems. The development of synthetic polymer-based scaffolds in recent years provides an alternate route to investigating cellular response to the presentation of microenvironmental cues in 3D. Initially bioinert, these scaffolds may be modified with chemical ligands to permit cell-matrix interactions and their mechanical properties may be precisely tuned to mimic different tissue sites. The goal of this dissertation is to develop and characterize a novel synthetic material for cell culture applications and to examine how physical and chemical factors in this microenvironment regulate breast cancer activation.

Specifically, we have developed a novel poly(ethylene glycol) (PEG)-based hydrogel scaffold for *in vitro* cell culture. PEG modified with thiols and peptides containing alloxycarbonyl-protected lysines (containing a reactive vinyl) react rapidly

upon the application of light in the presence of a photoinitiator, lithium acylphosphinate (~minutes). Scaffold mechanical properties are tuned by varying macromer concentration to mimic soft metastatic site tissue ECMs (Young's modulus ~ 600 – 6000 Pa). These properties remain stable during long-term culture (~weeks). We also demonstrate the covalent attachment and spatial presentation of peptides mimicking proteins found within metastatic tissue ECMs in these scaffolds. All cell lines remain viable (>70%) after encapsulation, with many at greater than 90% viability, indicating minimal negative effects of light and radicals on cell survival post-polymerization.

While initially well-defined, the properties of synthetic hydrogel scaffolds change as cells secrete soluble factors that permit cell-cell signaling and synthesize new proteins that provide additional binding sites with which cells may interact. To investigate these chemical property changes, we developed a shotgun proteomics technique to isolate and identify large proteins secreted within synthetic, polymer-based hydrogel scaffolds. Metastatic niche cells (adult human mesenchymal stem cells, hMSCs) were cultured within hydrogel scaffolds and large proteins, including fibronectin and collagen VI were identified. Additionally, a bead-based multiplex assay identified several soluble factors secreted by hMSCs (VEGF, IL-8), which may play a role in regulating cell function and fate.

Finally, the response and activation of estrogen receptor negative (MDA-MB-231) and estrogen receptor positive (T-47D) breast cancer cells cultured within synthetic hydrogels with discrete mechanical and chemical properties was determined. The highly aggressive MDA-MB-231 cells demonstrated the greatest levels of activation and spread within these synthetic matrices, while T-47D cells, which have

been associated with a dormant phenotype, exhibited only minimal response and formed multicellular spheroids. Specifically, hydrogels with high stiffness and matrix density restricted cancer cell growth, resulting in decreased spreading and smaller cell cluster volume. Individual and mixtures of peptides (GFOGER, RGDS, IKVAV) mimicking ECM proteins found within metastatic tissue sites and targeting cell surface receptors were also shown to affect response. GFOGER and RGDS, targeting integrin β1, among others, resulted in the highest levels of activation observed within microenvironments. Collectively, this work describes the development of a novel material scaffold with well-defined chemical and physical properties that may be used to identify critical factors in metastatic microenvironments that regulate breast cancer activation toward development of new treatments for recurrent cancers.

Chapter 1

INTRODUCTION

This chapter is adapted, in part, from *Biomaterials: Controlling Properties Over Time to Mimic the Dynamic Extracellular Matrix* by L. A. Sawicki and A. M. Kloxin, published in *Mimicking the Extracellular Matrix: The Intersection of Matrix Biology and Biomaterials*, Editors: G. A. Hudalla and W. L. Murphy, Chapter 9, 2015, with permission from the Royal Society of Chemistry.

1.1 Breast Cancer Metastasis, Dormancy, and Recurrence

Breast cancer is the most common cancer diagnosed in women at approximately 25 percent of cancers.[1,2] In 20 percent of patients that undergo successful treatment of the primary tumor, the cancer reoccurs within a metastatic tissue site, 5 to 10 years after treatment.[3] These late reoccurrences often are difficult to diagnose and treat, resulting in poor prognosis for patients.

Metastasis occurs through a series of steps, starting when the primary tumor grows and invades the native tissue (Figure 1.1). Cells then disseminate from the growing tumor, enter the bloodstream, and circulate through the body, where surviving cells may extravasate and settle within new tissue sites, most commonly the bone marrow, liver, and lungs.[4–6] It is hypothesized that failure to properly adhere within the metastatic tissue microenvironment, along with other cell-cell interactions, promotes the formation of dormant tumor cells or micrometastases that survive primary treatment and remain undetected for years.[7] Remodeling of the tissue due to

aging or wound healing is thought to trigger the release of tumor cells from dormancy, forming a new tumor.[8] However, the specific role of key factors in the microenvironment that regulate dormancy and recurrence post-metastasis are poorly understood.

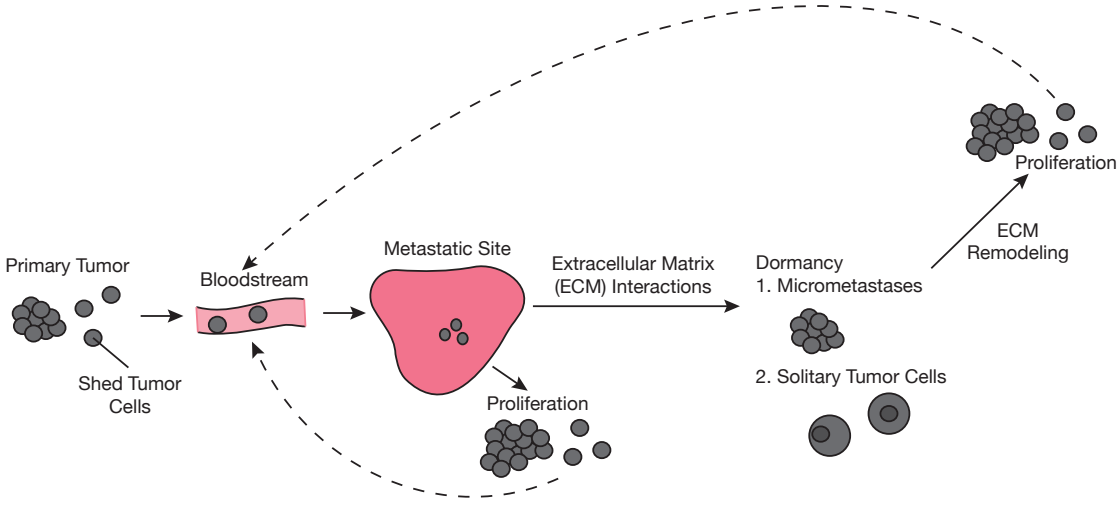

Figure 1.1: **Metastasis and recurrence of breast cancer.** The primary breast tumor sheds cells that travel through the bloodstream and may extravasate into a distant metastatic tissue site (e.g., bone marrow, liver, lungs).[4–6] At this site, the cells may interact with the ECM, immediately forming a new tumor. However, it is thought that lack of interactions with this new ECM causes tumor cells to form dormant micrometastases or solitary tumor cells.[7] Subsequent remodeling of this microenvironment with aging or wounding is thought to release the tumor cells from dormancy as a new set of chemical and physical cues are made present.

1.2 The Complex Microenvironment Surrounding Disseminated Tumor Cells

The extracellular matrix (ECM) surrounding cells presents a complex mixture of biochemical and biophysical factors that permit cell-matrix interactions and influence cell functions and fate, including migration, adhesion, and differentiation.[9]

These factors include large structural proteins (e.g., collagen, elastin, fibronectin, vitronectin, laminin) that provide a 3D mechanical support for cells and present integrin-binding sequences that allow cells to interact with the ECM structure.[10,11] Turnover of these proteins also occurs as niche cells (e.g., fibroblasts, mesenchymal stem cells) degrade existing proteins and deposit new structural proteins within tissues with aging, wounding, and disease.[12] Furthermore, small soluble factors (e.g., growth factors, cytokines, chemokines) are secreted by cells within the environment and drive additional cell response.[13–15]

1.2.1 Insoluble Factors

The structure of the native ECM is tissue specific and differs based on the type and concentration of structural proteins that define the tissue of interest. Collagens and elastin are the most prevalent structural proteins that define native tissues. Collagen I has a triple-helical conformation between three polypeptide strands that are held together by hydrogen bonds. These triple-helices self-assemble to form larger fibers that make up much of the strength and structure of the natural ECM.[16] Elastin is composed of two segments along its polypeptide chain – a hydrophobic region and an alpha-helical region rich in lysine and alanine that allow covalent cross-linking between elastin polypeptides. This structure overall is coil-like and gives elastin its ability to stretch and flex to a high degree.[10]

Other structural proteins present in native ECMs include fibronectin, laminins, and vitronectin. Fibronectin, a glycoprotein commonly found within connective tissue (e.g., bone marrow), is associated with cell adhesion to the ECM. It interacts with other proteins, cells, and with itself, assembling into fibrils that form linear and branched mesh structures around cells.[17] Laminin, found in the basil lamina, a

structure within the basement membrane of tissues, promotes cellular functions including adhesion, migration, and differentiation. The basement membrane is a thin layer of the ECM that underlies epithelial and endothelial cells and its structure is partly attributed to the assembly of laminins and their interactions with other ECM proteins.[18] Vitronectin, another fibrillar cell adhesion protein, also promotes spreading of cells within the ECM. This characteristic is partly responsible for vitronectin's role in promoting tumor cell survival and invasion in tissue as cancer progresses.[19]

Native ECM structure is not static with time as cells naturally secrete enzymes and new structural proteins that degrade and rebuild tissues, respectively. Wound healing and disease result in ECM remodeling as cells respond to disruptions in their surrounding environment. For example, in the case of healing a wound, a series of steps occur that cause remodeling of the native ECM (Figure 1.2). After wounding, the formation of a blood clot provides a provisional or temporary matrix that stimulates the migration and proliferation of fibroblasts in the wound site.[20] Enzymes secreted by cells in response to the wound degrade existing structural proteins and fibroblasts deposit new collagen to rebuild the ECM. The new collagen at the wound site is aligned randomly and denser than the original tissue, resulting in the different structural properties of scar tissue.[21,22]

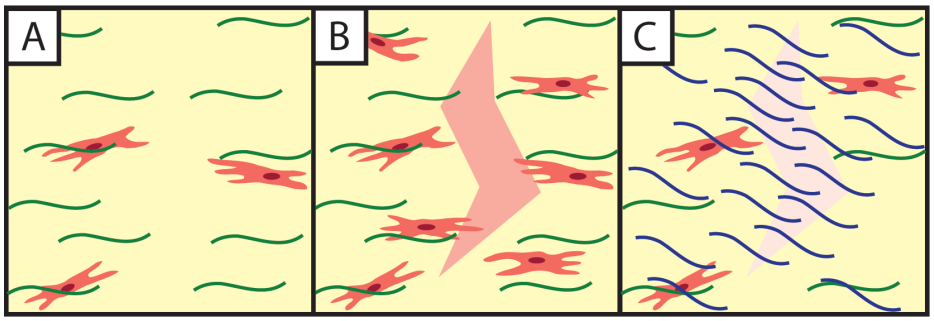

Figure 1.2: **Structural remodeling of the native ECM. A)** Healthy, native tissue provides a 3D support made up of proteins, surrounding cells. **B)** In response to wounding, or in aging, cells migrate into the microenvironment and degrade damaged proteins. **C)** These cells also secrete new proteins, changing the composition of proteins present in the ECM. It is thought that the differences in the ECM composition between (A) and (C) may cause the reactivation of dormant tumor cells that have entered a metastatic tissue site.

In combination, all of the structural proteins that build the native ECM give the native tissues its stiffness. Modulus, which can easily be measured experimentally, has been used to describe a wide range of native tissue mechanical properties. Table 1.1 provides the elastic moduli of various native tissues.[23–27] Tissues such as bone exhibit much higher moduli (E ~ 5.4-22 GPa), which denote a much stiffer material, while tissues such as bone marrow have lower moduli (E ~ 600 Pa), indicating softer, less rigid mechanical properties.

Table 1.1: **Elastic moduli of various native tissues.** The techniques used to measure the modulus of each tissue are listed.

Tissue Type	Measurement	Elastic Modulus
Bone	Tensile, micro-bending, indentation	5.4-22 GPa[23]
Bone Marrow	Shear	~600 Pa[24]
Brain	Indentation	260-490 Pa[25]
Cartilage	Compression	450-800 kPa[26]
Liver	Compression	640 Pa[25]
Lungs	Tension	5-6 kPa[25]
Skin	Shear	420-850 kPa[27]

Studies on the moduli of tissues over time have also been conducted to understand processes like aging, healing, and disease. The ECM naturally stiffens with age, which is partly attributed to an increase in random crosslinking between collagen fibers in the tissue.[28] This causes tissues to become less flexible; for example, skin becomes tough and more difficult to stretch. In the case of wound healing, the deposition of new proteins at a wound site leads to an increasingly fibrotic environment. The increase in density of protein fibers leads to a more densely packed matrix with higher modulus than uninjured tissue. Similar behavior is also observed in diseases such as pulmonary fibrosis, where the lungs stiffen as they are in a continuous wound healing state.[29]

1.2.2 Soluble Factors

In addition to large, structural proteins, a number of soluble cues are present in the native ECM, including growth factors, cytokines, and chemokines, and smaller molecules such as hormones. Growth factors can stimulate cell growth, proliferation, and differentiation, thus playing a major role in directing cell behavior within tissues.

For example, vascular endothelial growth factor (VEGF) contributes to processes like wound healing by promoting angiogenesis, the formation of new blood vessels from existing vessels. VEGF stimulates the migration and proliferation of endothelial cells that degrade and re-deposit basement membrane at wound sites while aligning to form new capillaries.[30] Cytokines were originally defined as soluble factors associated with hematopoietic and immune cells. Like growth factors, they function to promote growth, proliferation, and differentiation, and thus the term cytokine is often used interchangeably with growth factor.[31] For instance, interleukin-17 (IL-17) is a cytokine associated with the immune system that is upregulated upon injury to epithelial cells (wounding) and induces secretion of factors that control bacterial and fungal pathogens to prevent infection at the site of injury.[32] Chemokines are a class of small cytokines that direct the migration of cells within the ECM where they are expressed. They are often associated with leukocytes and immune response to wounding.[33] During chronic infections, many different chemokines are responsible for recruiting immune cells to affected tissue sites. For example, the chemokine CCL5 (RANTES) has been shown to play a role in sustaining immune response to viral infections by supporting the function of CD8 T immune cells.[34]

Soluble cues in the native ECM are in a constant state of flux as the body responds to changes in the environment. Returning to the example of wound healing, soluble factors secreted by cells at the wound site can stimulate the production and deposition of new proteins to rebuild the ECM. For example, in response to transforming growth factor beta 1 (TGF-β1) secretion, fibroblasts proliferate and deposit collagen-I within a wound site (Figure 1.3).[35] Cells sense these cues as gradients on the micron scale where different portions of the cell are in contact with

different concentrations of cues or as larger gradients on the millimeter scale with cues that appear uniform locally but change spatially as cells move along the gradient.[36]

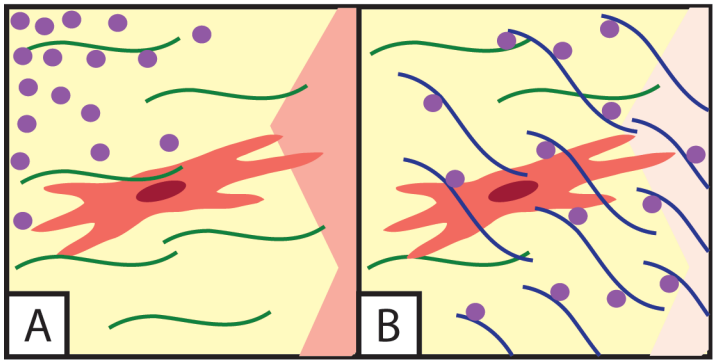

Figure 1.3: **Soluble factors secreted within microenvironments. A)** In wounding and aging, soluble factors are secreted within tissues. **B)** These soluble factors can signal cells present within the microenvironment to proliferate and deposit new proteins within the native ECM.

1.2.3 Metastatic Tissue Microenvironment Properties

The most common tissue sites for breast cancer recurrence, the bone marrow, liver, and lungs,[4–6] contain key structural proteins including fibronectin, laminin, vitronectin, and various collagens (collagen I and IV) at different compositions depending on tissue type and location within the tissue.[37] The basement membrane, through which cells must travel as they leave the bloodstream, is also hypothesized to play a role in metastasis and dormancy and is enriched with laminin, as is healthy mammary tissue.[38–40] These tissues also contain niche cells like fibroblasts and mesenchymal stem cells that remodel the base ECM by degrading proteins and secreting new structural and soluble factors.[41,42] Further, the mechanical properties of these tissues vary, from the stiffer lung tissue (Young's elastic modulus E ~ 5,000-

6,000 Pa)[25] to the softer bone marrow, liver, and basement membrane (E ~ 600-640 Pa).[24,25] The response of disseminated tumor cells to the host of biochemical and biophysical properties presented within the metastatic ECM is complex, and tools are needed to study cell-ECM interactions toward development of improved treatments for recurrent cancer.

1.3 Current Strategies to Investigate the Metastatic Microenvironment in Breast Cancer Recurrence

Two-dimensional (2D), three-dimensional (3D), and *in vivo* culture systems have been used to investigate the role of the ECM and tissue microenvironment in breast cancer response and recurrence. The biochemical and biophysical properties of these systems differ in terms of complexity and degree of user-directed property control, which may affect what cell response is observed for each system.[43]

Two-dimensional culture, commonly tissue culture poly(styrene) plates or glass slides, is one of the most widely used techniques for *in vitro* culture model studies. Plates and slides may be coated with different ECM proteins to study interactions between cells and select environmental cues. Soluble factors also may be introduced into the culture medium to further control cell response. For example, Barrios, et al. reported that cells cultured on tissue-culture polystyrene coated with fibronectin (FN) and treated with basic fibroblast growth factor (FGF-2) promotes dormancy through integrin $\alpha5\beta1$.[44] While the biochemical properties of these culture systems are highly tunable, control over mechanical properties is limited. Glass slides and poly(styrene) plates are highly stiff substrates with high Young's modus (E > 100,000 kPa),[45,46] and polarizes cells due to cell contact to the plate on one side and culture medium on the other side.[47] Alternate scaffolds and culture models are needed

to achieve appropriate mechanical properties and cell polarization to understand cell response.

At the other end of the spectrum, *in vivo* culture models allow researchers to capture cell-ECM interactions in the native tissue microenvironment. Seminal research by Weaver, et al. demonstrated that blocking β1 in tumor cells prior to injection into nude mice reduced malignancy, resulting in reduced tumor size and numbers.[48] Recently, it was demonstrated in a mouse xenograft model that disseminated breast cancer cells predominantly home to the bone marrow vasculature and dormant micrometastases form in E-selectin and stromal cell-derived factor-rich ECM.[49] While *in vivo* models provide a complete, native ECM, there is limited to no control over tissue biochemical and biomechanical properties, making it difficult to de-couple the effects of individual factors on cell response.

In recent years, three-dimensional culture scaffolds have been increasingly used to study cell-ECM interactions due to a native-like environment with appropriate polarization that also permits varying degrees of chemical and mechanical property control.[47,50,51] These scaffolds include naturally-derived substrates such as decellularized tissues, basement membrane extract, collagen I, fibrin, and hyaluronic acid, or synthetic polymer-based hydrogels such as poly (ethylene glycol) (PEG), poly(vinyl alcohol) (PVA), and poly(caprolactone) (PCL). To date, naturally-derived substrates have been primarily used in dormancy culture models. In particular, basement membrane extract (BME) or Matrigel, derived from the Engelbreth-Holm-Swarm (EHS) tumor, provides the necessary structure and many of the proteins (e.g., laminin, collagen IV, entactin) found within the native tumor.[52] Barkan, et al. reported enhanced proliferation of breast cancer cells (D2A1, D2.0R) cultured on BME

supplemented with FN through integrin β1 compared to cells cultured on BME alone.[53,54] While BME and other naturally-derived hydrogels provide necessary adhesion sites to sustain cells during culture and a 3D environment with correct polarization, complete control of the biochemical composition and biomechanical properties are limited due to batch-to-batch variability. Synthetic material scaffolds provide an alternate route for researchers to investigate cell-ECM interactions in 3D environments while permitting full control over chemical and mechanical properties.

1.4 Polymer-Based Synthetic Hydrogels for Cell Culture Applications

Polymer-based hydrogel materials are particularly attractive for their use as cell culture scaffolds due to a high degree of tunability. Initially bioinert, synthetic polymer scaffolds may be modified with proteins and peptides to allow cell-matrix interactions. Further, careful selection of reaction chemistry can permit independent control over biochemical and biomechanical properties in space and time. Taken together, the precise role of individual or combinations of key ECM factors may be discerned from these culture scaffolds.

Hydrogels are hydrophilic polymer networks, formed through physical or chemical crosslinking of polymer strands to generate a 3D network structure. For biomaterials-based applications, polymer selection is key to ensure cytocompatibility, with the most widely-used synthetic polymers including poly(ethylene glycol) (PEG), poly(2-hydroxyethyl methacrylate) (PHEMA), poly(vinyl alcohol) (PVA), and poly(caprolactone).[55] These polymers are bioinert, but may be chemically functionalized to permit modification with biochemical factors and drive cell-matrix interactions. Covalent and non-covalent coupling chemistries have been developed to

generate hydrogel scaffolds and modulate their mechanical and chemical properties to mimic those of the native ECM.

1.4.1 Triggering Mechanisms for Hydrogel Formation and Property Control

Chemical reactions triggered with initiators or catalysts are utilized to form and modify hydrogel scaffolds. These reactions must be cytocompatible so that the material can be made and modified in the presence of cells. Several cytocompatible coupling methods exist including photoinitiation, redox initiation, and base-catalyzed mechanisms, producing radicals or anions that drive polymerization or addition reactions to add crosslinks or pendant groups within biomaterials.

Photoinitiation mechanisms to form and modify biomaterials containing various functional groups (Table 1.2) must use both cytocompatible initiators and doses of light so that they can be used in the presence of cells. Ultraviolet (UV) (long wave, centered at 365 nm), visible (400-600 nm), and two-photon infrared (IR) irradiation have been used to initiate polymerization and dynamic property changes in many biomaterial applications. Irradiating cells with these wavelengths and exposure to initiator-generated radicals for longer periods of time can result in cell death or DNA damage;[56,57] however, reducing exposure times or light intensity can lessen the negative effects. Several cytocompatible wavelengths and irradiation doses (time * intensity) have been reported. UV light exposure of 6-10 mW/cm^2 at 365 nm (long wavelength UV) has limited to no adverse effects on cell survival if applied for less than 10 minutes, as measured by cytotoxicity, metabolism, and p53 expression; however, longer exposure times to 10 mW/cm^2 (30 minutes) does result in significant DNA damage (p53 activation).[57,58] Visible light is much less damaging to cells: for example, exposure to 80 mW/cm^2 at 470-490 nm results in minimal adverse effects

after periods of exposure longer than 5 minutes.[57] Moving into the infrared, cells remain viable under two-photon irradiation when exposed to pulse energies at or below 4 nJ and do not have significant intracellular ablation after exposure to 1.5 nJ irradiation.[59]

Depending on the light source, initiators can be selected from amongst the two classes of radical photoinitiators, which differ in their mechanism of radical generation. Type I photoinitiators cleave into two radicals upon application of light, whereas type II initiators enter an excited state after application of light and abstract a hydrogen from a coinitiator species.[60] Several known water-soluble, cytocompatible initiators include Irgacure 2959 (I2959, Type I), lithium phenyl-2,4,6-trimethylbenzoylphosphinate (LAP, Type I), and Eosin Y (Type II). I2959 works best with UV irradiation and has been shown to promote rapid polymerization rates with ~ 10 mW/cm2 at 365 nm.[61] LAP can be used with UV and limited visible wavelengths of light and has been shown to reduce polymerization times when compared to I2959.[60] Eosin Y has been used in visible light polymerizations, which may reduce any negative effects observed with UV light (e.g., DNA damage); however, as a Type II initiator it often requires a coinitiator and a catalyst to match the polymerization rates achieved with Type I photoinitiators. Despite its slower rate, a thiol−norbornene crosslinking system was recently reported to occur within minutes with only Eosin Y as the photoinitiator, no longer requiring a coinitiator or catalyst for the reaction to occur at a reasonable rate.[62] In two-photon polymerization, the light can be directed within specific cross-sections of the material to allow photopatterning of both biochemical and biophysical cues. A number of water-soluble photoinitiators can be used in two-photon photoinitiation, including I2959, rose bengal, eosin Y, erythrosin,

flavin adenine dinucleotide, methylene blue, WSPI, and G2CK, and have been used in synthetic ECM applications, including forming hydrogels and crosslinking proteins.[63]

Reduction-oxidation (redox) initiation mechanisms similarly can be used to initiate polymerization reactions over a range of temperatures, including cytocompatible temperatures (37 °C), at reasonable reaction rates for the formation or modification of biomaterials.[64] Traditional redox initiation mechanisms using metal ions for reduction are numerous; however, many of these are not considered cytocompatible. Over the years, new redox mechanisms using enzymes such as Glucose Oxidase (GOx)[65,66] and initiators such as ammonium persulfate (APS) with water soluble catalysts, such as ascorbic acid (AA)[67] or tetraethylmethylene diamine (TEMED),[68] have been used in the presence of cells as an alternative to light initiation mechanisms.

Of the various *in situ* coupling mechanisms, base-catalyzed addition is less commonly seen in biomaterial applications as there are fewer options for its use. One of the most prevalent applications of Michael-type addition is to form hydrogels with chemistries and tune their properties in the presence of cells. The use of a water-soluble base, such as triethanolamine (TEA), may be required for rapid *in situ* formation or modification reactions, such as the reaction of the Michael-type reaction of acrylates and thiols.[69]

Table 1.2: Initiation mechanisms for various cytocompatible coupling chemistries.

Chemistry	Photoinitiation	Redox Initiation	Base-catalyzed Addition
Acrylate[65,70]	◆	◆	
Diels-Alder[a, 71]			
Disulfide[b, 72,73]			
SPAAC[a, 74]			
Tetrazine−Norbornene[a, 75,76]			
Thiol−ene 1. Thiol−acrylate[66,69,77] 2. Thiol−allyl, −norbornene[62,78,79] 3. Thiol−maleimide[80]	◆ ◆	◆ ◆	◆ ◆

[a]These reactions proceed in aqueous conditions without initiator or catalyst.
[b]Formed via oxidation using base.

1.4.2 Covalent Coupling Chemistries

Hydrogels may be formed via chemical crosslinking between functional groups present on polymer and peptide macromers (Figure 1.4). These chemistries must be efficient and produce no toxic byproducts during reaction to ensure cytocompatibility for cell culture applications. Researchers have developed a toolbox of irreversible and reversible covalent chemistries to form and modify hydrogels for biomaterials applications as highlighted below.

1.4.2.1 Irreversible

Thiol−ene chemistries belong to a type of highly selective and efficient orthogonal reactions that have been termed ‘click’ chemistries.[77,78] The most common mechanism for thiol−ene reaction is free-radical polymerization. Upon free radical

initiation, a thiyl radical is created which attacks the carbon-carbon double bond (−ene). The radical propagates along the −ene and abstracts a hydrogen from another thiol to form a new thiyl radical in a chain transfer step. The process continues to alternate between radical propagation and chain transfer as the material polymerizes for formation or modification. Thiol−ene reactions can also occur as Michael-type additions in the presence of a base like TEA. Michael-type addition follows a similar scheme to free radical polymerization where the propagation of an anion replaces radical propagation. In thiol−ene Michael-type addition, the −ene must be electron deficient for the process to occur, where 'enes' that have been used in the presence of cells include acrylates,[69] vinyl sulfones,[81] and maleimides.[82]

Acrylate chemistry to create and modify biomaterials is considered a simplified technique as compared to "click" chemistries like the thiol−ene mechanism since only one type of reactive group is present. It forms a less homogeneous network as it relies on entanglement of polymer strands to create its network. Acrylate end groups react through a homopolymerization process and can be initiated through the various methods as described above. Additionally, acrylates can be coupled to thiols by step growth mechanism using Michael-type reaction[69] or by step growth polymerization using free radicals, which results in a mixed mode polymerization (i.e., thiol−acrylate addition reactions and acrylate homopolymerization by chain polymerization).[70]

Additional high-efficiency, orthogonal chemistries recently have been utilized to form and modify biomaterials in the presence of cells. A strain-promoted azide-alkyne cycloaddition (SPAAC) mechanism was developed, taking advantage of the ring strain on a cyclooctyne combined with a difluoromethylene electron-withdrawing

moiety to promote its reactivity with azides.[83] To create new biomaterials with the benefits of SPAAC while using more synthetically tractable monomers, a new inverse electron demand Diels-alder click reaction between tetrazine and norbornene or trans-cyclooctene was designed.[75,76] These materials can form readily at near physiological conditions in less than 5 minutes, faster than what has been observed for the SPAAC polymerization.

1.4.2.2 Reversible

Thiol−maleimide click chemistry is another form of thiol−ene chemistry formed through the Michael addition of a pendant thiol to an ene-containing maleimide ring. Their reaction is rapid under aqueous conditions, and biomaterials formed through this chemistry have been used in a variety of applications including the crosslinking of soft hydrogels.[84] While there have not been many cases reported using thiol−maleimide chemistry for cell-based applications, viable murine C2C12 myoblasts have been encapsulated in thiol−maleimide hydrogels, showing promise in applications beyond seeding cells on the surface of materials formed with this chemistry.[85] Generally considered stable, reverse Michael-type and exchange reactions have been shown to enable controlled degradation of the thioether succinimide bonds when an electron-withdrawing group is proximate to the thiol used in the thiol−maleimide reaction. Specifically, glutathione, a cysteine-rich peptide secreted by cells has been shown to promote this reversibility and exchange, which has implications in drug delivery and degradable ECM mimics.[86,87]

The covalent bonding of two free thiol groups through oxidation results in the formation of a disulfide bond, which is considered to be weak when compared to other covalent bonds. Gels and films that have been formed by disulfide bonds between

thiol-modified monomers show a high degree of cytocompatibility, however, disulfide bonds generally form on a slower time scale than the other chemistries that have been described (~hours). This "weak" bond is relatively easy to cleave to re-generate thiols and so the reaction is considered reversible. Various methods to dissociate disulfides to alter biomechanical properties have been studied including exposure to glutathione,[86,87] LAP,[72] and dithiothreitol (DTT).[73]

The Diels-Alder reaction occurs between a diene and dienophile to form a cyclohexene and can occur under cytocompatible, aqueous conditions.[88] The reaction is reversible, primarily at high temperatures; however, a recent development has led to a Diels-Alder reaction mechanism that is reversible under physiological conditions.[71] Bonds between terminal maleimides and furans allow a reversible Diels-Alder cycloaddition at cytocompatible temperatures (37 °C), although more rapid release was observed with increasing temperatures. These studies demonstrated the temporal release of biochemical cues, with future implications in designing an ECM mimic where both biochemical and biomechanical cues are dynamically altered.

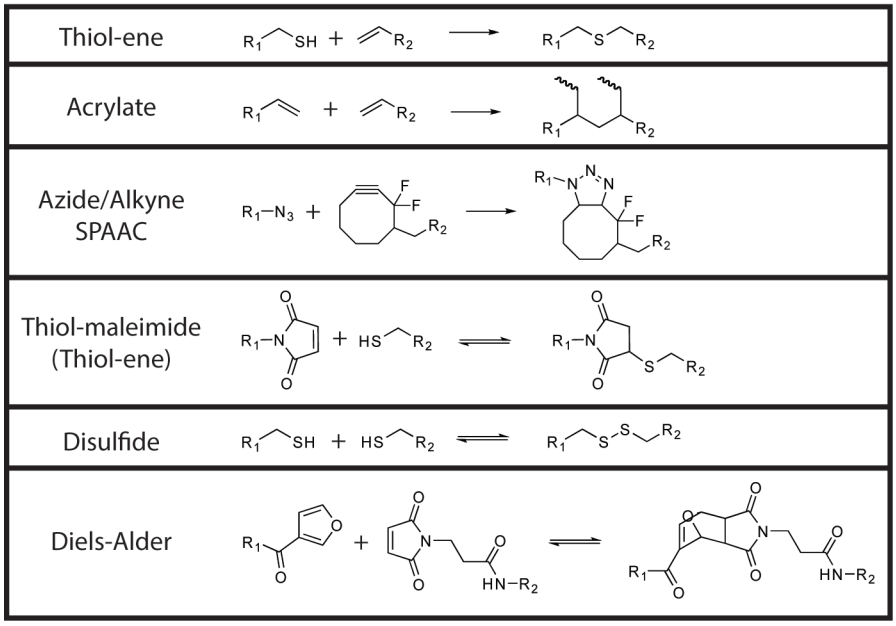

Figure 1.4: **Covalent coupling chemistries.** The generalized reaction schematics for irreversible and reversible coupling chemistries used to form hydrogels are shown.

1.4.3 Non-Covalent Interactions

An alternate technique to forming hydrogels is through non-covalent interactions, such ionic interaction, hydrogen bonding, and hydrophobic assembly. Gels formed via these mechanisms are generally less stable, allowing dynamic changes to the microenvironment through disruption of the weak interaction bonds.

Select peptides and proteins naturally assemble into higher ordered structures due to hydrogen bonding (noncovalent) between amino acids that is stabilized by disulfide bonds (covalent). These include collagen mimetic peptides (CMPs) based on the sequence $(GPO)_n$,[89] stimuli-responsive peptides such as the sequence $C(FKEF)_2C$,[90] and triblock proteins made through recombinant DNA techniques.[91] Hydrogen bonding in proteins and peptides occurs between the oxygen on a carbon

and the hydrogen on the amine in the "backbone" of two neighboring amino acids. This bonding leads to assembled structures, beta sheets or alpha helices (Figure 1.5 A and B), that can influence how cells interact with proteins in the native environment. Researchers are designing methods to mimic peptide and protein structures within biomaterials, as these are key components of the native ECM, through noncovalent interactions that promote self-assembly.

Peptide-amphiphiles are one of the most widely studied type of self-assembling peptides and have been used to create scaffolds that mimic the native ECM structure and composition.[92] The assembly of hydrophobic and hydrophilic regions of the peptides into beta sheets or alpha helical structures can be controlled by pH and structural changes can be made by altering the pH over time. For example, a peptide designed with alternating valine (V) and lysine (K) amino acid residues, which have a high propensity toward forming β-sheet structures, adopts a β-hairpin secondary structure promoted by the inclusion of the tetrapeptide $V^{D}PPT$. Changes in pH promote the folding of the designed peptide across the tetrapeptide that is further stabilized by the alternating hydrophobic and hydrophilic V and K amino acid sequence.[93] Thus, selective peptide design has allowed progress in controlling the formation of nanostructures within synthetic matrices.

Block copolymers contain multiple regions or "blocks" of different polymers (Figure 1.5 C) within their polymer chain. They have been used to make self-assembling biomaterials that respond to environmental cues such as pH and temperature, which can dynamically alter their structural properties. These materials work in a similar manner to peptide-amphiphiles, containing hydrophobic and hydrophilic polymer regions that assemble when exposed to various environmental

cues like the presence of water at varying pH. Some have also been designed to contain blocks of peptides and blocks of polymer to provide a more accurate mimic of the native ECM, allowing cells to adhere and interact better within the synthetic material.[94]

There are a number of block copolymer hydrogels for applications in drug delivery and tissue engineering including polystyrene-poly(ethylene oxide) (PS-PEO) diblock and PS-PEO-PS triblock copolymer blends that form hydrogels with spherical domains resulting from assembly of the hydrophobic and hydrophilic blocks of the copolymer.[95] Hydrogels formed from oppositely charged poly(allyl glycidyl ether-b-ethylene glycol-b-allyl glycidyl ether) triblock copolyelectrolytes were shown to soften with increasing salt concentration, which has implications for the design of future block copolymers with tunable mechanical properties.[96] The sizes of the structures formed by the different domains in self-assembled block copolymers exist on the nano- to micro-scale and can be controlled by changing the ratio and type of monomers, the lengths of the blocks within the monomers, and the pH or salt concentration in the environment.[97,98]

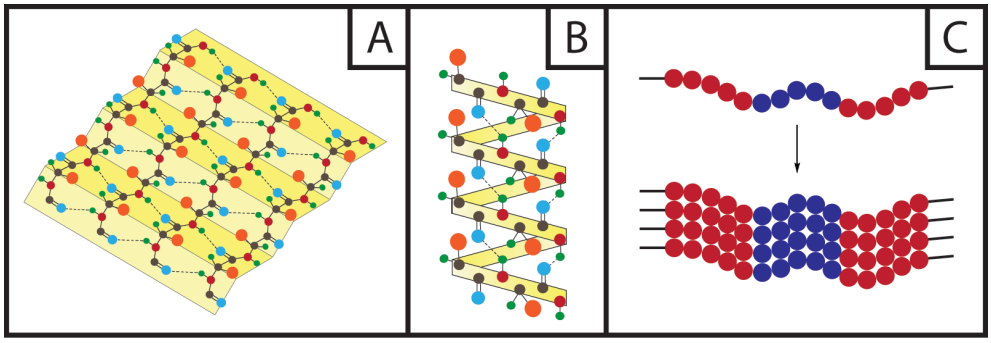

Figure 1.5: **Self-assembling structures used within hydrogels. A)** β-sheet secondary peptide structure. **B)** α-helical secondary peptide structure. **C)** Diblock co-polymers.

1.4.4 Mechanical Properties

Cells respond to ECM stiffness and structure in disease and processes in the body such wound healing and aging,[99] processes which also have been implicated in metastasis and recurrence. The ability to tune the bulk mechanical properties of a synthetic material to mimic those of different tissue ECM will provide additional insight into cell response within 3D *in vitro* culture systems.

While stiffness is a defined a material property (k), the term 'stiffness' is often used as a descriptor of how stiff or soft a material is and modulus (E, Young's modulus; G, shear modulus) is used as an indirect measure of this, where:

$$G = \rho_x RTQ^{-1/3} \qquad \text{Eq. 1.1}$$

and ρ_x is the crosslink density, R is the ideal gas constant, T is the temperature, and Q is the volumetric swelling ratio of the material. The key parameter used to control modulus is crosslink density, with an increased crosslink density corresponding to an increased modulus or stiffer material. In practice, crosslink density has been adjusted through changing macromer concentration or macromer molecular weight.[100–102] Increasing the macromer concentration increases the number of functional groups available to react and form crosslinks, creating a material with higher modulus. Adjusting the macromer molecular weight changes the distance between crosslinks, with lower molecular weight associated with shorter distances between crosslinks and increased modulus.

While it is desirable for the mechanical properties of hydrogels to be stable during long-term culture, cell restriction within a crosslinked polymer network can result in decreased viability at late time points. Network degradation allows cell spreading and growth within synthetic microenvironments, and improves long-term viability (Figure 1.6). Several chemical handles for degradation include esters,[103]

amides,[104] and thioesters[105] to permit hydrolysis of the bulk of the gel or photodegradable groups like the o-nitrobenzyl groups that cleave upon light application to the bulk or targeted regions within the gel.[106–108] Hydrolysis occurs during exposure to water or culture medium, and the scaffold will eventually dissolve, which may limit the length of culture while retaining the desired mechanical properties. Photodegradation allows user-directed control over the mechanical properties, but is limited to when the light is applied, so additional modes of degradation may be required for viability during long-term culture. Toward generating cell-responsive microenvironments, researchers have incorporated peptide crosslinks that cleave in the presence of cell-secreted enzymes, allowing local degradation and subsequently cell spreading, and growth within the microenvironment (Table 1.3).[109] Degradation rates may be tuned with the selection of different peptide sequences depending on desired length of culture and enzymes secreted by cells in culture.

Table 1.3: Common enzymatically-degradable peptide sequences utilized for cell-triggered degradation of biomaterials. Cleavage enzymes and k_{cat}/K_m values ($M^{-1}s^{-1}$) are reported for each sequence.[109] Larger k_{cat}/K_m correspond with faster degradation rates.

Sequence	MMP-1	MMP-2	MMP-3	MMP-7	MMP-8	MMP-9	MTI-MMP
GPQG↓IAGQ	60.6	180	16.7	110	1,570	93.9	—
GPQG↓IWGQ	434	555	56.0	—	11,100	214	—
PVG↓LIG	—	121,000	—	—	—	3,600	—
IPVS↓LRSG	98	82,000	2,300	9,700	—	11,500	4,300

1.4.5 Biochemical Properties

Biochemical factors within the native ECM promote cell-matrix interactions, controlling cell response and fate. Toward mimicking these interactions, proteins,

peptides, and soluble chemical factors have been incorporated within synthetic ECMs (Figure 1.6).

Whole ECM proteins including fibronectin, laminin, elastin, and collagen may be added to synthetic hydrogel scaffolds through covalent incorporation or encapsulation to allow adhesion to the matrix. However, batch-to-batch variability, denaturation, aggregation, and presentation of multiple binding sites can make it difficult to identify key factors regulating cell repsonse.[47] Short peptide sequences that are part of whole ECM proteins have been identified to target and bind specific cell-surface receptors. For example, arginine-glycine-aspartic acid-serine (RGDS), a peptide found within the protein fibronectin, as well many others, has been shown to bind cells through a variety of cell-surface integrins (αVβ3 (strongest), α5β1, α8β1, αVβ1, αVβ5, αVβ6, αVβ8, αIIbβ3)[110,111] and promote adhesion.[112] Peptides that mimic laminin (YIGSR, IKVAV),[113,114] collagen (GFOGER, DGEA),[115,116] and others have also been studied, generating a toolbox of peptides for researchers to incorporate within synthetic scaffolds. These peptide sequences may be functionalized with chemical moieties (e.g., thiols, azides, norbornenes) to allow covalent incorporation within networks. It is important to note that the collagen-based sequence, GFOGER, is often paired with $(POG)_n$ repeat units to promote the assembly of triple helices which provides additional nanostructure that can enhance cell binding and response.[117] Researchers are developing additional techniques to generate structured peptides through assembly and cyclization to further enhance response.[118]

Several techniques have been developed to incorporate soluble factors within microenvironments to modulate cell response. The simplest is through the addition of the factor to culture medium which diffuses into the network. Over time, the factor

degrades, and is replenished with replacement of the medium. Binding peptide sequences have been designed to sequester soluble factors, enhancing stability and allowing controlled release of the factor in the microenvironment. For example, the sequence KRTGQYKL, which exhibits binding affinity for FGF-2, was covalently linked into the gels to sequester the factor after its diffusion into the material. Enhanced FGF-2 binding was achieved by the conjugation of multiple peptides to poly(acrylic acid) polymer chains prior to hydrogel polymerization. The spacing created by the poly(acrylic acid) chain decreased steric hindrance, and the presence of multiple peptides increased the number of binding sites, creating greater affinity for the growth factor. This increase in affinity binding also resulted in extended growth factor release, with potential in applications such as controlled growth factor delivery and directing cell fate.[119]

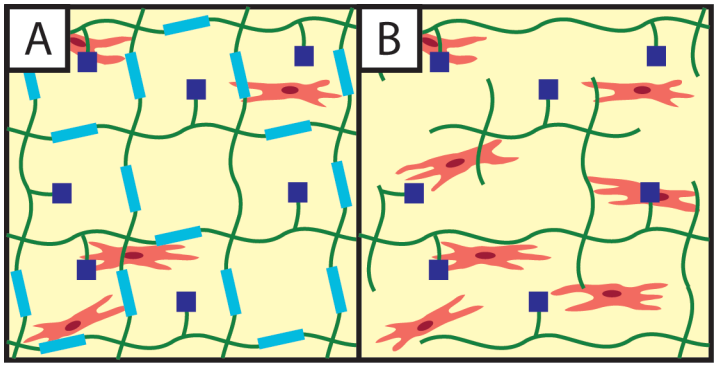

Figure 1.6: **Cells in synthetic microenvironments. A)** Cells are encapsulated within 3D synthetic microenvironments containing polymers (green), degradable peptide crosslinks (light blue), and pendant peptides (dark blue) to promote interactions with the matrix. **B)** Cells respond to the environment by adhering to pendant peptides, degrading peptide crosslinks, and proliferating/migrating within the microenvironment.

1.4.6 Synthetic Hydrogels for Cancer Cell Culture Applications

Recently, several 3D polymer-based material scaffolds have been reported for cancer cell culture, drug screening, and drug delivery applications. These scaffolds permit flexibility in their design so that isolated chemical or mechanical factors may be investigated in their control over response. For example, Girard, et al. developed 3D nanofibrous scaffolds to investigate epithelial-to-mesenchymal transition (EMT), associated with cancer metastasis. Scaffolds electrospun from polymers poly(lactic-co-glycolic acid) (PLGA), polylactic acid (PLA), and methoxypolyethylene glycol (mPEG), permitted the formation of tumoroids from cancer cells seeded into the scaffold through control of charge and topography of the scaffold.[120] Loessner, et al. reported the use of a poly(ethylene glycol) (PEG)-based hydrogel crosslinked with peptides (enzymatically- or non-degradable) and containing an adhesive peptide (RGDS) to promote binding within matrices. Epithelial ovarian cancer cells (OV-MZ-6) cultured within these scaffolds formed spheroids, which responded to matrix modulus and presence of an adhesive peptide and were resistant to paclitaxel, behavior matching that observed *in vivo*.[121] In another PEG-based hydrogel system, Gill, et al. investigated EMT in lung adenocarcinoma (344SQ) cells. Mechanical properties (modulus) and chemical factors (adhesive peptide RGDS, TGFβ1) were varied within these networks to permit the formation of lumenized spheroids in culture.[122]

1.5 Development of a Synthetic PEG-Based Scaffold to Investigate Breast Cancer Dormancy and Recurrence

Inspired by seminal work toward understanding late recurrence of breast cancer *in vitro* and the development of synthetic 3D material systems for cancer cell culture, we plan to address the need for a tunable material scaffold to study breast cancer dormancy and activation. The overall goal of this thesis is to develop a novel

PEG-based hydrogel scaffold for the 3D *in vitro* culture of breast cancer cells to identify critical ECM cues responsible in regulating dormancy and recurrence. Specifically, we aim to *i)* generate a PEG-based hydrogel with tunable biochemical and biomechanical properties (Chapter 2) *ii)* develop a technique to identify proteins secreted by metastatic tissue niche cells within synthetic hydrogel scaffolds (Chapter 3), and *iii)* culture breast cancer cells within synthetic microenvironments mimicking the biochemical and biomechanical properties of metastatic tissue ECM and identify their response (Chapter 4). In chapter 5, a summary of the work and overview of future applications of the developed system will be presented.

REFERENCES

1. Siegel, R. L., Miller, K. D. & Jemal, A. Cancer Statistics, 2015. *CA Cancer J Clin*. **65** (1), 5–29 (2015).

2. Ferlay, J., Steliarova-Foucher, E., *et al.* Cancer incidence and mortality patterns in Europe: Estimates for 40 countries in 2012. *Eur J Cancer*. **49** (6), 1374–1403 (2013).

3. Brewster, A. M., Hortobagyi, G. N., *et al.* Residual Risk of Breast Cancer Recurrence 5 Years After Adjuvant Therapy. *J Natl Cancer Inst*. **100** (16), 1179–1183 (2008).

4. Weigelt, B., Peterse, J. L. & van't Veer, L. J. Breast Cancer Metastasis: Markers and Models. *Nat Rev Cancer*. **5** 591–602 (2005).

5. Nguyen, D. X., Bos, P. D. & Massagué, J. Metastasis: from dissemination to organ-specific colonization. *Nat Rev Cancer*. **9** 274–284 (2009).

6. Scully, O. J., Bay, B., Yip, G. & Yu, Y. Breast Cancer Metastasis. *Cancer Genomics and Proteomics*. **9** 311–320 (2012).

7. Barkan, D., Green, J. E. & Chambers, A. F. Extracellular matrix: A gatekeeper in the transition from dormancy to metastatic growth. *Eur J Cancer*. **46** (7), 1181–1188 (2010).

8. Lu, P., Weaver, V. M. & Werb, Z. The extracellular matrix: A dynamic niche in cancer progression. *J Cell Biol*. **196** (4), 395–406 (2012).

9. Lester, B. R. & McCarthy, J. B. Tumor cell adhesion to the extracellular matrix and signal transduction mechanisms implicated in tumor cell motility, invasion and metastasis. *Cancer Metastasis Rev*. **11** 31–44 (1992).

10. Alberts, B., Johnson, A., Lewis, J., Raff, M., Roberts, K. & Walter, P. Cell junctions, cell adhesion, and the extracellular matrix. *Mol Biol Cell*. 1065–1125 (2002).

11. Hynes, R. O. The Extracellular Matrix: Not Just Pretty Fibrils. *Science*. **326** (5957), 1216–1219 (2009).

12. Bonnans, C., Chou, J. & Werb, Z. Remodelling the extracellular matrix in development and disease. *Nat Publ Gr*. **15** (12), 786–801 (2014).

13. Chang, C., Werb, Z. & Werb, Z. The many faces of metalloproteases: cell growth, invasion, angiogenesis and metastasis. *Trends Cell Biol*. **11** (11), 37–43 (2001).

14. Schultz, G. S. & Wysocki, A. Interactions between extracellular matrix and growth factors in wound healing. *Wound Repair Regen*. **17** 153–162 (2009).

15. Raman, D., Baugher, P. J., Mon, Y. & Richmond, A. Role of chemokines in tumor growth. *Cancer Lett*. **256** 137–165 (2007).

16. Shoulders, M. D. & Raines, R. T. Collagen Structure and Stability. *Annu Rev Biochem*. **78** 929–958 (2009).

17. Singh, P., Carraher, C. & Schwarzbauer, J. E. Assembly of Fibronectin Extracellular Matrix. *Annu Rev Cell Dev Biol*. **26** 397–419 (2010).

18. Durbeej, M. Laminins. *Cell Tissue Res*. **339** 259–268 (2010).

19. Desgrosellier, J. S. & Cheresh, D. A. Integrins in cancer: biological implications and therapeutic opportunities. *Nat Rev Cancer*. **10** (1), 9–22 (2010).

20. Singer, A. J. & Clark, R. A. F. Cutaneous Wound Healing. *N Engl J Med*. **341** (10), 738–746 (1999).

21. Martin, P. Wound Healing — Aiming for Perfect Skin Regeneration. *Science*. **276** (5309), 75–81 (1997).

22. Kwan, K. H. L., Liu, X., To, M. K. T., Yeung, K. W. K., Ho, C. & Wong, K. K. Y. Modulation of collagen alignment by silver nanoparticles results in better mechanical properties in wound healing. *Nanomedicine Nanotechnology, Biol Med*. **7** (4), 497–504 (2011).

23. Rho, J., Kuhn-Spearing, L. & Zioupos, P. Mechanical properties and the hierarchical structure of bone. *Med Eng Phys*. **20** 92–102 (1998).

24. Winer, J. P., Janmey, P. A., Mccormick, M. E. & Funaki, M. Bone Marrow-Derived Human Mesenchymal Stem Cells Become Quiescent on Soft Substrates but Remain Responsive to Chemical or Mechanical Stimuli. *Tissue Eng Part A*. **15** (1), 147–154 (2009).

25. Levental, I., Georges, P. C. & Janmey, P. A. Soft biological materials and their

impact on cell function. *Soft Matter*. **3** (3), 299–306 (2007).

26. Mansour, J. M. *Biomechanics of cartilage*. *Kinesiol Mech pathomechanics Hum Mov*. (Lippincott Williams and Wilkins, Philadelphia: 2003).

27. Agache, P. G., Monneur, C., Leveque, J. L. & De Rigal, J. Mechanical Properties and Young's Modulus of Human Skin in Vivo. *Arch Dermatol Res*. **269** 221–232 (1980).

28. Frantz, C., Stewart, K. M. & Weaver, V. M. The extracellular matrix at a glance. *J Cell Sci*. **123** 4195–4200 (2010).

29. Liu, F., Mih, J. D., *et al.* Feedback amplification of fibrosis through matrix stiffening and COX-2 suppression. *J Cell Biol*. **190** (4), 693–706 (2010).

30. Bao, P., Kodra, A., *et al.* The Role of Vascular Endothelial Growth Factor in Wound Healing. *J Surg Res*. **153** (2), 347–358 (2009).

31. Yorio, T., Clark, A. F. & Wax, M. B. *Ocular therapeutics: eye on new discoveries*. (Academic: Amsterdam; Boston; London, 2008).

32. Cua, D. J. & Tato, C. M. Innate IL-17-producing cells: the sentinels of the immune system. *Nat Rev Immunol*. **10** 479–489 (2010).

33. Cameron, M. J. & Kelvin, D. J. *Cytokines, chemokines and their receptors*. (Landes Bioscience: 2000).

34. Crawford, A., Angelosanto, J. M., Nadwodny, K. L., Blackburn, S. D. & Wherry, E. J. A Role for the Chemokine RANTES in Regulating CD8 T Cell Responses during Chronic Viral Infection. *PloS Pathog*. **7** (7), e1002098 (2011).

35. Leask, A. & Abraham, D. J. TGF-B signaling and the fibrotic response. *FAESB J*. **18** (7), 816–827 (2004).

36. Sant, S., Hancock, M. J., Donnelly, J. P., Iyer, D. & Khademhosseini, A. Biomimetic Gradient Hydrogels for Tissue Engineering. *Can J Chem Eng*. **88** (6), 899–911 (2011).

37. Barney, L. E., Jansen, L. E., Polio, S. R., Galarza, S., Lynch, M. E. & Peyton, S. R. The predictive link between matrix and metastasis. *Curr Opin Chem Eng*. **11** 85–93 (2016).

38. Chen, Q. K., Lee, K., Radisky, D. C. & Nelson, C. M. Extracellular matrix proteins regulate epithelial-mesenchymal transition in mammary epithelial

cells. *Differentiation*. **86** (3), 126–132 (2013).

39. Theocharis, A. D., Skandalis, S. S., Gialeli, C. & Karamanos, N. K. Extracellular matrix structure. *Adv Drug Deliv Rev*. **97** 4–27 (2016).

40. Voulgari, A. & Pintzas, A. Epithelial-mesenchymal transition in cancer metastasis: Mechanisms, markers and strategies to overcome drug resistance in the clinic. *Biochim Biophys Acta - Rev Cancer*. **1796** (2), 75–90 (2009).

41. Wu, Y., Chen, L., Scott, P. G. & Tredget, E. E. Mesenchymal Stem Cells Enhance Wound Healing Through Differentiation and Angiogenesis. *Stem Cells*. **25** 2648–2659 (2007).

42. Fang, M., Yuan, J., Peng, C. & Li, Y. Collagen as a double-edged sword in tumor progression. *Tumor Biol*. **35** 2871–2882 (2014).

43. Baker, B. M. & Chen, C. S. Deconstructing the third dimension– how 3D culture microenvironments alter cellular cues. *J Cell Sci*. **125** (13), 3015–3024 (2012).

44. Barrios, J. & Wieder, R. Dual FGF-2 and Intergrin α5β1 Signaling Mediate GRAF-Induced RhoA Inactivation in a Model of Breast Cancer Dormancy. *Cancer Microenviron*. **2** 33–47 (2009).

45. Atala, A. & Yoo, J. J. *Essentials of 3D biofabrication and translation*. (Academic Press: 2015).

46. Skardal, A., Mack, D., Atala, A. & Soker, S. Substrate elasticity controls cell proliferation, surface marker expression and motile phenotype in amniotic fluid-derived stem cells. *J Mech Behav Biomed Mater*. **17** 307–316 (2013).

47. Tibbitt, M. W. & Anseth, K. S. Hydrogels as extracellular matrix mimics for 3D cell culture. *Biotechnol Bioeng*. **103** (4), 655–663 (2009).

48. Weaver, V. M., Petersen, O. W., *et al.* Reversion of the Malignant Phenotype of Human Breast Cells in Three-Dimensional Culture and In Vivo by Integrin Blocking Antibodies. *J Cell Biol*. **137** (1), 231–245 (1997).

49. Ghajar, C. M., Peinado, H., *et al.* The perivascular niche regulates breast tumour dormancy. *Nat Cell Biol*. **15** (7), 807–17 (2013).

50. Lee, J., Cuddihy, M. J. & Kotov, N. A. Three-Dimensional Cell Culture Matrices: State of the Art. *Tissue Eng Part B*. **14** (1), 61–86 (2008).

51. Pampaloni, F., Reynaud, E. G. & Stelzer, E. H. K. The third dimension bridges

the gap between cell culture and live tissue. *Nat Rev Mol Cell Biol*. **8** 839–845 (2007).

52. Hughes, C. S., Postovit, L. M. & Lajoie, G. A. Matrigel: A complex protein mixture required for optimal growth of cell culture. *Proteomics*. **10** 1886–1890 (2010).

53. Barkan, D., Kleinman, H., *et al.* Inhibition of Metastatic Outgrowth From Single Dormant Tumor Cells by Targeting the Cytoskeleton. *Cancer Res*. **68** (15), 6241–6250 (2009).

54. Barkan, D. & Green, J. E. An In Vitro System to Study Tumor Dormancy and the Switch to Metastatic Growth. *J Vis Exp*. **54** e2914 (2011).

55. Hoffman, A. S. Hydrogels for biomedical applications. *Adv Drug Deliv Rev*. **64** 18–23 (2012).

56. Fedorovich, N. E., Oudshoorn, M. H., Geemen, D. Van, Hennink, W. E., Alblas, J. & Dhert, W. J. A. The effect of photopolymerization on stem cells embedded in hydrogels. *Biomaterials*. **30** (3), 344–353 (2009).

57. Bryant, S. J., Nuttelman, C. R. & Anseth, K. S. Cytocompatibility of UV and visible light photoinitiating systems on cultured NIH/3T3 fibroblasts in vitro. *J Biomater Sci Polym Ed*. **11** (5), 439–457 (2000).

58. Guvendiren, M. & Burdick, J. A. Stiffening hydrogels to probe short- and long-term cellular responses to dynamic mechanics. *Nat Commun*. **3** 792–799 (2012).

59. Tibbitt, M. W., Kloxin, A. M., Dyamenahalli, U. & Anseth, K. S. Controlled two-photon photodegradation of PEG hydrogels to study and manipulate subcellular interactions on soft materials. *Soft Matter*. **6** (20), 5100–5108 (2010).

60. Fairbanks, B. D., Schwartz, M. P., Bowman, C. N. & Anseth, K. S. Photoinitiated polymerization of PEG-diacrylate with lithium phenyl-2,4,6-trimethylbenzoylphosphinate: polymerization rate and cytocompatibility. *Biomaterials*. **30** (35), 6702–6707 (2009).

61. Williams, C. G., Malik, A. N., Kim, T. K., Manson, P. N. & Elisseeff, J. H. Variable cytocompatibility of six cell lines with photoinitiators used for polymerizing hydrogels and cell encapsulation. *Biomaterials*. **26** (11), 1211–1218 (2005).

62. Shih, H. & Lin, C. Visible-Light-Mediated Thiol-Ene Hydrogelation Using

Eosin-Y as the Only Photoinitiator. *Macromol Rapid Commun*. **34** 269–273 (2013).

63. Torgersen, J., Qin, X., Li, Z., Ovsianikov, A. & Liska, R. Hydrogels for Two-Photon Polymerization: A Toolbox for Mimicking the Extracellular Matrix. *Adv Funct Mater*. **23** 4542–4554 (2013).

64. Odian, G. *Principles of polymerization*. (John Wiley & Sons: 2004).

65. Johnson, L. M., Fairbanks, B. D., Anseth, K. S. & Bowman, C. N. Enzyme-Mediated Redox Initiation for Hydrogel Generation and Cellular Encapsulation. *Biomacromolecules*. **10** 3114–3121 (2009).

66. Hume, P. S., Bowman, C. N. & Anseth, K. S. Biomaterials Functionalized PEG hydrogels through reactive dip-coating for the formation of immunoactive barriers. *Biomaterials*. **32** (26), 6204–6212 (2011).

67. Temenoff, J. S., Shin, H., Conway, D. E., Engel, P. S. & Mikos, A. G. In Vitro Cytotoxicity of Redox Radical Initiators for Cross-Linking of Oligo(poly(ethylene glycol) fumarate) Macromers. *Biomacromolecules*. **4** 1605–1613 (2003).

68. Kloxin, A. M., Tibbitt, M. W. & Anseth, K. S. Synthesis of photodegradable hydrogels as dynamically tunable cell culture platforms. *Nat Protoc*. **5** (12), 1867–1887 (2010).

69. Metters, A. & Hubbell, J. Network Formation and Degradation Behavior of Hydrogels Formed by Michael-Type Addition Reactions. *Biomacromolecules*. **6** 290–301 (2005).

70. Salinas, C. N. & Anseth, K. S. Mixed Mode Thiol-Acrylate Photopolymerizations for the Synthesis of PEG-Peptide Hydrogels. *Macromolecules*. **41** (16), 6019–6026 (2008).

71. Koehler, K. C., Anseth, K. S. & Bowman, C. N. Diels−Alder Mediated Controlled Release from a Poly(ethylene glycol) Based Hydrogel. *Biomacromolecules*. **14** 538–547 (2013).

72. Fairbanks, B. D., Singh, S. P., Bowman, C. N. & Anseth, K. S. Photodegradable, photoadaptable hydrogels via radical-mediated disulfide fragmentation reaction. *Macromolecules*. **44** (8), 2444–2450 (2011).

73. Shu, X. Z., Liu, Y., Palumbo, F. S., Luo, Y. & Prestwich, G. D. In situ crosslinkable hyaluronan hydrogels for tissue engineering. *Biomaterials*. **25**

1339–1348 (2004).

74. Johnson, J. A., Baskin, J. M., Bertozzi, C. R., Koberstein, T. & Turro, N. J. Copper-free click chemistry for the in situ crosslinking of photodegradable star polymers. *Chem Commun*. **26** 3064–3066 (2008).

75. Alge, D. L., Azagarsamy, M. A., Donohue, D. F. & Anseth, K. S. Synthetically tractable click hydrogels for three-dimensional cell culture formed using tetrazine-norbornene chemistry. *Biomacromolecules*. **14** (4), 949–953 (2013).

76. Blackman, M. L., Royzen, M. & Fox, J. M. Tetrazine Ligation: Fast Bioconjugation Based on Inverse-Electron-Demand Diels-Alder Reactivity. *J Am Chem Soc*. **130** 13518–13519 (2008).

77. Hoyle, C. E. & Bowman, C. N. Thiol-ene click chemistry. *Angew Chemie - Int Ed*. **49** (9), 1540–1573 (2010).

78. Hoyle, C. E., Lowe, A. B. & Bowman, C. N. Applications of click chemistry themed issue and polymer synthesis. *Chem Soc Rev*. **39** (4), 1355–1387 (2010).

79. McCall, J. D., Lin, C. & Anseth, K. S. Affinity Peptides Protect Transforming Growth Factor Beta During Encapsulation in Poly(ethylene glycol) Hydrogels. *Biomacromolecules*. **12** 1051–1057 (2011).

80. Luo, Y. & Shoichet, M. S. A photolabile hydrogel for guided three-dimensional cell growth and migration. *Nat Mater*. **3** 249–253 (2004).

81. Lutolf, M. P., Lauer-Fields, J. L., *et al.* Synthetic matrix metalloproteinase-sensitive hydrogels for the conduction of tissue regeneration: Engineering cell-invasion characteristics. *Proc Natl Acad Sci United States Am*. **100** (9), 5413–5418 (2003).

82. Fu, Y. & Kao, W. J. In situ forming poly (ethylene glycol)-based hydrogels via thiol-maleimide Michael-type addition. *J Biomater Res A*. **98A** (2), 201–211 (2011).

83. Hodgson, S. M., Bakaic, E., Stewart, S. A., Hoare, T. & Adronov, A. Properties of Poly(ethylene glycol) Hydrogels Cross-Linked via Strain-Promoted Alkyne−Azide Cycloaddition (SPAAC). *Biomacromolecules*. **17** 1093–1100 (2016).

84. Nie, T., Baldwin, A., Yamaguchi, N. & Kiick, K. L. Production of heparin-functionalized hydrogels for the development of responsive and controlled growth factor delivery systems. *J Control Release*. **122** 287–296 (2007).

85. Phelps, E. A., Enemchukwu, N. O., *et al.* Maleimide Cross-Linked Bioactive PEG Hydrogel Exhibits Improved Reaction Kinetics and Cross-Linking for Cell Encapsulation and In Situ Delivery. *Adv Mater*. **24** 64–70 (2012).

86. Baldwin, A. D. & Kiick, K. L. Tunable Degradation of Maleimide-Thiol Adducts in Reducing Environments. *Bioconjug Chem*. **22** 1946–1953 (2011).

87. Baldwin, A. D. & Kiick, K. L. Reversible maleimide–thiol adducts yield glutathione-sensitive poly(ethylene glycol)–heparin hydrogels. *Polym Chem*. **4** (1), 133–143 (2013).

88. Nandivada, B. H., Jiang, X. & Lahann, J. Click Chemistry: Versatility and Control in the Hands of Materials Scientists. *Adv Mater*. **19** 2197–2208 (2007).

89. Cejas, M. A., Kinney, W. A., *et al.* Thrombogenic collagen-mimetic peptides : Self-assembly of triple helix-based fibrils driven by hydrophobic interactions. *Proc Natl Acad Sci United States Am*. **105** (25), 8513–8518 (2008).

90. Bowerman, C. J. & Nilsson, B. L. A Reductive Trigger for Peptide Self-Assembly and Hydrogelation. *J Am Chem Soc*. **132** 9526–9527 (2010).

91. Petka, W. A., Harden, J. L., Mcgrath, K. P., Wirtz, D. & Tirrell, D. A. Reversible Hydrogels from Self-Assembling Artificial Proteins. *Science*. **281** (5375), 389–392 (1998).

92. Hartgerink, J. D., Beniash, E. & Stupp, S. I. Self-Assembly and Mineralization of Peptide-Amphiphile Nanofibers. *Science*. **294** (5547), 1683–1688 (2001).

93. Schneider, J. P., Pochan, D. J., Ozbas, B., Rajagopal, K., Pakstis, L. & Kretsinger, J. Responsive Hydrogels from the Intramolecular Folding and Self-Assembly of a Designed Peptide. *J Am Chem Soc*. **124** (50), 15030–15037 (2002).

94. Nowak, A. P., Breedveld, V., Pakstis, L. & Ozbas, B. Rapidly recovering hydrogel scaffolds from self-assembling diblock copolypeptide amphiphiles. *Nature*. **417** 424–428 (2002).

95. Guo, C. & Bailey, T. S. Highly distensible nanostructured elastic hydrogels from AB diblock and ABA triblock copolymer melt blends. *Soft Matter*. **6** 4807–4818 (2010).

96. Hunt, J. N., Feldman, K. E., *et al.* Tunable , High Modulus Hydrogels Driven by Ionic Coacervation. *Adv Mater*. **23** 2327–2331 (2011).

97. Lopresti, C., Massignani, M., *et al.* Controlling Polymersome Surface Topology at the Nanoscale by Membrane Confined Polymer/Polymer Phase Separation. *ACS Nano*. **5** (3), 1775–1784 (2011).

98. Krogsgaard, M., Behrens, M. A., Pedersen, J. S. & Birkedal, H. Self-Healing Mussel-Inspired Multi-pH-Responsive Hydrogels. *Biomacromolecules*. **14** 297–301 (2013).

99. Discher, D. E., Janmey, P. & Wang, Y. Tissue Cells Feel and Respond to the Stiffness of Their Substrate. *Science*. **310** 1139–1143 (2005).

100. Shih, H. & Lin, C. Cross-Linking and Degradation of Step-Growth Hydrogels Formed by Thiol−Ene Photoclick Chemistry. *Biomacromolecules*. **13** 2003–2012 (2012).

101. Anseth, K. S., Bowman, C. N. & Brannon-peppas, L. Mechanical properties of hydrogels and their experimental determination. *Biomaterials*. **17** 1647–1657 (1996).

102. Kloxin, B. A. M., Kloxin, C. J., Bowman, C. N. & Anseth, K. S. Mechanical Properties of Cellularly Responsive Hydrogels and Their Experimental Determination. *Adv Mater*. **22** 3484–3494 (2010).

103. Jo, Y. S., Gantz, J., Hubbell, A. & Lutolf, M. P. Tailoring hydrogel degradation and drug release via neighboring amino acid controlled ester hydrolysis. *Soft Matter*. **5** 440–446 (2009).

104. Larson, R. A. & Weber, E. J. *Reaction mechanisms in environmental organic chemistry*. (CRC press: 1994).

105. Bracher, P. J., Snyder, P. W., Bohall, B. R. & Whitesides, G. M. The Relative Rates of Thiol–Thioester Exchange and Hydrolysis for Alkyl and Aryl Thioalkanoates in Water. *Orig Life Evol Biosph*. **41** 399–412 (2011).

106. Zhao, H., Sterner, E. S., Coughlin, E. B. & Theato, P. o-Nitrobenzyl Alcohol Derivatives: Opportunities in Polymer and Materials Science. *Macromolecules*. (45), 1723–1736 (2012).

107. Kloxin, A. M., Kasko, A. M., Salinas, C. N. & Anseth, K. S. Photodegradable Hydrogels for Dynamic Tuning of Physical and Chemical Properties. *Science*. **324** (5923), 59–63 (2009).

108. Griffin, D. R. & Kasko, A. M. Photodegradable Macromers and Hydrogels for Live Cell Encapsulation and Release. *J Am Chem Soc*. **134** 13103–13107

(2012).

109. Patterson, J. & Hubbell, J. A. Enhanced proteolytic degradation of molecularly engineered PEG hydrogels in response to MMP-1 and MMP-2. *Biomaterials*. **31** (30), 7836–7845 (2010).

110. Rice, J. J., Martino, M. M., Laporte, L. De, Tortelli, F., Briquez, P. S. & Hubbell, J. A. Engineering the Regenerative Microenvironment with Biomaterials. *Adv Healthc Mater*. **2** 57–71 (2013).

111. Ruoslahti, E. RGD and other recognition sequences for integrins. *Annu Rev Cell Dev Biol*. **12** 697–715 (1996).

112. Massia, S. P. & Hubbell, J. A. An RGD Spacing of 440 nm Is Sufficient for Integrin avß3-mediated Fibroblast Spreading and 140 nm for Focal Contact and Stress Fiber Formation. *J Cell Biol*. **114** (5), 1089–1100 (1991).

113. Ali, S., Saik, J. E., Gould, D. J., Dickinson, M. E. & West, J. L. Immobilization of Cell-Adhesive Laminin Peptides. *Biores Open Access*. **2** (4), 241–249 (2013).

114. Weber, L. M. & Anseth, K. S. Hydrogel encapsulation environments functionalized with extracellular matrix interactions increase islet insulin secretion. *Matrix Biol*. **27** (8), 667–673 (2008).

115. Shekaran, A. & Garcia, A. J. Extracellular matrix-mimetic adhesive biomaterials for bone repair. *J Biomed Mater Res - Part A*. **96A** (1), 261–272 (2011).

116. Mehta, M., Madl, C. M., Lee, S., Duda, G. N. & Mooney, D. J. The collagen I mimetic peptide DGEA enhances an osteogenic phenotype in mesenchymal stem cells when presented from cell-encapsulating hydrogels. *J Biomed Mater Res - Part A*. **103A** (11), 3516–3525 (2015).

117. Li, Y. & Yu, S. M. Targeting and mimicking collagens via triple helical peptide assembly. *Curr Opin Chem Biol*. **17** (6), 968–975 (2013).

118. Aimetti, A. A., Shoemaker, R. K., Lin, C. & Anseth, K. S. On-resin peptide macrocyclization using thiol–ene click chemistry. *Chem Commun*. **46** (23), 4061–4063 (2010).

119. Lin, C. & Anseth, K. S. Controlling Affinity Binding with Peptide-Functionalized Poly(ethylene glycol) Hydrogels. *Adv Funct Mater*. **19** 2325–2331 (2009).

120. Girard, Y. K., Wang, C., *et al.* A 3D Fibrous Scaffold Inducing Tumoroids: A Platform for Anticancer Drug Development. *PLoS One*. **8** (10), e75345 (2013).

121. Loessner, D., Stok, K. S., Lutolf, M. P., Hutmacher, D. W., Clements, J. A. & Rizzi, S. C. Biomaterials Bioengineered 3D platform to explore cell-ECM interactions and drug resistance of epithelial ovarian cancer cells. *Biomaterials*. **31** (32), 8494–8506 (2010).

122. Gill, B. J., Gibbons, D. L., *et al.* A synthetic matrix with independently tunable biochemistry and mechanical properties to study epithelial morphogenesis and EMT in a lung adenocarcinoma model. *Cancer Res*. **72** (22), 6013–6023 (2012).

Chapter 2

DESIGN OF THIOL−ENE PHOTOCLICK HYDROGELS USING FACILE TECHNIQUES FOR CELL CULTURE APPLICATIONS

The information in this chapter is adapted, with permission from the Royal Society of Chemistry, from *Design of thiol−ene photoclick hydrogels using facile techniques for cell culture applications* by L. A. Sawicki and A. M. Kloxin, published in *Biomaterials Science*, Volume 2, Number 11, pages 1612-1626, November 2014.

2.1 Abstract

Thiol–ene 'click' chemistries have been widely used in biomaterials applications, including drug delivery, tissue engineering, and controlled cell culture, owing to their rapid, cytocompatible, and often orthogonal reactivity. In particular, hydrogel-based biomaterials formed by photoinitiated thiol–ene reactions afford spatiotemporal control over the biochemical and biomechanical properties of the network for creating synthetic materials that mimic the extracellular matrix or enable controlled drug release. However, the use of charged peptides functionalized with cysteines, which can form disulfides prior to reaction, and vinyl monomers that require multistep syntheses and contain ester bonds, may lead to undesired inhomogeneity or degradation under cell culture conditions. Here, we designed a thiol–ene hydrogel formed by the reaction of allyloxycarbonyl-functionalized peptides and thiol-functionalized poly(ethylene glycol). Hydrogels were polymerized by free radical initiation under cytocompatible doses of long wavelength ultraviolet light in the presence of water-soluble photoinitiators (lithium acylphosphinate, LAP, and 2-

hydroxy-1-[4-(2-hydroxyethoxy)phenyl]-2-methyl-1-propanone, Irgacure 2959). Mechanical properties of these hydrogels were controlled by varying the monomer concentration to mimic a range of soft tissue environments, and hydrogel stability in cell culture medium was observed over weeks. Patterns of biochemical cues were created within the hydrogels post-formation and confirmed through the incorporation of fluorescently-labeled peptides and Ellman's assay to detect free thiols. Human mesenchymal stem cells remained viable after encapsulation and subsequent photopatterning, demonstrating the utility of the monomers and hydrogels for three-dimensional cell culture. This facile approach enables the formation and characterization of hydrogels with well-defined, spatially-specific properties and expands the suite of monomers available for three-dimensional cell culture and other biological applications.

2.2 Introduction

Click chemistries for the formation and modification of biomaterials have garnered significant and growing interest for numerous applications, including drug delivery, tissue engineering, and controlled cell culture.[1,2] A number of functional groups undergo efficient and highly selective click reactions under a variety of cytocompatible conditions, making them well suited for the manipulation of biomaterial properties in the presence of cells.[3,4] These reactions include radically initiated thiol–ene and thiol–yne,[5,6] thiol-Michael addition,[7,8] spontaneous reaction of azides with strained alkynes,[9,10] and spontaneous reaction of tetrazine with norbornene and transcyclooctene,[11,12] which have been used to examine the effects of matrix properties on cell behavior,[6,7,9,11] to label cells and biomolecules,[10,12] and to form carriers for drug delivery.[13] Amongst these, thiol–ene click chemistries have been

examined broadly for the formation and modification of hydrogel-based biomaterials owing to their ease of use and the availability of thiols in many biomolecules.[14]

Hydrogels formed by thiol–ene click reactions have been constructed with a range of cytocompatible polymers and copolymers, such as poly(ethylene glycol) (PEG),[15] hyaluronic acid,[16] and poly(ethylene glycol)–poly(lactic acid),[17] and modified with peptides and proteins, such as GPQG↓IWGQ,[18] IPVS↓LRSG,[18] and RGDS,[19] to impart specific biological activity.[16,20] Various vinyl functional groups have been investigated for this purpose, including norbornene,[19] vinyl sulfone,[8] and allyl ether.[21] For example, the Michael-type addition of thiols on peptides with vinyl groups (‘ene's) on vinyl sulfone-modified PEG has been widely employed to design hydrogels with controlled, cell-responsive properties for use in drug delivery or tissue engineering.[8,22] These reactions proceed *via* a step growth mechanism,[5,14] resulting in a homogeneous network structure with robust mechanical properties for applications in cell culture and delivery.[23]

Photoinitiated thiol–ene systems are particularly attractive for hydrogel formation and modification because they allow user-directed control over the presentation of biophysical or biochemical cues in space and in time to promote specific cellular functions and toward mimicking the dynamic structure or composition of the native extracellular matrix (ECM) *in vitro*.[24,25] Peptides modified with cysteines and polymers modified with acrylates (mixed step and chain growth mechanism) or norbornenes (step growth mechanism) have been extensively used owing to their rapid reaction under cytocompatible photopolymerization conditions.[19,26,27] For example, Fairbanks *et al.* first demonstrated that norbornene-modified PEG reacts within minutes with cysteine-modified, enzymatically degradable

crosslinking peptides in the presence of a radical initiator to form hydrogels by step growth free radical polymerization.[19] This strategy (vinyl-modified PEG) has been used to encapsulate a number of cell types including, but not limited, to osteoblasts, chondrocytes, mesenchymal stem cells (MSCs), and smooth muscle cells.[28] These chemistries also have been used to create new biomaterial systems, such as a hydrogel formed by the reaction of norbornene-modified hyaluronic acid with a dithiol crosslinker and modified with patterns of biochemical cues at select time points.[16]

Despite their great utility, there are a few potential concerns when using these existing thiol–ene photoclick systems. Recently, Shih and Lin observed that ester bonds present in polymers modified with various vinyl groups (*e.g.*, acrylic acid or norbornene carboxylic acid) degrade over relatively short times in water or cell culture conditions (*i.e.*, days to weeks), where the hydrolysis rate is affected by the incorporation of different charged peptide sequences.[29] Preprogrammed degradation afforded by hydrolysis allows cell spreading within the matrix; however, it is often desirable for the rate of degradation to respond dynamically to cell secreted enzymes or an externally-applied stimulus (*e.g.*, light). Toward designing alternate systems with controlled degradation (*e.g.*, cell-secreted enzymes or light), polymer precursors modified with amine functional groups instead of hydroxyls have been utilized, introducing more water-stable amide bonds upon reaction with carboxylic acid-containing functional groups.[30,31] Despite this increased stability, there typically is increased cost or synthetic processing associated with using these materials. Additionally, the formation of disulfide bonds between cysteine-modified charged peptides[32] before reaction may deplete the concentration of thiols present in the

reaction solution, resulting in an off-stoichiometry mixture, defects in the network structure, and slower polymerization times.[33,34]

Herein, an approach to rapid thiol–ene photoclick polymerization between a vinyl-modified peptide and thiol-modified PEG is presented (Figure 2.1). A multiarm PEG thiol is used as the 'backbone' of the hydrogel structure with thiols on each arm connected by ether bonds. The PEG backbone is not charged, limiting potential disulfide formation,[35] and ether bonds neighboring thiol functional groups provide a water-stable base for the introduction of enzymatically degradable peptide sequences for cell-dictated degradation. The alloxycarbonyl (alloc) group, which is used to protect the amines of amino acids (*e.g.*, lysine) during peptide synthesis, is incorporated within pendant (single)[15,36,37] and crosslink (double) peptide sequences to provide vinyls for reaction with the PEG thiol backbone. The use of lithium acylphosphinate (LAP) as a photoinitiator, which has increased rates of initiation and polymerization relative to other water-soluble photoinitiators,[38] allows the rapid reaction of the alloc-modified peptides with the multiarm PEG thiol to form hydrogels under cytocompatible doses of long wavelength ultraviolet (UV) light (10 mW/cm^2, 365 nm).[39] Further, these monomers may be purchased commercially or synthesized with relatively simple techniques presented here, making the system accessible to researchers in a variety of fields. In this article, the polymerization, mechanical properties, stability, cytocompatibility, and spatial patterning of these robust thiol–ene photoclick hydrogels are characterized to define and demonstrate their potential for use as three-dimensional (3D) mimics of the ECM, particularly for the evaluation of cell–matrix interactions. In addition to the application of these materials in controlled cell culture models, we believe this approach may be useful for the *in situ*

modification of assembling peptides (*e.g.*, adding functionalities to supramolecular structures to allow electrical conduction, enhance imaging, or promote specific biological interactions)[40,41] and even in membrane applications (*e.g.*, forming stable, charged PEG-based membranes for batteries).[42]

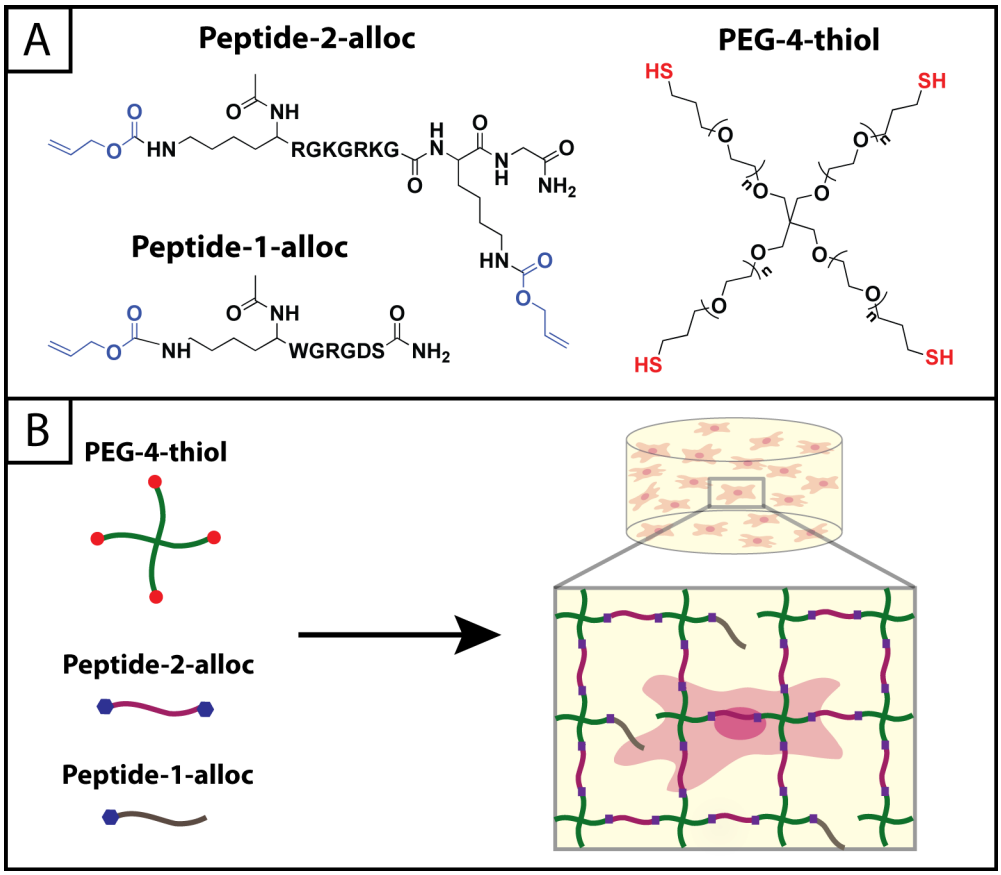

Figure 2.1: **Hydrogels formed by thiol–ene photoclick reactions for cell culture applications. A)** Monomers functionalized with thiols or with alloc groups were synthesized for hydrogel formation using thiol–ene click chemistry: multi-armed PEG was modified with thiols (right) and peptides containing alloc-protected lysines (1 or 2) (left). Upon the application of light, these functional groups react by a step growth mechanism, where an initiating species generates a thiyl radical that attacks the pendant 'ene' and forms a stable covalent bond between the monomers in solution.[19] **B)** This material system is promising for cell encapsulation and three-dimensional cell culture, where the thiol-modified PEG is crosslinked with alloc-containing peptides in the presence of cells allowing their encapsulation for *in vitro* studies. Capitalizing on the spatial control enabled by the thiol-ene photoclick reaction, pendant peptides (containing one alloc) can be added within the network during or after gel formation to promote cell-matrix interactions.

2.3 Materials and Methods

2.3.1 Synthesis of PEG-Thiol Macromer

Poly(ethylene glycol)-tetrathiol (PEG4SH) is commercially available (JenKem Technology USA, Creative PEGWorks) or can be synthesized as was done here using a modified version of published protocols.[43] Briefly, four-arm PEG (M_n ~ 20,000 g/mol, 10 g) (JenKem USA) was dissolved in anhydrous tetrahydrofuran (THF, 70 mL) (Fisher Scientific) and purged with argon, and argon-purged sodium hydroxide (NaH, 4× molar excess with respect to –OH groups) (Sigma Aldrich) suspended in THF was transferred *via* cannula under argon to the dissolved PEG. Allyl bromide (3× molar excess with respect to –OH groups) (Acros Organics) dissolved in 30 mL of THF subsequently was added. The PEG-allyl solution was refluxed overnight at 40 °C under argon and precipitated in ice cold ethyl ether to generate allyl ether-modified PEG (PEG4AE). The PEG4AE was dissolved in dichloromethane (40 mL) (Fisher Scientific) with a photoinitiator (2,2-dimethoxy-1,2-diphenylethan-1-one, I651, 0.5% w/w) (Acros Organics) and trace trifluoroacetic acid (TFA, ~100 μL) (Acros Organics) and purged with argon. Thioacetic acid (2× molar excess with respect to allyl) (Acros Organics) was added, and the solution was purged with argon and subsequently exposed to UV light (365 nm at 10–15 mW/cm^2 for 45 minutes) to yield PEG-thioacetate (PEG4TA) after precipitation in ice cold diethyl ether. Last, PEG4TA was dissolved in 60–70 mL of water and purged with argon. An equal volume of 1 M sodium hydroxide (Fisher Scientific) purged with argon was added to the PEG4TA (0.5 M final concentration) to generate the thiol end groups on the final PEG4SH product. The reaction immediately was neutralized with hydrochloric acid (final pH 1–2) (Fisher Scientific) and PEG4SH extracted with chloroform and trace TFA (to

prevent disulfide formation) and precipitated in ice cold diethyl ether. To wash and collect all intermediates and the final product after precipitation, samples were centrifuged at 0 °C for 20 minutes at 4400 rpm for a total of 3 washes and desiccated under vacuum at room temperature overnight. All intermediates and the final product were characterized with proton nuclear magnetic resonance (^{1}H NMR) in DMSO: PEG4AE 5.1–5.2 (m, 1H) 5.2–5.3 (m, 1H) 5.8–5.9 (m, 1H); PEG4TA 2.3 (s, 3H); PEG4SH 2.3 (m, 1H) for a single arm of the tetrafunctional monomer (Supplementary Information, Figure 2.7).

2.3.2 Synthesis of Alloc-Functionalized Peptides

The pendant cell adhesion sequence **K(alloc)**GWGRGDS (RGDS), a ubiquitous sequence found in many ECM proteins including fibronectin and vitronectin,[44] was synthesized to promote cell adhesion (amino acid(s) with reactive functional groups in bold). Non-degradable, water-soluble crosslinking sequences were synthesized: **K(alloc)**RGKGRKG**K(alloc)**G[37] (RGKGRK2alloc) (primary sequence used in hydrogel development) and **K(alloc)**GKGWGKG**K(alloc)**G (GKGWGKG2alloc) and **C**GKGWGKG**C**G (GKGWGKG2SH) (sequences with reduced charge and including tryptophan for easily assessing their concentration). Additionally, an enzymatically degradable, water-soluble crosslinking sequence K**K(alloc)**GGPQG↓IWGQG**K(alloc)**K (GPQGIWGQ2alloc) (broadly degradable by matrix metalloproteinases (MMP)-1, 2, 3, 8 and 9)[18] was synthesized to promote cell viability and allow spreading in longer cell culture and photopatterning experiments. Each was synthesized by standard solid phase peptide synthesis (SPPS) techniques using Fmoc chemistry on MBHA rink amide resin (0.59 mmol/g; 0.25 mmol scale) (Novabiochem) with a peptide synthesizer (Protein Technologies PS3). Fmoc-

protected amino acids, including the commercially-available alloc-protected lysine, and *o*-(benzotriazol-1-yl)-*N*,*N*,*N*′,*N*′-tetramethyluronium hexafluorophosphate (HBTU) (4× excess) (Chem-Impex International) were loaded into cartridges and coupled on resin. Fmoc deprotection was carried out using 20% piperidine (Sigma Aldrich) in *N*,*N*-dimethylformamide (DMF) (Fisher Scientific) prior to each amino acid coupling in 0.4 M methylmorpholine in DMF. Peptide products were cleaved in 95% v/v trifluoroacetic acid (TFA), 2.5% v/v triisopropylsilane (TIPS) (Acros Organics), and 2.5% v/v water with 5% w/v dithiothreitol (DTT) (Research Products International Corporation) to prevent disulfide formation and 2.5% w/v phenol (Sigma Aldrich) to protect tryptophan (W). After cleavage from the resin, peptides were precipitated in ice cold diethyl ether, centrifuged at 3000 rpm and 4 °C for 5 minutes for a total of three washes and desiccated under vacuum overnight at room temperature. Dry raw peptide product was purified by high-performance liquid chromatography (HPLC) and analyzed by matrix-assisted laser desorption/ionization (MALDI, crystallized with α-cyano-4-hydroxycinnamic acid, Acros Organics) or electrospray ionization (ESI) mass spectrometry to confirm synthesis of each desired peptide (Supplementary Information, Figure 2.8).

A fluorescently-labeled pendant peptide, Alexa Fluor® 488-AhxWGRGDS**K(alloc)**G (AF488RGDS), also was designed for photopatterning experiments using published protocols.[37] After Fmoc deprotection of Ahx on the N′-terminus of the peptide, 1 mg Alexa Fluor® 488 Carboxylic Acid, 2,3,5,6-Tetrafluorophenyl Ester, 5-isomer (Invitrogen) was stirred with 0.25 mmol peptide on resin in 4 mL DMF and 50 μL *N*,*N*′-diisopropylethylamine (DIPEA) (Chem-Impex International) overnight. The peptide was cleaved from resin, precipitated, and

analyzed by HPLC and ESI mass spectrometry (Supplementary Information, Figure 2.8).

2.3.3 Synthesis of LAP Initiator

The LAP initiator was synthesized using previously-described methods.[38] Briefly, 2,4,8-trimethylbenzoyl chloride (1.6 g, 0.009 mol) (Sigma Aldrich) was added to dimethyl phenylphosphonite (1.5 g, 0.009 mol) (Acros Organics) and reacted overnight at room temperature under argon. Lithium bromide (4× molar excess) (Sigma Aldrich) in 2-butanone (Sigma Aldrich) was added to the reaction solution and heated to 50 °C for 10 minutes. The white precipitate was filtered and rinsed 3 times with 2-butanone, and the final powder product dried and analyzed by ^{1}H NMR, matching literature (Supplementary Information, Figure 2.9).[38]

2.3.4 Hydrogel Formation

All monomers and initiators were prepared in Dulbecco's phosphate buffered saline (PBS) (Life Technologies) immediately before polymerization. For the various experiments described below, solutions of PEG4SH, RGKGRK2alloc (unless noted otherwise), and RGDS (7.5, 10, 12.5 wt% with respect to PEG, 2 mM RGDS) were prepared at stoichiometric ratios of thiol functional groups to alloc functional groups (1:1 SH:alloc) and containing a photoinitiator, either LAP (1.1 and 2.2 mM) or Irgacure 2959 (I2959) (2.2 mM). Hydrogels were formed upon irradiation of the monomer-initiator solution with cytocompatible doses of long wavelength UV light (365 nm at 10 mW/cm^2, International Light IL1400A Radiometer/Photometer) in the specific geometries described below.

2.3.5 Rheometry

Hydrogels were formed *in situ* on a photorheometer (TA AR-G2 with UV light attachment, Exfo Omnicure Series 2000 light source, 365 nm filter, SilverLine UV Radiometer M007-153) to estimate the polymerization times for different initiator types and monomer concentrations. I2959 (2.2 mM) or LAP (1.1 or 2.2 mM) photoinitiators were added to 10 wt% PEG monomer solutions containing stoichiometrically balanced amounts (1:1 SH:alloc) of RGKGRK2alloc to compare the effects of initiator type on polymerization time (n = 3). PEG monomer solutions (7.5, 10, and 12.5 wt%) containing stoichiometrically balanced amounts of RGKGRK2alloc and RGDS (2 mM) were mixed with 2.2 mM LAP to compare the effects of monomer concentration on polymerization time (n = 6). Finally, PEG4SH or PEG4AE monomer solutions (10 wt%) containing stoichiometrically balanced amounts of alloc (RGKGRK2alloc, GKGWGKG2alloc, GPQGIWGQ2alloc) or thiol-modified crosslinkers (PEG2SH, GKGWGKG2SH) were mixed with 2.2 mM LAP to compare the effects of crosslinker and functional group chemistry on polymerization time (n = 3). These solutions were placed between parallel plates (8 mm diameter, 200 μm gap) and UV light (365 nm at 10 mW/cm^2) applied 1 minute after starting rheometric measurements. Storage (G') and loss moduli (G'') were recorded over time at 2% applied strain and 6 rad/s frequency. From the data, an approximate time for complete gelation was defined to be when the percent change in modulus between consecutive data points was less than 0.1%.

For swollen modulus experiments, 7.5, 10, and 12.5 wt% hydrogels were polymerized within a 1 mm thick mold (2 microscope slides treated with Rain-X separated by a 1 mm rubber gasket). After polymerization, discs (8 mm diameter) were punched from the gel slab and swollen overnight in PBS. Strain sweeps (1 rad/s

frequency, 1–100% strain) and frequency sweeps (1–100 rad/s frequency, 5% strain) were conducted on swollen gels to determine the linear viscoelastic regime for the material. The swollen gels were then placed between parallel plates on the rheometer and G' and G'' were measured at 5% strain and 5 rad/s frequency (within the linear viscoelastic regime) (n = 6).

2.3.6 Hydrogel Swelling

Experiments to determine volumetric swelling ratios (Q) were performed on 7.5, 10, and 12.5 wt% hydrogels. Discs (8 mm diameter) were punched from gels polymerized between glass slides separated by a 1 mm thick gasket, ensuring sufficient mass for measuring dry weight, and swollen overnight in PBS. After recording swollen mass (M_s), the gels were lyophilized and the dry masses were measured (M_d) (n = 6). Volumetric swelling ratio was calculated by the relationships:

$$q = \frac{M_s}{M_d}, Q = 1 + \frac{\rho_{polymer}}{\rho_{solvent}}(q - 1) \qquad \text{Eq. 2.1}$$

where q is the mass swelling ratio, $\rho_{polymer}$ = 1.07 g/mL for PEG,[45] and $\rho_{solvent}$ = 1.00 g/mL for PBS.

Experiments to determine gel stability after polymerization were performed on gels incubated in PBS and cell culture medium at 37 °C over a 3 week time course. Gels (10 wt%) were polymerized for 5 minutes in 5 mm diameter molds (1 mL syringes with tips cut off) under sterile conditions and placed in sterile PBS and cell culture medium. M_s and M_d were recorded for the gels after 1, 7, 14, and 21 days (n = 6). Values for the volumetric swelling ratio (Q) were calculated as described above.

2.3.7 Detection of Unreacted Thiols

To initially quantify the photoaddition of biochemical cues, hydrogels (10 wt% with respect to PEG) were polymerized (1 or 5 minutes) between glass slides separated by a 0.254 mm thick gasket (McMaster-Carr) and off-stoichiometry such that approximately 2 mM free thiol remained in the unswollen gel after polymerization. Discs (5 mm diameter) were punched from these gels for further treatment and analysis. Half of the gel discs were swollen in PBS containing LAP initiator (2.2 mM) and excess pendant peptide (20 mg/mL RGDS) and incubated at room temperature for 1 hour. After 1 hour, these gels were exposed to UV light for 1 or 5 minutes to initiate the photoaddition of the RGDS. The other half of the gels remained in PBS as a control. Free thiol concentrations in the gels were quantitatively detected by Ellman's assay as described below.

Briefly, the swollen volume of the gels was predicted using the measured Q value (estimated at 19.3 μL for the 0.254 mm thick, 5 mm diameter discs). Ellman's reaction buffer (20.7 μL) containing 0.1 M sodium phosphate (Sigma Aldrich) and 1 mM ethylenediaminetetraacetic acid (Sigma Aldrich) at pH 7.5–8 was added to the gels for a total volume of 40 μL. Ellman's reagent (7.2 μL, 4 mg in 1 mL reaction buffer) (Fisher Scientific) was diluted in 360 μL of reaction buffer and added to each well containing a gel. Gels were incubated in the reagent for 1 hour and 30 minutes, the estimated time for the diffusion of the yellow NTB^{2-} dianion out of the gel so that the supernatant and gel colors match (by visual inspection). Finally, a calibration curve of L-cysteine hydrochloride monohydrate (Sigma Aldrich) (0–2 mM) was made to calculate the concentration of thiols detected in each gel. Absorbance of each condition was measured at 405 nM (Biotek Synergy H4 automated plate reader).

To determine the free thiol concentration in conditions for photopatterning in the presence of encapsulated cells, 10 wt% gels were polymerized in syringe tips (20 μL) such that approximately 2 mM free thiol remained in the unswollen gel after polymerization. Gels polymerized for 1 and 5 minutes were placed immediately in PBS as a control (n = 3). Additional gels polymerized for 1 minute immediately were placed in solutions of PBS containing 3 mg/mL RGDS and 2.2 mM LAP and incubated at 37 °C for 30 minutes (n = 3) or 1 hour 30 minutes (n = 3). After incubation, these gels were exposed to a second dose of UV light for 1 minute to attach the biochemical cue (RGDS) to remaining free thiols. Free thiol concentrations in the gels were quantitatively detected by Ellman's assay as described above, accounting for larger gel size (swollen volume = 84.8 μL; add 15.2 μL of PBS to gel in well plate for 100 μL total volume; add 18 μL Ellman's reagent in 900 μL Ellman's buffer to each well).

2.3.8 Spatially-Specific Photopatterning of Biochemical Cues

Hydrogels (10 wt%) were polymerized between glass slides spaced by a 0.254 mm gasket and off-stoichiometry to have a final free thiol concentration of 2 mM within the as prepared gel (prior to equilibrium swelling). The hydrogel was left on one of the glass slides for subsequent treatments and rinsed with PBS for 1 hour. Rinsed gels were placed in solution containing pendant peptides (AF488RGDS or RGDS) mixed with 2.2 mM LAP initiator for 1 hour and 30 minutes to allow diffusion of the peptides and initiator into the gel network prior to subsequent patterning. Photomasks with lines of increasing thickness (0.2–1 mm width) or square patterns (0.4 mm edge) purchased from Advanced Reproductions Corporation were placed ink-side down on top of the samples and exposed to collimated UV light (Inpro

Technologies collimating adaptor, Exfo Omnicure Series 2000 light source) for 1 minute (365 nm at 10 mW/cm^2). Gels were rinsed 3× for 40 minutes each with PBS to remove excess pendant peptide after photoaddition. Samples containing the patterned AF488RGDS were imaged with a confocal microscope (Zeiss 510 NLO). Ellman's reagent was applied to the gels containing RGDS and imaged immediately on a stereomicroscope (Zeiss Stemi 2000-C).

2.3.8.1 Culture and Encapsulation of Human Mesenchymal Stem Cells

Human mesenchymal stem cells (hMSCs) isolated from human bone marrow (Lonza)[46] were cultured on tissue-culture treated polystyrene in cell culture medium[46] and harvested at ~70–80% confluency (Passage 2, 3) for experiments. For evaluating the effects of light, cells were trypsinized from culture plates, counted (hemocytometer), centrifuged (5 minutes, 1000 rpm), and plated at a density of 20,000 cells/cm^2 in 96-well plates. For cell encapsulation and photopatterning experiments, cells were trypsinized from culture plates, counted (hemocytometer), centrifuged (5 minutes, 1000 rpm), and resuspended at desired densities in monomer solution (10 wt%) with and without RGDS. The mixtures of cells in monomer solution were polymerized in syringe molds at cytocompatible wavelengths and doses of UV light (365 nm at 10 mW/cm^2), encapsulating cells within the hydrogel matrix.

2.3.9 Metabolic Activity of hMSCs in Photopatterned and Non-Patterned Hydrogels

Cells were suspended in monomer solution (10 wt%, 3000 cells/μL) containing 2 mM RGDS and polymerized in syringe tip molds (20 μL) for 1 and 5 minutes (n = 6, non-patterned). Immediately after polymerization, gels were placed in cell culture medium to rinse out unreacted monomer and photoinitiator (30 minutes). After

rinsing, the medium was replaced with fresh medium and gels were incubated at 37 °C for subsequent analysis. For photopatterned gels, cells were suspended in monomer solution (10 wt%, 3000 cells/μL) without RGDS and polymerized for 1 minute such that 2 mM free thiols remained in the unswollen gel for subsequent modification. After polymerization, the gels were incubated in PBS containing 3 mg/mL RGDS and 2.2 mM LAP for 30 minutes or 1 hour 30 minutes at 37 °C before exposure to a second dose of UV light (1 minute) to covalently link RGDS within the network (n = 6). Patterned gels were immediately placed in cell culture medium (30 minutes) to rinse out excess monomer and photoinitiator. At 1 and 3 days post-encapsulation (D1 and D3), metabolic activity was assessed by CellTiter 96 (Promega) (n = 3 each condition, each time point).

To assess the effect of light alone on cell function, plated cells (20,000 cells/cm^2) were exposed to UV light (1 min of 365 nm at 10 mW/cm^2). Metabolic activity was assessed by CellTiter 96 at D1 and D3 compared to control (no light) (n = 3 each condition, each time point).

2.3.10 Viability of hMSCs in Photopatterned and Non-Patterned Hydrogels

To initially study the viability of cells encapsulated in hydrogels, 3000 cells/μL were encapsulated in non-degradable gels (10 wt%, 2 mM RGDS before swelling) polymerized for 1 and 5 minutes. Additional studies were performed to determine the effect of cell density on viability post-encapsulation, with cells encapsulated in non-degradable gels (10 wt%, 2 mM RGDS before swelling) at 3000 and 30,000 cells/μL. Viability was quantified at 3 days post-encapsulation with a LIVE/DEAD® Viability/Cytotoxicity Kit for mammalian cells (Invitrogen), and gels were imaged with a confocal microscope (Zeiss 510 NLO).

To study the viability of cells in photopatterned hydrogels over longer times in culture, cells were encapsulated in gels (10 wt%, 20 μL, 3000 cells/μL) crosslinked with the degradable (GPQGIWGQ2alloc) peptide sequence such that 2 mM free thiol remained in unswollen gels post-polymerization (1 minute). Gels were placed in PBS containing 3 mg/mL RGDS and 2.2 mM LAP for 1 hour and exposed to a second dose of UV light (1 minute) to allow attachment of RGDS to the network. Viability was assessed 6 days after encapsulation with the LIVE/DEAD® Viability/Cytotoxicity Kit for mammalian cells, providing time for hMSCs to partially degrade and attach to the hydrogel matrix.

2.4 Results and Discussion

Click chemistries for hydrogel formation are of interest in many biomaterials applications. Their efficient reactions under mild conditions enable hydrogel formation and modification in the presence of proteins and cells,[3,28] which is especially useful for designing materials that mimic native tissue environments *in vitro* for cell culture. Light-mediated thiol–ene click reactions in particular are of great utility for control over the presentation of biomechanical and biochemical cues in space and time within these systems. Here, we describe a new approach to utilizing thiol–ene chemistry for hydrogel formation and spatially-specific patterning in cell culture applications with alloc-functionalized peptides and thiol-terminated PEG. This strategy enables rapid and consistent polymerization of hydrogels controlled by the application of light, the formation of a stable bioinert base matrix, and the spatial presentation of biochemical cues within the hydrogel network.

2.4.1 Initiator Selection Allows Rapid Polymerization Under Cytocompatible Conditions

Thiol–ene reactions for biomaterial applications can occur spontaneously in aqueous solutions in the presence of a base catalyst or upon the introduction of free radicals, depending on vinyl group selection.[14,47] For example, base-catalyzed polymerization of hydrogels in the presence of cells by Michael-type addition reactions between thiols and vinyl sulfones or maleimides has been used to understand cell behavior, invasion, and differentiation in synthetic mimics of the ECM.[7,22] Additionally, for control over when and where the reaction takes place, polymerizations of hydrogels by a photoinitiated, free radical step growth reaction between thiols and vinyls (*e.g.*, norbornene) have been used with cytocompatible doses of UV or visible light depending on initiator selection (*e.g.*, Irgacure 2959,[39] lithium acylphosphinate,[38] or Eosin Y[30]). While the spatiotemporal control afforded by photopolymerization is quite useful, minimizing exposure to light, particularly wavelengths in the UV, is crucial for polymerizations done in the presence of cells.[39,48] Light-mediated reaction conditions that are cytocompatible and rapid for the polymerization of monomers in aqueous solutions often are limited and are needed to reduce the exposure time of cells and proteins to light and reactive components (particularly free radicals). Toward addressing this, we aimed to establish conditions for the photopolymerization of monomers functionalized with thiols and allocs to expand the suite of reactions for cell encapsulation.

Previously, the general reaction of allyl- and thiol-functionalized monomers for hydrogel formation was considered too slow for gel formation in the presence of cells, which may be due to a rate-limiting chain transfer step,[49] and has been described with limited use in cell culture applications for the modification of synthetic hydrogel

matrices with pendant alloc-modified peptide tethers.[15,37] Here, we examined water-soluble initiator and monomer compositions to identify cytocompatible conditions for alloc-based hydrogel formation. Hydrogels were polymerized *in situ* on a rheometer to monitor polymerization times of gels formed with different water-soluble photoinitiators (LAP and I2959) and initial monomer concentrations (7.5, 10, 12.5 wt% with respect to PEG). Two initiator concentrations were selected (1.1 and 2.2 mM) to match concentrations that have been used to polymerize other types of hydrogels in the presence of cells,[39] as cell viability previously has been observed to be sensitive to the concentration of LAP owing to robust free radical generation with irradiation at 365 nm.[38]

The rheological data collected by *in situ* polymerization of hydrogels demonstrates the efficiency of the LAP initiator for the radical reaction of thiol with vinyl functional groups. The slope of the moduli over time for the 1.1 and 2.2 mM LAP conditions becomes approximately 0 after complete gelation, whereas the I2959 continues to slowly increase (slope = 1.5 to 5 Pa/s) (Figure 2.2 A) indicating a less rapid reaction. While presentation of hydrogel moduli (y-axis) on a log scale is typical, we have chosen to present moduli on an absolute (normalized) scale to demonstrate the efficiency of the LAP initiator in achieving complete gelation when compared directly to I2959. Further, the polymerization times of the gels formed using 1.1 and 2.2 mM LAP were determined to be approximately 5 and 15 times faster than those using I2959 as the initiator (2.60 ± 0.03 and 0.96 ± 0.05 min, respectively, vs. 13.59 ± 1.15 min) (Figure 2.2 B). This order of magnitude difference in polymerization time is comparable to differences observed between LAP and I2959 in the polymerization of other functional groups, such as the chain growth polymerization of PEG-diacrylate

with LAP (10 times faster than with I2959),[38] and arises from the increased absorbance of and radical generation by LAP relative to I2959 at long wavelengths of UV light (365 nm). Moving forward, we focused on the 2.2 mM LAP polymerization condition, which provided the most rapid gel formation. However, the 1.1 mM LAP condition may be attractive for investigations in the future for specific cell culture applications as higher initiator concentrations can result in lower cell viability.[39]

In addition to comparing the effect of different initiating conditions on polymerization rates, the concentration of monomers initially present also must be considered. The availability of terminal functional groups for reaction influences the time to complete gelation, especially at low concentrations where the distance between functional groups is greater and, after reaction of one end group, can decrease the probability of reaction with a functional group on a different monomer.[50] We observe that the lowest initial monomer concentration (7.5 wt%) corresponds to the longest polymerization time (3.00 ± 0.22 min) while the higher concentrations (10, 12.5 wt%) polymerize in shorter time periods (0.79 ± 0.03, 0.88 ± 0.11 min) (Figure 2.2 B). The polymerization time for the 7.5 wt% gels is statistically different from the 10 and 12.5 wt% gels ($p < 0.05$); however, the 10 and 12.5 wt% gels are not ($p > 0.05$). The more rapid polymerization times of the higher concentration conditions may be attributed to the increased concentration of functional groups.

Finally, we investigated the polymerization of several different alloc-modified peptides (RGKGRK2alloc, GKGWGKG2alloc, GPQGIWGQ2alloc) with PEG4SH to understand if there may be any effects of peptide sequence on polymerization time (Figure 2.2 C). We observed the most rapid polymerization with the highly charged RGKGRK2alloc crosslinking peptide followed by the less charged

GPQGIWGQ2alloc and GKGWGKG2alloc peptides (40 seconds slower), indicating that charge may play a role in the polymerization of the system and should be considered when designing and utilizing different peptide sequences. All peptides led to complete gelation within 2.5 minutes after UV light was applied and, consequently, are promising and appropriate for cell encapsulation, as discussed further below. We briefly compared to the polymerization of PEG4AE with different thiol-containing crosslinkers (PEG2SH, GKGWGKG2SH) to examine the effect of monomer chemistry on the polymerization rate (Supplementary Information, Figure 2.10). The polymerization of this 'inverse' system was consistently slower than the alloc system, which may be related to the reactivity of the allyl and thiol groups being affected by neighboring substituents (*i.e.*, oxycarbonyl [alloc] *vs.* ether [AE][51] or neighboring amino acids[52]). Further, in our hands, we observe variability in the final moduli and polymerization times for PEG4AE and peptide2SH gels, which we speculate is partially due to the propensity for disulfide formation between thiols on these charged peptides.[32] Presentation of thiols from PEG, as demonstrated with the peptide2alloc system, allows consistent formation of hydrogels under cytocompatible conditions.

A

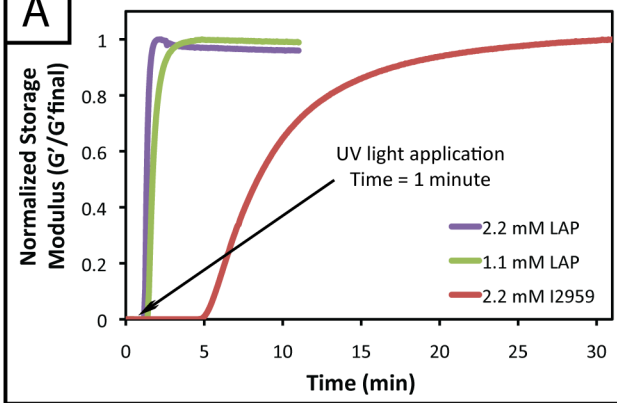

B

	Condition	Polymerization Time (min)
Initiators	2.2 mM LAP	0.96 ± 0.05
	1.1 mM LAP	2.60 ± 0.03
	2.2 mM I2959	13.59 ± 1.15
PEG Weight Percent	7.5	3.00 ± 0.22
	10	0.79 ± 0.03
	12.5	0.88 ± 0.11

C

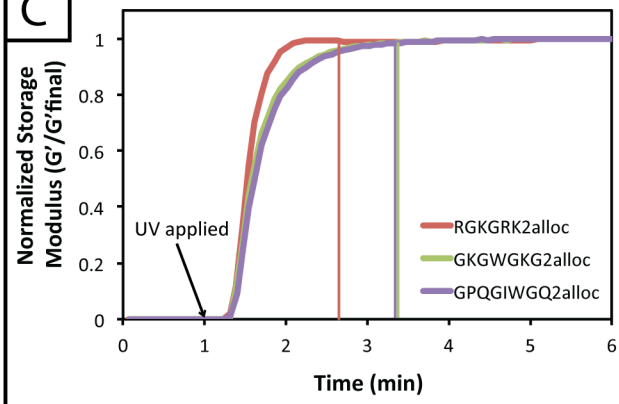

Figure 2.2: ***In situ* polymerization of PEG hydrogels with different photoinitiators. A)** Hydrogels (10 wt% with respect to PEG) were polymerized *in situ* on a rheometer to monitor gel formation over time using various initiator conditions. After 1 minute on the rheometer, UV light (10 mW/cm^2, 365 nm) was applied to samples. The storage moduli of gels polymerized using 1.1 and 2.2 mM LAP initiator begin to increase within 30 seconds after light application and finish forming in approximately 1-3 minutes (modulus levels off). Gels polymerized using 2.2 mM I2959 begin to form 4 minutes after UV light application and reach complete formation in approximately 13-14 minutes of exposure. The rapid polymerizations observed for the LAP initiator are relevant for cell culture applications. Representative data for each condition is shown here. **B)** Complete polymerization, defined here as the point where the change in modulus between consecutive data points is less than 0.1 %, was determined for various initiator and monomer concentrations. As shown in (A), the LAP initiator exhibits the most rapid polymerization, with times of 0.96 ± 0.05 and 2.60 ± 0.03 minutes for 2.2 and 1.1 mM LAP, respectively. Complete polymerization for I2959, at the highest concentration compared to LAP (2.2 mM), occurs in 13.59 ± 1.15 minutes. Using 2.2 mM LAP, hydrogels from various initial monomer concentrations (7.5, 10, and 12.5 wt% with respect to PEG) were polymerized. The 7.5 wt% condition exhibited the slowest polymerization rate of 3.00 ± 0.22 minutes due to fewer functional groups that are available to react. The 10 and 12.5 wt% gels polymerized in 0.79 ± 0.03 and 0.88 ± 0.11 minutes as the number of functional groups in solution is higher at the start of polymerization. **C)** Hydrogels were polymerized with different alloc-modified peptides to evaluate any effect of peptide chemistry on polymerization rate. The less charged GKGWGKG2alloc and GPQGIWGQ2alloc peptides take 40 seconds longer to polymerize than the charged RGKGRK2alloc peptide, although this is not as significant as the effects of weight percent and the type and concentration of initiator on polymerization time.

2.4.2 Hydrogel Mechanical Properties Tuned to Mimic Soft Tissue Environments

One common approach used to control or tune the initial mechanical properties of hydrogels is varying the monomer concentration.[53] Controlling the hydrogel mechanical properties, as measured by modulus, can be critical in cell culture and

regenerative medicine applications, where the elasticity, or "stiffness", of the microenvironment that surrounds a cell has been shown to affect cell function and fate.[54,55] These properties also must be consistent from gel-to-gel for a well-defined, controlled material system. Here, we aimed to establish hydrogel compositions with a range of equilibrium-swollen moduli that mimic different soft tissues. Toward this, we measured the swollen storage moduli (G') and volumetric swelling ratios (Q) of hydrogels formed from different initial monomer concentrations (7.5, 10, and 12.5 wt% with respect to PEG) (Figure 2.3).

We demonstrate for our material system that, by increasing the concentration of monomer in the gel-forming solution, we can increase the modulus (Figure 2.3 B; 7.5 wt%, G' = 553 ± 81 Pa; 10 wt%, G' = 1343 ± 49 Pa; 12.5 wt%, G' = 2147 ± 87 Pa), creating gels with a range of elasticity comparable to native soft tissues (around the range of neural tissues to muscle, $E \sim$ 1 to 10 kPa, where $E \approx 3G$).[55] Assuming that the theory of rubber elasticity holds for these swollen gels, the behavior can be attributed to an increase in crosslink density (ρ_x) by:[56]

$$G = \rho_x RTQ^{-1/3} \qquad \text{Eq. 2.2}$$

Similarly, we observed decreasing swelling ratios for increasing monomer concentrations (Figure 2.3 C; 7.5 wt%, Q = 41.4 ± 1.3; 10 wt%, Q = 33.3 ± 0.6; 12.5 wt%, Q = 29.2 ± 0.4). Increased crosslink density inhibits how much a gel is able to swell, thus the inverse relationship between ρ_x and Q is expected and observed. The results for the moduli and swelling ratios also were found to be statistically significant ($p < 0.05$), indicating that the material system may be easily tuned to have specific mechanical properties by varying the concentration of monomer present within a gel.

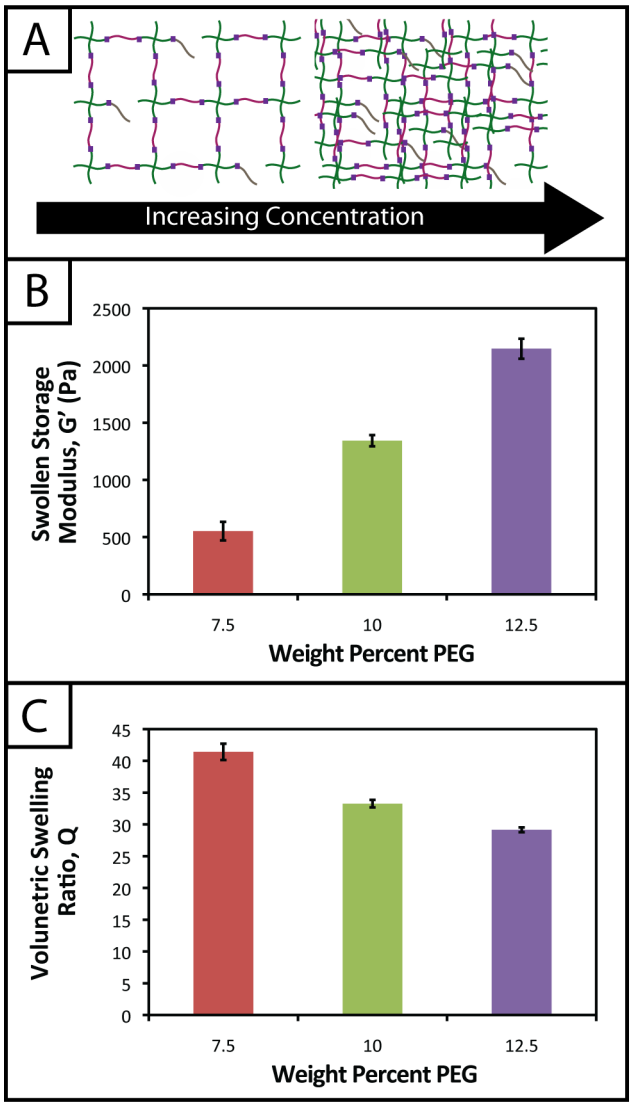
A
Increasing Concentration
B
Swollen Storage Modulus, G' (Pa)
2500
2000
1500
1000
500
0
7.5
10
12.5
Weight Percent PEG
C
Volunetric Swelling Ratio, Q
45
40
35
30
25
20
15
10
5
0
7.5
10
12.5
Weight Percent PEG

Figure 2.3: **Hydrogel mechanical properties tuned to mimic soft tissue environments. A)** To adjust the mechanical properties of hydrogels, monomer concentration in solution prior to polymerization may be increased or decreased to increase or decrease crosslink density and thus modulus, respectively. **B)** Hydrogels from different initial monomer concentrations (7.5, 10, and 12.5 wt% with respect to PEG) were polymerized and swollen in PBS to demonstrate tunable hydrogel mechanical properties. The lowest average swollen storage modulus was observed for the 7.5 wt% gels (553 ± 81 Pa), and increased with higher monomer concentrations (1343 ± 49 Pa and 2147 ± 87 Pa). **C)** Another important mechanical property to consider in the design of controlled hydrogel mimics of the ECM is the volumetric swelling ratio. In accordance with modulus measurements, for the gels polymerized with an initial monomer concentration of 12.5 wt% (with respect to PEG), the lowest volumetric swelling ratio is observed (29.2 ± 0.4), and the volumetric swelling ratio increases for lower concentrations (7.5 and 10 wt% with respect to PEG) (Q = 41.4 ±1.3 and 33.3 ±0.6).

2.4.3 Hydrogel Stability Demonstrated for Long-Term Culture

Hydrogel degradation over time often is desirable for cell culture applications to allow cellular processes, such as growth, proliferation, and migration, which can be constrained or hindered by a tightly crosslinked material.[57] However, nonspecific degradation in aqueous solutions (*e.g.*, hydrolytic cleavage of bonds within functional groups) can limit the degree of user control over materials properties afforded by the addition of enzymatically degradable peptide crosslinks[18] or photodegradable chemistries,[58] resulting in unintended or premature hydrogel degradation such that the gel does not remain intact for appropriate time periods during cell culture. For example, Shih and Lin have shown that step growth PEG-tetranorbornene-based thiol–ene hydrogels completely degrade in 2–3 weeks at physiological pH (pH ~ 7.4), where the norbornene is linked to PEG by an ester bond leading to hydrolytic degradation. Specifically, the degradation rate of these hydrogels was influenced by the peptide crosslinker sequence, where peptides containing hydrophobic or aromatic residues

exhibited slower degradation (*e.g.*, CGGGC sequence $k_{hyd} = 0.049 \pm 0.001$ day^{-1}, CGGLC sequence $k_{hyd} = 0.036 \pm 0.002$ day^{-1}).[29]

In the hydrogel system presented here, we aimed to create monomers free of ester bonds to allow the creation of hydrogels that are stable under cell culture conditions. To assess the stability of the resulting hydrogels, we monitored the volumetric swelling ratio (Q) of 10 wt% gels incubated in PBS and cell culture medium at 37 °C over a period of three weeks (Figure 2.4), a typical length for many two and three-dimensional cell culture experiments.[3] For both conditions, the Q values qualitatively are constant during the time course, and there is no substantial degradation during the incubation period. Quantitatively, the p-values for the gels incubated in PBS for different times are all greater than 0.05, indicating no statistical significance between the gels for each time points and thus that degradation does not occur. For the gels incubated in culture medium, when comparing days 1–14, the p-values are all greater than 0.05. However, the day 21 time point is statistically different from the day 1 and 7 time points ($p < 0.05$), indicating a slight change in swelling by 3 weeks. We hypothesize that nonspecific degradation of the peptide crosslinker could be occurring over time in growth medium, which is more complex than PBS and contains serum laden with enzymes, resulting in this small but statistically significant increase in swelling. Despite this small swelling change, the hydrogels remain robust and intact over multiple weeks in culture. The swelling ratios of hydrogels in PBS versus media also are statistically significant for the entire incubation period, which we speculate results from differences in the composition of PBS and growth media. With this base system, various degradable peptide crosslinks derived from ECM proteins (*e.g.*, GPQG↓IWGQ or IPVS↓LRSG derived from

collagen I) can be incorporated within the gels to allow cell-controlled matrix degradation, where the degradation rate of the matrix can be tuned by peptide selection for different applications.[18]

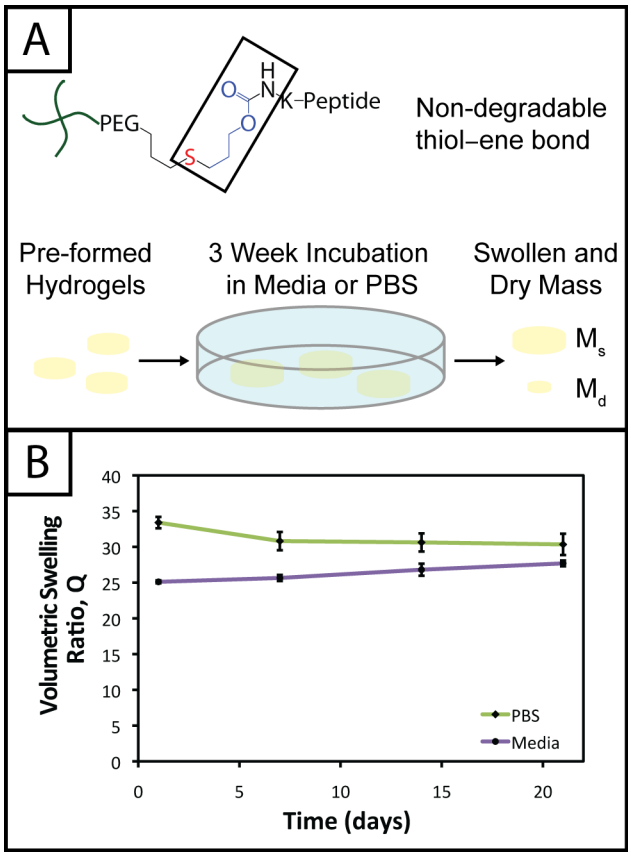

Figure 2.4: **Hydrogel stability toward long-term cell culture. A)** The thiol–ene system is linked by a carbamate bond between a thiol-functionalized PEG macromer and an alloc-functionalized peptide, which both lack hydrolytically cleavable bonds (e.g., esters). To evaluate gel stability for controlled cell culture over several weeks, 10 wt% hydrogels (with respect to PEG) were incubated in cell culture medium and PBS for 3 weeks and volumetric swelling ratios (Q) measured. **B)** The swelling of gels incubated in PBS did not significantly change ($p > 0.05$ for all samples) indicating stability over the time period ($Q = 33.4 \pm 0.8$, 30.8 ± 1.3, 30.6 ± 1.3, 30.3 ± 1.5). The swelling of gels incubated in growth media slightly increased through the incubation period such that the first two and last Q values are different ($p < 0.05$), although consecutive points are not ($p > 0.05$), which may be attributed partly to non-specific degradation of the hydrogel by enzymes present in the more complex growth medium ($Q = 25.1 \pm 0.2$, $25.6 \pm .4$, 26.8 ± 0.8, 27.6 ± 0.4).

2.4.4 Biochemical Cues Spatially Patterned within Hydrogels

One benefit that photoclick chemistry provides in the design of hydrogels is the ability to control the presentation of biochemical cues in space or time.[59] Native tissues are dynamic environments with gradients and defined regions of biological cues occurring at different times, and the ability to capture this complexity in synthetic systems is important for understanding and directing cellular processes.[25] Here, we studied the photoaddition of a model biochemical cue to our material (i) to establish if excess free thiols could be modified after hydrogel formation and (ii) to demonstrate control over the spatial presentation of these cues. Specifically, an alloc-modified integrin binding peptide (RGDS or AF488RGDS) was coupled homogenously or in specific regions to hydrogels containing free thiols using photopatterning.

While one of our goals was to develop a hydrogel from accessible materials, we also aimed to use simple techniques to characterize this system. Ellman's assay, which can identify free thiols in solution, is one such technique that has been used to quantify free thiols in materials post-polymerization.[60,61] We have utilized this assay in a non-destructive method to quantify free thiols in our hydrogels such that, if desired, gels may be rinsed of reagent, treated with tris(2-carboxyethyl)phosphine (TCEP), rinsed of TCEP, and re-used in additional studies. In addition to quantifying free thiols, we wanted to demonstrate that Ellman's reagent also could be used to observe biochemical patterns created in gels with a reasonable degree of resolution as an inexpensive and rapid alternative or complementary approach to using a fluorescently-tagged cue (Figure 2.5 A).

Toward achieving this, 10 wt% gels (0.254 mm thick between glass slides) initially were polymerized off stoichiometry so that free thiols (2 mM at preparation prior to equilibrium swelling) remained for later modification with the pendant RGDS

peptide. Adjusting for swelling, the free thiol concentration at equilibrium was estimated to be roughly ~0.61 ± 0.05 mM, so the free thiol concentration in hydrogels as measured by Ellman's assay will be lower than 2 mM. The free thiol concentrations of off-stoichiometry gels polymerized for 1 and 5 minutes subsequently was determined by Ellman's assay to be 1.13 ± 0.09 mM and 0.97 ± 0.10 mM, respectively (Figure 2.5 B, −RGDS condition). The gels polymerized for 1 and 5 minutes do not have statistically different thiol concentrations ($p > 0.05$), supporting the results in Figure 2.2 B that the 10 wt% gels are completely formed in under one minute.

To initially determine if a model biochemical cue could be added to these gels, pre-formed gels incubated in RGDS monomer (20 mg/mL ~20× excess to SH) with LAP (2.2 mM) were exposed to UV light for 1 and 5 minutes. The thiol concentration after modification was determined for each condition by Ellman's (1 min = 0.01 ± 0.01 mM, 5 min = 0.003 ± 0.003 mM) (Figure 2.5 B, +RGDS condition). These concentrations correspond to 93.1 and 94.8% modification of the remaining free thiols and 98.5 and 99.0% total thiol modification, indicating high coupling efficiency of the pendant peptide. There are slightly fewer free thiols in the gels polymerized for 5 minutes indicating that a longer polymerization time results in higher conversion of functional groups; however, there is no statistical significance between the two conditions indicating that the effects of longer polymerization are ultimately negligible. Hydrogels polymerized off-stoichiometry (2 mM free thiol at preparation) were then incubated in growth medium at 37 °C for 3 days to determine if cues could be added at different times during culture. Only trace free thiols were observed with Ellman's assay after this 3-day incubation (0.008 ± 0.002 mM), indicating the formation of disulfides either with components in the culture medium or between free

thiol end groups on PEG. To test this hypothesis, TCEP (10 mM in PBS) was added to the gels for 1 hour to break potential disulfide bonds. Gels subsequently were rinsed, and the presence of free thiols was detected with Ellman's (1.54 ± 0.09 mM) (Supplementary Information, Figure 2.11). This recovery of thiols confirms that a large portion of free thiols post-polymerization were lost to disulfide formation upon incubation in culture medium. While the application TCEP could be investigated as an approach to allow temporal photopatterning, reducing agents such as it will negatively affect cell viability[62] and may not be a practical option for *in situ* photopatterning. However, different orthogonal chemistries[2] could be utilized within this base hydrogel system to allow the temporal addition of cues throughout long-term cell culture in future investigations.

With the ability to add cues to the matrix after initial formation, spatially-defined regions of various cues of interest can be created toward directing the organization and function of cells in three dimensions.[10,22,63] Fluorescently-labeled cues are typically used to observe biochemical patterns in hydrogel-based matrices with a high degree of resolution; however, this approach requires additional expense and time for peptide labeling and fluorescence imaging. For a rapid and inexpensive assessment of patterning, we examined using Ellman's reagent to observe spatially-defined patterns as a simple alternative or complementary approach for preliminary evaluations. Hydrogels photopatterned with the AF488RGDS peptide demonstrate spatial resolution of cue addition (Figure 2.5 C) in the *x*, *y*, and *z*-directions for patterns of arbitrary shapes (wide and narrow lines, squares). Next, to test Ellman's as an alternative to fluorescently-labeled evaluation, non-labeled RGDS was patterned into gels, and the gels were imaged under a light microscope immediately after the

application of Ellman's reagent (Figure 2.5 D). At short time periods (<5 minutes), we observed resolution of the patterns; however, as the products from reaction with Ellman's reagent diffused throughout the gel, the pattern began to disappear (Supplementary Information, Figure 2.12). While Ellman's reagent is limited by the fast diffusion of the reaction products, resulting in the short-term observation of patterns in the *x*–*y* plane only, we envision using this test in initial or follow-up studies of photopatterning in thiol–ene hydrogels because it is easy to use and provides almost instant results. Initially, one could test the ability to pattern a hydrogel before building or purchasing a more expensive fluorescently-tagged peptide. In later experiments, one could quickly confirm that a different peptide or peptide sequence is patterned into the same system without having to build another labeled peptide and use an epi-fluorescent or confocal microscope.

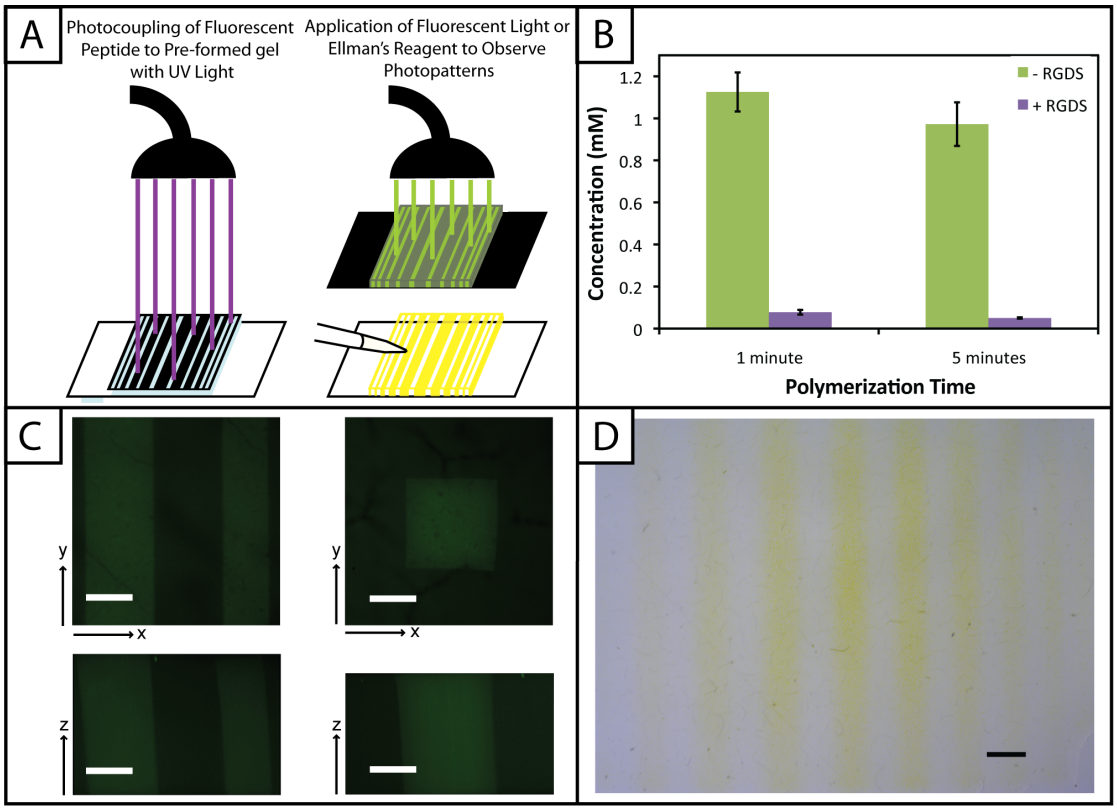
A
Photocoupling of Fluorescent Peptide to Pre-formed gel with UV Light
Application of Fluorescent Light or Ellman's Reagent to Observe Photopatterns
B
- RGDS
+ RGDS
Concentration (mM)
1.2
1
0.8
0.6
0.4
0.2
0
1 minute
5 minutes
Polymerization Time
C
y
x
z
D

Figure 2.5: **Biochemical cues spatially patterned within hydrogels. A)** To create patterns of biochemical cues, hydrogels are polymerized off-stoichiometry ([SH] > [alloc]) and incubated with excess pendant RGDS or AF488RGDS peptide. Gels were irradiated through photomasks printed with black lines or squares for 1 and 5 minutes (left). Samples are subsequently analyzed with fluorescent light or Ellman's reagent to determine the modification of free thiols with pendant biochemical cues (right). **B)** Gels (10 wt% with respect to PEG) were polymerized with 2.2 mM LAP for 1 and 5 minutes off stoichiometry (2 mM free thiol at preparation). After equilibrium swelling, the initial free thiol concentration in these gels were 1.13 ± 0.09 and 0.97 ± 0.10 mM, respectively, as determined by Ellman's assay. Only 0.01 ± 0.01 and 0.003 ± 0.003 mM free thiol remained after adding the RGDS tether indicating the efficient coupling of the model biochemical cue to the hydrogel network. **C)** Following the setup shown in (A), arbitrary patterns (squares, 1600 μm^2; lines of different thickness, 200 - 1000 μm) of a fluorescent peptide (AF488RGDS) were created within pre-formed hydrogels and imaged on a confocal microscope for analysis. Resolution of the pattern is observed in the x-, y-, and z-planes indicating selective coupling to only regions of the gel that were exposed to light. (Scale bar, 200 μm) **D)** As a quick and inexpensive alternative to fluorescence, a non-fluorescent pendant peptide (RGDS) was photopatterned (lines of different thickness) into pre-formed hydrogels. Ellman's reagent was directly applied to the top of these gels to identify regions lacking the pendant peptide (yellow) with resolution in the x- and y-planes over short times (< 5 min). (Scale bar, 1 mm)

2.4.5 Encapsulated Stem Cells Remain Viable and Metabolically Active within Patterned and Non-Patterned Hydrogels

Hydrogel systems for cell culture or delivery must not only be cytocompatible, but cells also must be able to withstand their polymerization conditions for encapsulation within the matrix. PEG, the primary component of the materials presented here, has been used in a variety of hydrogel systems owing to its bioinert nature, providing a blank slate for the presentation of peptide sequences or whole proteins to elicit specific cellular responses.[25] Furthermore, cells must be able to

withstand multiple doses of UV light and radical initiator for the creation of biochemical patterns within gels to direct cell behavior in three dimensions.

To evaluate the cytocompatibility of the initial polymerization conditions, we encapsulated adult human mesenchymal stem cells, hMSCs, within non-degradable gels (10 wt%, 2.2 mM LAP, 2 mM RGDS, 3000 cells/μL) polymerized for different lengths of time. Specifically, based on our rheometric measurements, hydrogels were polymerized for the minimum amount of time required to completely polymerize 10 and 12.5 wt% samples (1 minute) and in excess of the minimum amount of time to polymerize 7.5 wt% samples (5 minutes). In addition, cell density was kept low to promote primarily cell–matrix interactions and fully understand the limits of cell viability in the system when encapsulating a dilute, single-cell suspension. Cell viability and metabolic activity subsequently were evaluated 1 and 3 days after polymerization to determine polymerization conditions appropriate for the initial encapsulation and culture of cells, respectively.

A membrane integrity assay (LIVE/DEAD® Viability/Cytotoxicity Kit) of cells encapsulated in gels (Figure 2.6 A) showed a higher percentage of living cells in gels polymerized for 1 minute (87 ± 2%) in comparison to 5 minutes (81 ± 4%) at day 3 in culture. While decreased cell viability is observed for the 5 minute polymerization condition, which could limit the use of gels with lower modulus in cell culture (*e.g.*, 7.5 wt%), viability can be rescued by adjustment of experimental parameters, including increased cell–cell contact (*i.e.*, controlling the density of encapsulated cells),[64] incorporating biomimetic peptides that promote additional cell–matrix interactions,[20,65] and lower initiator concentration (*i.e.*, reducing concentration of radicals during polymerization but at some cost to polymerization time).[38] We

increased the encapsulation density of cells in non-degradable gels polymerized for 5 minutes (3000 to 30,000 cells/μL) and demonstrated a corresponding increase in viability (83 ± 2% to 92 ± 1%) (Supplementary Information, Figure 2.13). Accordingly, cell encapsulation density can be adjusted as appropriate to support viability and function depending on the experimental variables to be studied and should be considered in experimental design when using this system.

The metabolic activity of cells, an indicator of cell viability and function, also was monitored 1 and 3 days after encapsulation using CellTiter 96. Constant metabolic activity over time was observed in the gels polymerized for 1 and 5 minutes over three days ($p > 0.05$) (Figure 2.6 B). Initially (D1) the metabolic activity of the gels polymerized for 5 minutes is statistically different ($p < 0.05$) from gels polymerized for only one minute. However, by day 3, the metabolic activity of the gels polymerized for 1 and 5 minutes is statistically similar ($p > 0.05$), indicating that the initial effects of the polymerization are most apparent for longer irradiation time periods but do not impact cell metabolic activity past the initial treatment. Here, the short-term effects of encapsulation on cell survival appear minimal and similar to that observed in other hydrogels formed by free radical initiation,[38,48] indicating that this new hydrogel system could support cell culture or delivery in various experimental applications.

Note that all conditions in the metabolic activity experiments presented above were normalized to cells encapsulated in hydrogels with 1 minute of light exposure. While normalization to encapsulated cells without UV exposure is desirable, the hydrogel system presented cannot be easily formed without light. To assess any effect of UV light alone on cell function, hMSCs were seeded in 96-well plates and

metabolic activity monitored 1 and 3 days after exposure to UV. Light exposure did not significantly affect hMSC metabolic activity at either D1 or D3 post-irradiation (p > 0.05, compared to no UV control) (Supplementary Information, Figure 2.14). This result is consistent with the reports of others for single doses of UV light at 10 mW/cm^2.[66]

Toward utilizing this system for patterning gels with biochemical cues during cell culture, we sought to establish relatively mild photopatterning conditions to enable the application of multiple doses of light and radicals within 24 hours of encapsulation. We first incubated gels with 2 mM free thiols prior to swelling in serum-free and serum-containing, phenol red-free growth medium for 2 hours at 37 °C. Only 0.26 ± 0.02 and 0.24 ± 0.04 mM free thiols remained after incubation indicating free thiol consumption at a rate much faster than 24 hours (Supplementary Information, Figure 2.11); consequently, gels need to be incubated in PBS, rather than culture medium, for photopatterning in the presence of cells. A balance must be struck between allowing time for diffusion of the peptide and initiator into the gels while minimizing the time that cells are incubated in PBS during this process. To address this, we polymerized gels in geometries in which cell encapsulation experiments were conducted (10 wt%, 20 μL gels in syringe tips) for 1 minute and placed them immediately in the patterning solution (PBS containing 3 mg/mL RGDS ~3× excess to SH and 2.2 mM LAP). Gels were incubated at 37 °C for 30 minutes or 1 hour and 30 minutes, times longer and shorter than the time estimated for diffusion of the monomer to the center of the gel assuming Fickian diffusion (t_d ~ 65 minutes):

$$t_d = \frac{L^2}{\mathcal{D}} \qquad \text{Eq. 2.3}$$

where L is half the thickness of the unswollen gel (~0.625 mm) and $\mathcal{D}$ the diffusion coefficient (~10^{-6} cm^2/s based on proteins of similar molecular weight as the RGDS peptide).[67] A second dose of UV light (1 minute) was applied to covalently link RGDS within the hydrogel. As previously observed, free thiol concentration in gels polymerized for 1 and 5 minutes (without patterning) was not statistically different ($p > 0.05$) and the patterned gels exhibit significantly lower concentrations of free thiols post-patterning ($p < 0.05$ compared to that after 1 and 5 minute gel formation) at 0.30 ± 0.01 and 0.21 ± 0.02 mM, respectively (Figure 2.6 C). These two photopatterning conditions have statistically different thiol concentrations after polymerization ($p < 0.05$), suggesting that the peptide and initiator may not have fully penetrated the gel during this incubation time. To test this hypothesis, gels (10 wt%, 20 μL in syringe tips, 1 minute polymerization) were incubated with AF488RGDS (3 mg/mL) and LAP (2.2 mM) in PBS for 30 minutes, 1 hour, and 1 hour 30 minutes, and exposed to UV light for 1 minute to allow covalent attachment of the fluorescent peptide. *Z*-Stack images through the entire gel depth (confocal) indicate consistent patterning of the peptide through the gel depth for all conditions (Figure 2.6 D; Supplementary Information, Figure 2.15). We speculate that the slight differences seen between the thiol concentrations after patterning by Ellman's assay (Figures 2.5 B and 2.6 C) are the result of small variations between batches of PEG-4SH monomer and hydrogels or the relative excesses at which the cues were tagged (20× for proof-of-concept and 3× for patterning in the presence of cells).

To compare the effects of these photopatterning conditions on cell activity and viability, cells encapsulated in non-degradable gels (3000 cells/μL, 1 minute UV exposure) were incubated for 30 minutes or 1 hour 30 minutes in PBS containing

RGDS and LAP and a second dose of UV light subsequently was applied for 1 minute. Cell metabolic activity for these photopatterning conditions is statistically similar to the 1 minute hydrogel formation condition at days 1 and 3 ($p > 0.05$), indicating that exposure to multiple polymerizations (formation + patterning) has a minimal effect on cell function (Figure 2.6 B). There appears to be a slight, but not statistically significant, decrease in metabolic activity for each condition between days 1 and 3. We hypothesize that this negligible decrease results from minor damage to cells in all cases by the radically-mediated polymerizations, which shows up in reduced metabolic activity at day 3. No statistical difference is observed between any condition at day 3. Taken together, no specific effect of the photopatterning process is observed, and the photopatterning conditions assessed here are appropriate for use in cell culture.

Finally, toward long-term culture of cells in patterned gels, hMSCs were encapsulated in cell-degradable gels crosslinked with a MMP-cleavable peptide sequence[18] (GPQGIWGQ2alloc) and treated with 3 mg/mL RGDS and 2.2 mM LAP in PBS for 1 hour (between the minimum and maximum incubation times tested for photopatterning) before a second dose of UV light was applied to photopattern RGDS within the network. After 6 days of culture, cells were stained with the LIVE/DEAD® Viability/Cytotoxicity Kit and imaged on a confocal microscope to observe cell viability and any spreading within the network. Viability greater than 90% was observed and a few cells exhibited protrusions (Figure 2.6 E), indicative of adhesion to and degradation of the matrix. Based on these results, this approach for cell encapsulation and matrix photopatterning is promising for future studies to probe stem cell–material interactions and direct cell function and fate *in vitro*.

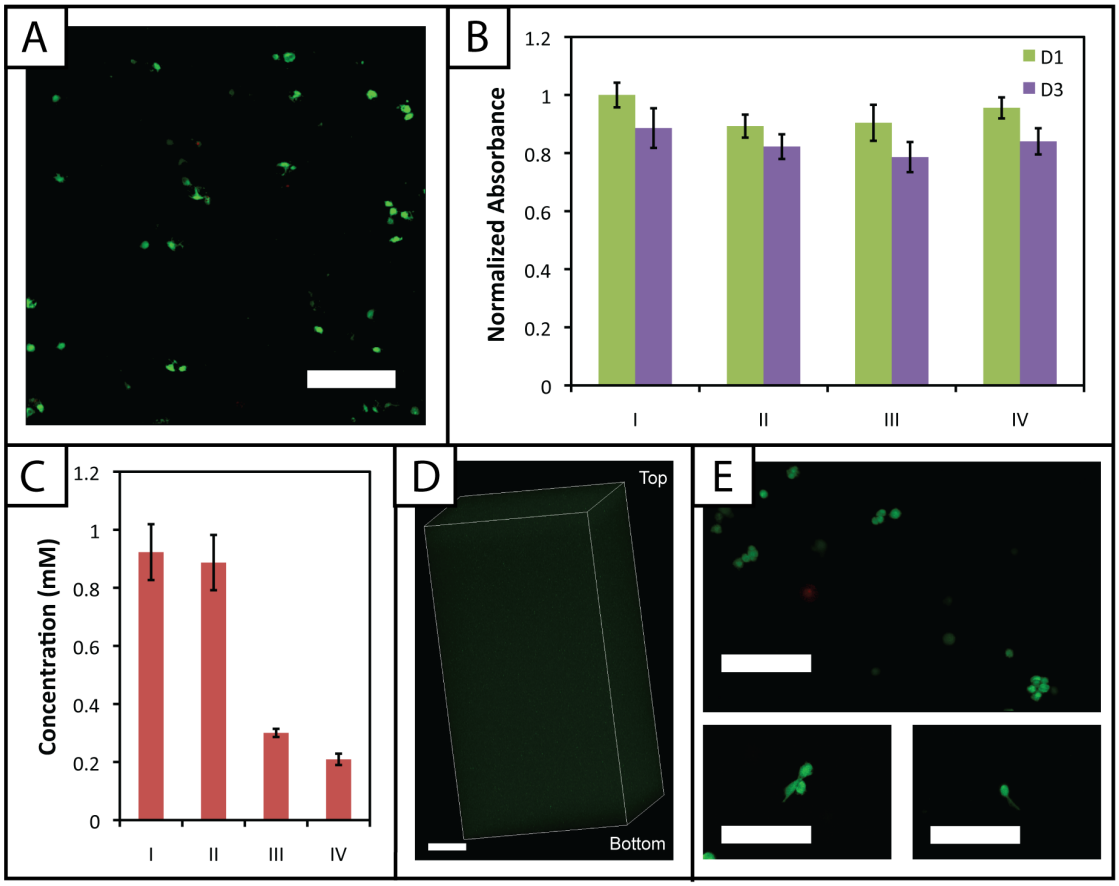
A
B
Normalized Absorbance
1.2
1
0.8
0.6
0.4
0.2
0
D1
D3
I
II
III
IV
C
Concentration (mM)
1.2
1
0.8
0.6
0.4
0.2
0
I
II
III
IV
D
Top
Bottom
E

Figure 2.6: **Encapsulated stem cells remain viable within patterned and non-patterned hydrogels. A)** Cells were mixed with PEG and peptide monomers and encapsulated to demonstrate the utility of this material system for cell culture in three dimensions. Cells stained green indicate viable cells with intact membranes, whereas cells stained red indicate cells with compromised cell membranes that are dead or dying. Approximately 87 ± 2 and 81 ± 4 % of cells were viable after encapsulation and culture for 3 days in 10 wt% gels (with respect to PEG) polymerized for 1 and 5 minutes with 2.2 mM LAP. (Confocal projection; Scale bar, 200 μm) **B)** Metabolic activity of the encapsulated cells also was assessed as a second measure of cell viability and function in response to polymerization and short-term culture (normalized to the gels polymerized for 1 minute 1 day after encapsulation). Various encapsulation and photopatterning conditions were tested (I) 1 minute encapsulation, (II) 5 minutes encapsulation, (III) 1 minute encapsulation + 30 minutes PBS/RGDS/LAP + 1 minute photopatterning, (IV) 1 minute encapsulation + 1 hour 30 minutes PBS/RGDS/LAP + 1 minute photopatterning. Condition II for day 1 is statistically different ($p < 0.05$) from I, indicating that longer exposure times to UV and radicals can initially affect viability. However, at day 3, conditions I and II are statistically similar, indicating 'recovery' of the cells post-encapsulation. The photopatterning conditions III and IV are statistically similar to I at days 1 and 3; thus, incubation in PBS and a second dose of UV light do not significantly impact cell function. **C)** Ellman's assay was conducted on hydrogels processed under conditions used in panel B (I, II, III, and IV). The initial encapsulation conditions I and II have statistically similar free thiol concentrations, consistent with prior gel formation results. The photopatterning conditions III and IV are statistically different from I and II, indicating the ability to covalently attach peptides within the network post-polymerization under mild conditions for cell culture. Further, III and IV are statistically different from each other, suggesting that photopatterning may be diffusion-limited in thicker gels used for cell encapsulation. To evaluate this, **D)** gels incubated with 3 mg/mL AF488RGDS and 2.2 mM LAP for 30 minutes were patterned with a second dose of UV light for 1 minute. Uniform attachment of the fluorescent cue is observed throughout the entire gel depth (~1.6 mm). (Confocal z-stack; Scale Bar, 200 μm) **E)** Cells encapsulated in a MMP-degradable hydrogel patterned with RGDS remain viable (> 90%) over 6 days in culture (top). Several encapsulated cells began to form protrusions by day 6, characteristic of degradation and cell adhesion to the matrix (bottom). (Scale bars, 200 μm)

2.5 Conclusions

In summary, we presented a novel hydrogel system formed by thiol–ene photoclick chemistry through reaction of thiol-modified PEG and alloc-modified peptides. Use of the LAP photoinitiator allowed rapid polymerization with cytocompatible doses of UV light and the formation of hydrogels with appropriate mechanical properties to mimic soft tissues. These hydrogels remain stable in cell culture conditions and encapsulated cells are viable within the network. Biochemical cues were selectively patterned within the gels to demonstrate spatial control over matrix properties, and cells remained viable. Further, the monomers used in the design of this system may be synthesized using established protocols or commercially purchased, making the material accessible for the facile and consistent formation of robust hydrogels to mimic the ECM. In the future, this base material may be used with orthogonal click chemistries to allow control over biochemical and biomechanical properties over days to weeks to study cell response to changes in the surrounding environment and provides a useful platform to adapt for a variety of biomaterials applications, including cell culture, tissue engineering, and drug delivery. Specifically, toward application in culture and directing hMSC fate, gels could be patterned with individual or multiple biochemical cues in spatially defined regions to drive cellular processes, including adhesion, migration, proliferation, or differentiation.[68,69]

2.6 Acknowledgements

This work was supported by the Institutional Development Award from the National Institutes of Health (P20GM103541), the Pew Charitable Trusts (00026178), a National Science Foundation Career Award (DMR-1253906), and the National Science Foundation IGERT SBE2 program at the University of Delaware (fellowship

to LAS). The authors thank the Delaware Biotechnology Institute at the University of Delaware for training and access to confocal microscopy at the BioImaging Center, Mr. Matthew Rehmann for generously providing hMSCs isolated from bone marrow and the cysteine-modified peptide, Prof. Christopher J. Kloxin and Mr. Stephen Ma for generously providing photomasks, Prof. Wilfred Chen for use of the automated plate reader, and Mr. Eric Macedo for training in polymer and peptide synthesis techniques.

2.7 Supplementary Information

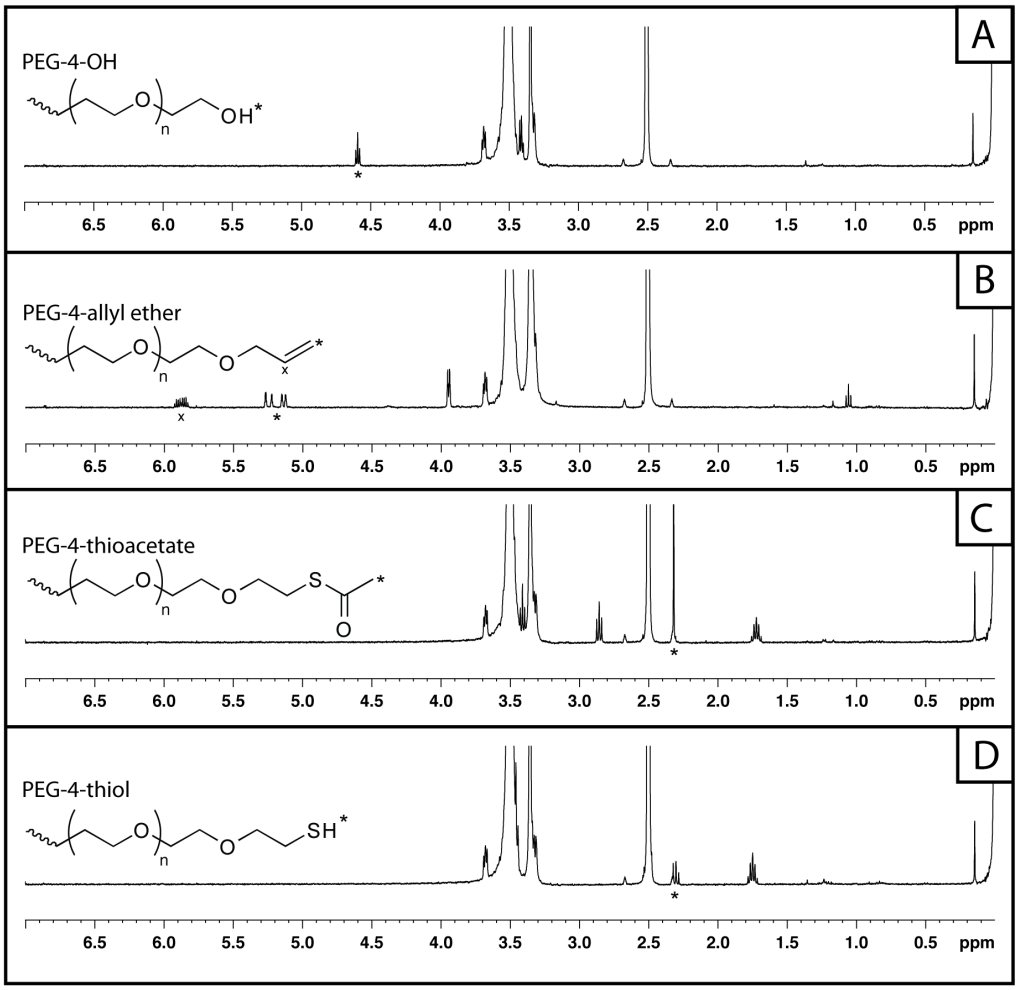

Figure 2.7: **^{1}H NMR of product and intermediates in PEG4SH synthesis in DMSO. A)** The hydrogen on the hydroxyl group of the initial PEG 20k monomer is identified at 4.6 (m, 1H). **B)** After reaction with allyl bromide, the hydroxyl peak on the PEG disappears and allyl ether peaks appear at 5.1-5.2 (m, 1H), 5.2-5.3 (m, 1H), and 5.8-5.9 (m, 1H), respectively. **C)** Conversion of the PEG-4-allyl ether (PEG4AE) to PEG-4-thioacetate results in the disappearance of allyl ether associated peaks, replaced by a peak at 2.3 (s, 3H), corresponding to the methyl group on the thioacetate. **D)** After final conversion of PEG-4-thioacetate, the product PEG-4-thiol (PEG4SH) was confirmed by the presence of a peak at 2.3 (m, 1H) indicating the hydrogen on free thiol groups. This peak has the same shift as that of the thioacetate peak, but is a multiplet and corresponds to one hydrogen.

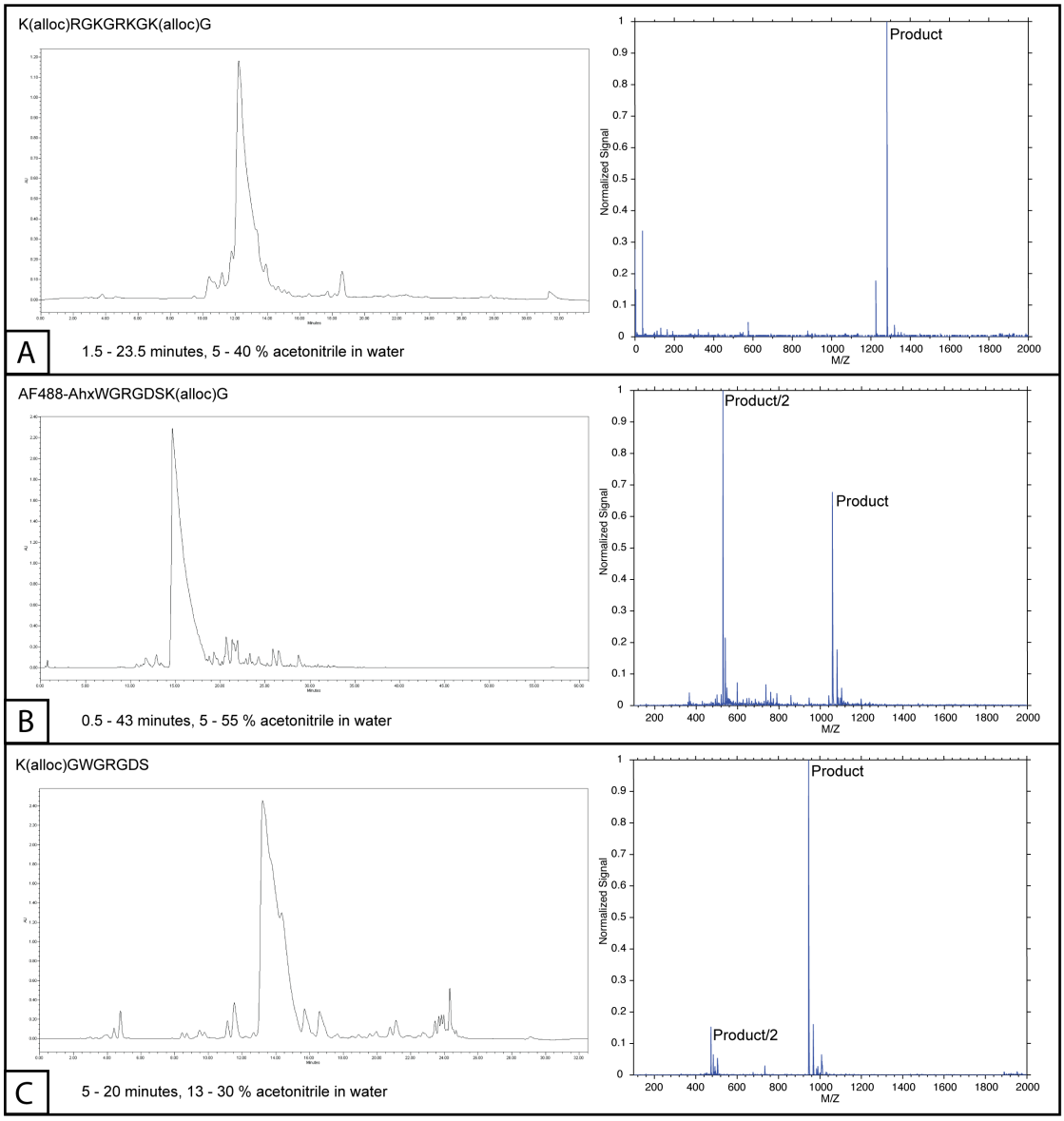
K(alloc)RGKGRKGK(alloc)G
Product
Normalized Signal
M/Z
A
1.5 - 23.5 minutes, 5 - 40 % acetonitrile in water
AF488-AhxWGRGDSK(alloc)G
Product/2
Product
Normalized Signal
M/Z
B
0.5 - 43 minutes, 5 - 55 % acetonitrile in water
K(alloc)GWGRGDS
Product
Product/2
Normalized Signal
M/Z
C
5 - 20 minutes, 13 - 30 % acetonitrile in water

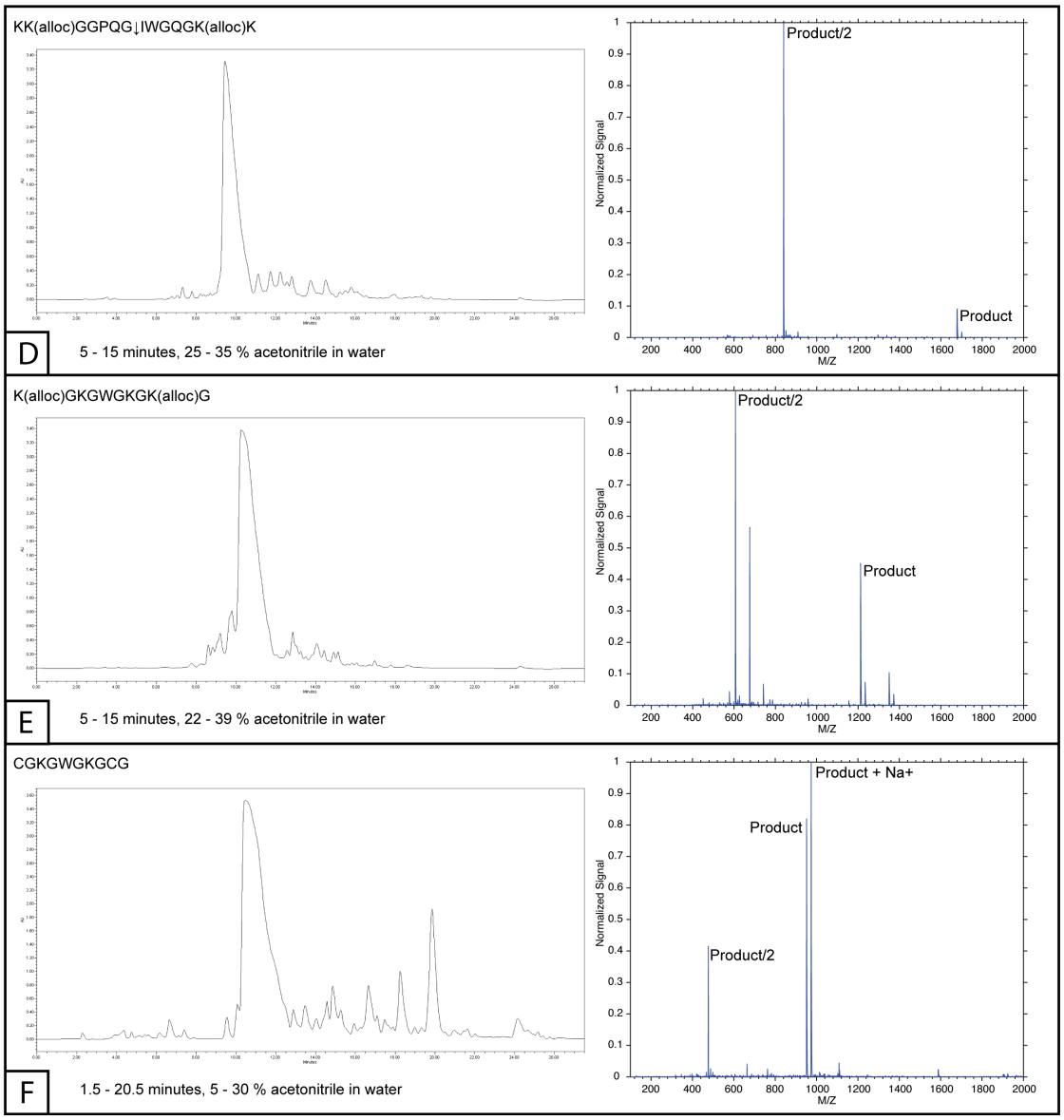
KK(alloc)GGPQG↓IWGQGK(alloc)K
Product/2
Product
Normalized Signal
M/Z
D
5 - 15 minutes, 25 - 35 % acetonitrile in water
K(alloc)GKGWGKGK(alloc)G
Product/2
Product
Normalized Signal
M/Z
E
5 - 15 minutes, 22 - 39 % acetonitrile in water
CGKGWGKGCG
Product + Na+
Product
Product/2
Normalized Signal
M/Z
F
1.5 - 20.5 minutes, 5 - 30 % acetonitrile in water

Figure 2.8: **HPLC traces, MALDI-MS, and ESI-MS spectra for the purification and identification of synthesized peptides. A)** The major peak observed with HPLC (left) was collected for the purification of K(alloc)RGKGRKGK(alloc)G (RGKGRK2Alloc) crosslinker peptide. The final product was confirmed by MALDI-MS (MW = 1282 g/mol, N'-terminus acetylation). **B)** The major peak observed with HPLC (left) contains AF488-AhxWGRGDSK(alloc)G (AF488RGDS). The crude product was analyzed by ESI-MS (MW = 1059 g/mol). Note that the molecular weight is for AhxWGRGDSK(alloc)G because the AF488AhxWGRGDSK(alloc)G is a minor species (approximately 1 for every 220 AhxWGRGDSK(alloc)G). **C)** The major HPLC peak (left) for the pendant K(alloc)GWGRGDS (RGDS) was analyzed by ESI-MS and the final product confirmed. (MW = 946 g/mol). **D)** The major HPLC peak (left) analyzed by ESI-MS (right) confirmed the synthesis of KK(alloc)GGPQG↓IWGQGK(alloc)G (GPQGIWGQ2alloc, MW = 1680 g/mol, N'-terminus acetylation). **E)** The major HPLC peak (left) of K(alloc)GKGWGKGK(alloc) (GKGWGKG2alloc) was analyzed by ESI-MS to confirm synthesis of the final product (MW = 1213 g/mol, N'-terminus acetylation). **F)** The HPLC peak (left) of CGKGWGKGCG (GKGWGKG2SH) was analyzed by ESI-MS and the final product confirmed (MW = 952 g/mol).

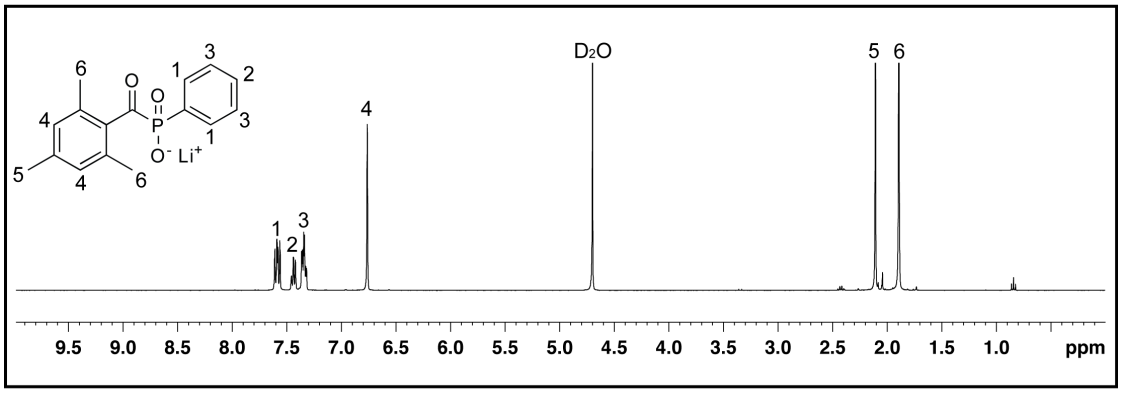

Figure 2.9: **^{1}H NMR of lithium acylphosphinate initiator in D_2O.** Peaks labeled 1-6 are identified on the NMR spectra corresponding to hydrogens on each ring of the initiator.

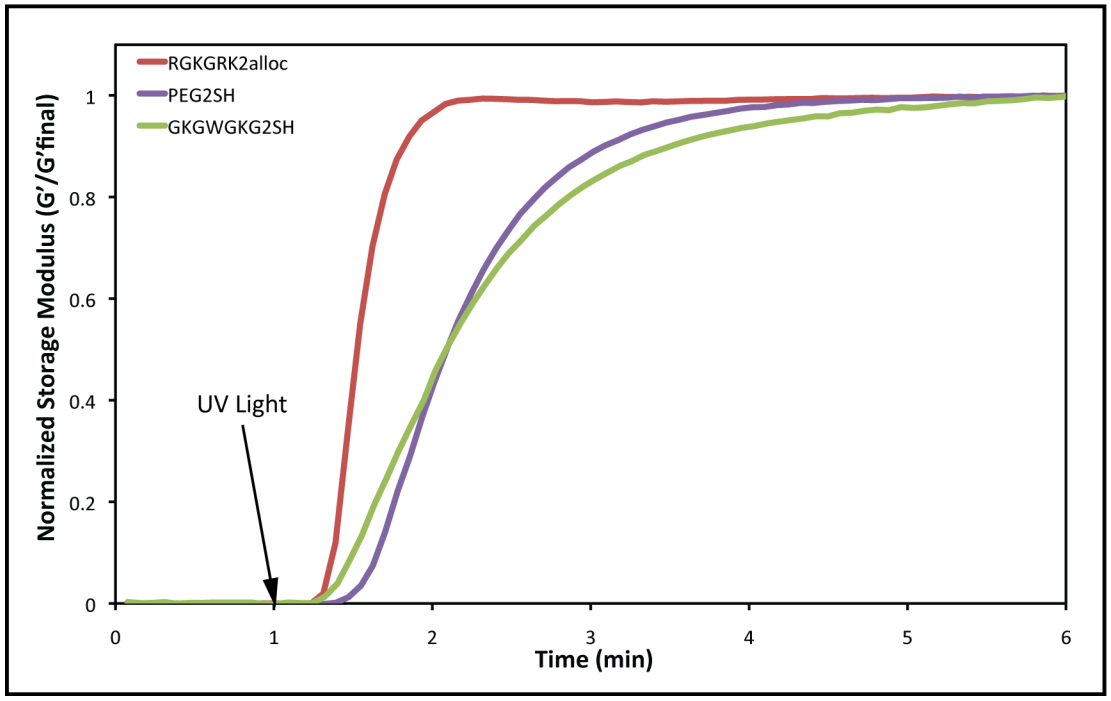

Figure 2.10: **Polymerization of thiol−ene hydrogels with various peptides and functionalities.** Hydrogels (10 wt%) were polymerized with different initial monomer solutions to investigate the effects of peptide sequence and functionality on polymerization rate. The highly charged RGKGRK2alloc crosslinking peptide exhibits the fastest polymerization when reacted with PEG4SH. The PEG2SH crosslinking molecule, when reacted with PEG4AE, exhibits a slower polymerization than RGKGRK2alloc with PEG4SH, which may be due to either the lack of charge in the reacting monomers or the change of the reacting functional groups. Finally, the GKGWGKG2SH peptide with PEG4AE exhibited the slowest reaction, with the modulus continuing to slowly increase at 6 minutes. This reaction may be partly affected by functional group chemistry as well as disulfides, as the moduli (normalized here to the final modulus at 6 minutes) were an order of magnitude lower than the other gel conditions tested and the modulus appeared to continue to increase slowly over time. Ellman's assay was used to measure free thiols in the peptide stock solution to insure 1:1 stoichiometry and total peptide concentration also was checked with absorbance at 280 nm; however, this decreased polymerization rate and modulus were consistently observed.

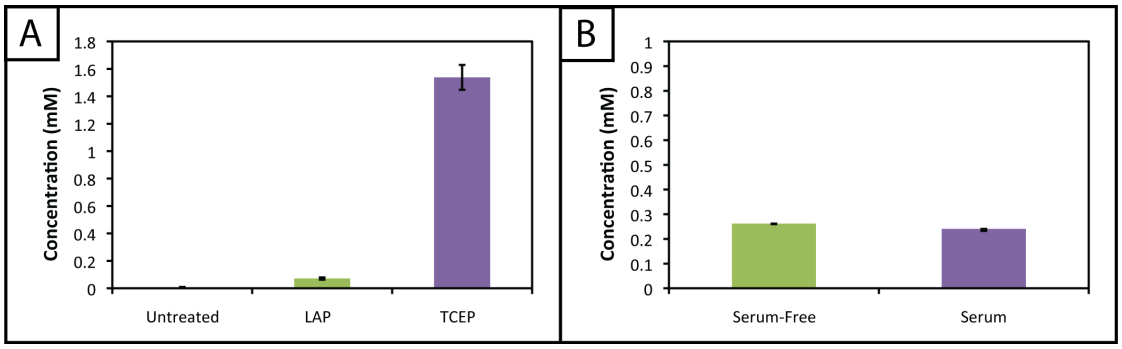

Figure 2.11: **Ellman's assay to determine free thiol concentration in hydrogels over time in cell culture medium. A)** Hydrogels incubated in growth medium for 3 days were analyzed by Ellman's assay to determine if culture conditions affected temporal addition of biochemical cues. After 3 days in culture medium, only trace thiols were detected in the 'Untreated' condition by Ellman's assay (< 0.01 mM), indicating the formation of disulfide bonds over time. To test the hypothesis that disulfides were forming, TCEP, a strong reducing agent, was added to the samples and free thiol concentrations were found to be 1.54 ± 0.09 mM, indicating that extensive disulfide formation occurred during incubation with cell culture medium. In the literature, LAP has been shown to cleave disulfide bonds in disulfide-bonded PEG-tetrathiol hydrogels, and we wanted to determine if this could be applied in a PEG-peptide system.[43] Samples were incubated with LAP and irradiated with UV light. A slightly higher concentration of free thiols was present after irradiation with light (0.07 ± 0.01 mM); however, this concentration would not be a sufficient for the addition of biochemical cues to direct cell function. In future studies, orthogonal click chemistries will be investigated to allow long-term temporal control over biochemical properties. **B)** Hydrogels incubated in serum-free and serum-containing phenol red-free cell culture medium for 2 hours have decreased thiol concentrations (0.26 ± 0.02 and 0.24 ± 0.04 mM), indicating rapid consumption of free thiols in culture medium and that photopatterning must be performed immediately in PBS.

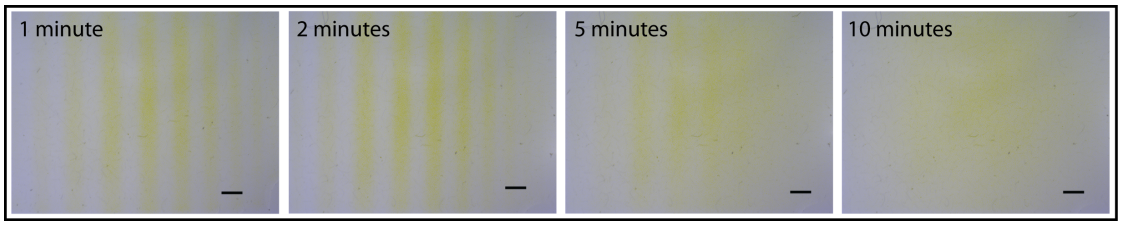

Figure 2.12: **Discrete time lapse of photopatterned hydrogels in the presence of Ellman's reagent.** A photopatterned hydrogel was incubated with Ellman's reagent, and imaged at 1, 2, 5, and 10 minutes to monitor diffusion of the yellow TNB^{2-} ion through the sample. At 1 and 2 minutes, unpatterned regions are vibrant yellow; however, as time increases to 5 minutes, the pattern becomes less resolved and eventually disappears by 10 minutes. Samples should be imaged immediately for the best resolution of patterns. (Scale bars, 200 μm)

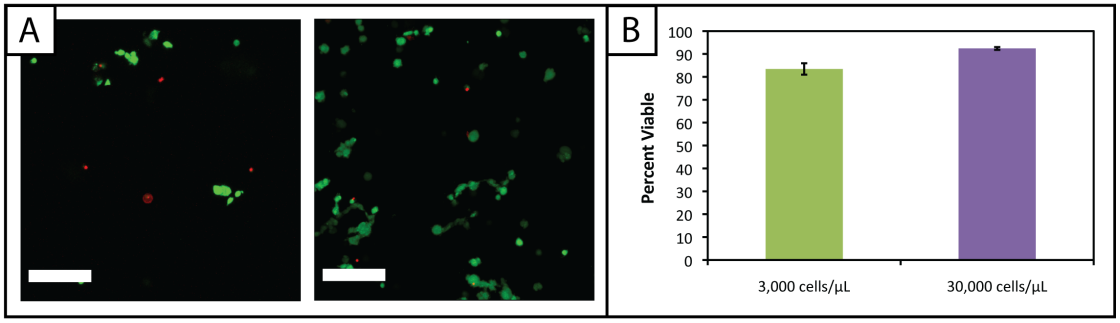

Figure 2.13: **Cell encapsulation and viability at different seeding densities**. **A)** Viability of cells encapsulated in 10 wt% hydrogels at 3000 (left) and 30000 (right) cells/μL was determined 3 days after encapsulation. Live (green) and dead (red) cells were identified with a LIVE/DEAD® Viability/Cytotoxicity Kit. (Scale bars, 200 μm) **B)** Approximately 83 ± 2% of cells remain viable in gels with 3000 cells/μL, whereas a statistically higher percent of cells ($p < 0.05$) remain viable in gels with 30,000 cells/μL at 92 ± 1%.

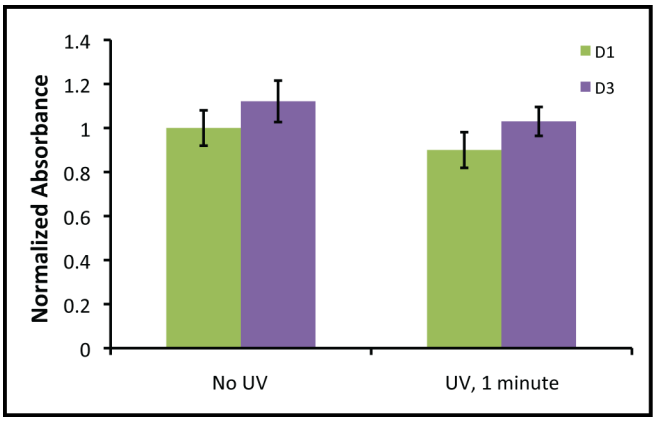

Figure 2.14: **Metabolic activity of cells treated with UV light in 2D.** Cells seeded on plates were treated with UV light for 1 minute. Metabolic activity was monitored 1 and 3 days after treatment (D1 and D3) to determine the potential effects. All absorbances were normalized to the "No UV" condition at D1. Exposure to UV light alone does not have an apparent effect on metabolic activity ($p > 0.05$) when compared to the "No UV" condition. Further, an increase in metabolic activity is seen at D3, indicating that the cells are able to recover from (and potentially proliferate after) exposure.

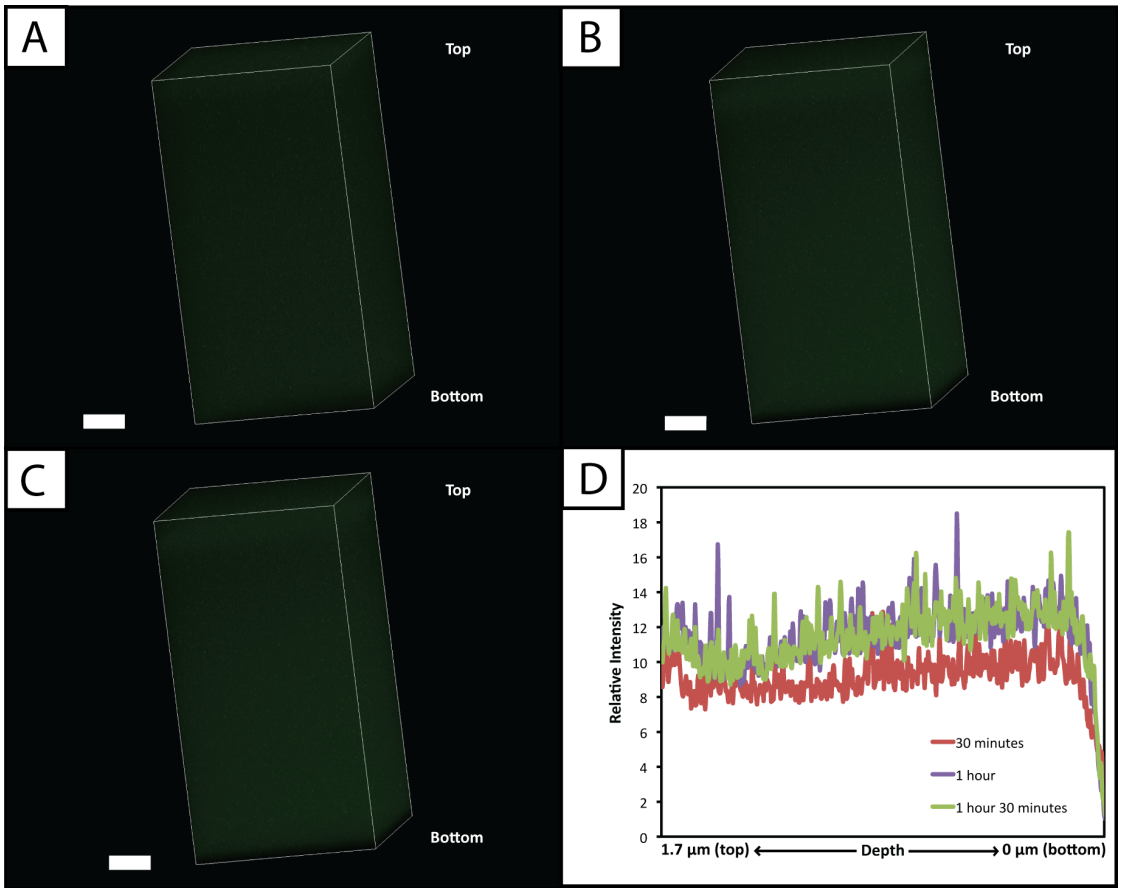

Figure 2.15: **Whole gels patterned with AF488RGDS to determine depth of diffusion and patterning**. Gels (20 µL) were incubated with photopatterning solution (3 mg/mL AF488RGDS, 2.2 mM LAP, PBS) for **A)** 30 minutes, **B)** 1 hour, and **C)** 1 hour 30 minutes, before applying a second dose of UV light for 1 minute. Confocal imaging through the gel depth indicates attachment and uniform patterning of the fluorescent peptide. (Scale bars, 200 µm) **D)** The relative intensity of the fluorophore for all three conditions is approximately the same (within noise), indicating that the incubation times are sufficient to achieve uniform patterning throughout the gel. The decrease in intensity at 0 µm indicates the bottom of the gel has been reached (also seen in A-C, where the image is darker).

REFERENCES

1. Kolb, H. C., Finn, M. G. & Sharpless, K. B. Click Chemistry: Diverse Chemical Function from a Few Good Reactions. *Angew Chemie - Int Ed*. **40** (11), 2004–2021 (2001).

2. Xi, W., Scott, T. F., Kloxin, C. J. & Bowman, C. N. Click Chemistry in Materials Science. *Adv Funct Mater*. **24** (18), 2572–2590 (2014).

3. Kharkar, P. M., Kiick, K. L. & Kloxin, A. M. Designing degradable hydrogels for orthogonal control of cell microenvironments. *Chem Soc Rev*. **42** (17), 7335–7372 (2013).

4. Iha, R. K., Wooley, K. L., Nystro, A. M., Burke, D. J., Kade, M. J. & Hawker, C. J. Applications of Orthogonal "Click" Chemistries in the Synthesis of Functional Soft Materials. *Chem Rev*. **109** (11), 5620–5686 (2009).

5. Kade, M. J., Burke, D. J., Hawker, C. J. & Burke, D. J. The Power of Thiol-ene Chemistry. *J Polym Sci Part A Polym Chem*. **48** 743–750 (2010).

6. Lomba, M., Oriol, L., *et al.* In Situ Photopolymerization of Biomaterials by Thiol-yne Click Chemistry. *Macromol Biosci*. **11** 1505–1514 (2011).

7. Robinson, K. G., Nie, T., Baldwin, A. D., Yang, E. C., Kiick, K. L. & Akins, R. E. Differential effects of substrate modulus on human vascular endothelial, smooth muscle, and fibroblastic cells. *J Biomed Mater Res - Part A*. **100 A** (5), 1356–1367 (2012).

8. Lutolf, M. P. & Hubbell, J. A. Synthesis and Physicochemical Characterization of End-Linked Poly(ethylene glycol)-co-peptide Hydrogels Formed by Michael-Type Addition. *Biomacromolecules*. **4** (3), 713–722 (2003).

9. Zheng, J., Smith Callahan, L. A., *et al.* Strain-Promoted Crosslinking of PEG-based Hydrogels via Copper-Free Cycloaddition. *ACS Macro Lett*. **1** (8), 1071–1073 (2013).

10. DeForest, C. A., Polizzotti, B. D. & Anseth, K. S. Sequential click reactions for synthesizing and patterning three-dimensional cell microenvironments. *Nat Mater*. **8** (8), 659–664 (2009).

11. Alge, D. L., Azagarsamy, M. A., Donohue, D. F. & Anseth, K. S. Synthetically tractable click hydrogels for three-dimensional cell culture formed using tetrazine-norbornene chemistry. *Biomacromolecules*. **14** (4), 949–953 (2013).

12. Selvaraj, R. & Fox, J. M. trans-Cyclooctene — a stable, voracious dienophile for bioorthogonal labeling. *Curr Opin Chem Biol*. **17** (5), 753–760 (2013).

13. Baldwin, A. D. & Kiick, K. L. Reversible maleimide–thiol adducts yield glutathione-sensitive poly(ethylene glycol)–heparin hydrogels. *Polym Chem*. **4** (1), 133–143 (2013).

14. Hoyle, C. E. & Bowman, C. N. Thiol-ene click chemistry. *Angew Chemie - Int Ed*. **49** (9), 1540–1573 (2010).

15. Polizzotti, B. D., Fairbanks, B. D. & Anseth, K. S. Three-Dimensional Biochemical Patterning of Click-Based Composite Hydrogels via Thiolene Photopolymerization. *Biomacromolecules*. **9** (4), 1084–1087 (2008).

16. Gramlich, W. M., Kim, I. L. & Burdick, J. A. Biomaterials Synthesis and orthogonal photopatterning of hyaluronic acid hydrogels with thiol-norbornene chemistry. *Biomaterials*. **34** (38), 9803–9811 (2013).

17. Nuttelman, C. R., Rice, M. A., Rydholm, A. E., Salinas, C. N., Darshita, N. & Anseth, K. S. Macromolecular Monomers for the Synthesis of Hydrogel Niches and Their Application in Cell Encapsulation and Tissue Engineering. *Prog Polym Sci*. **33** (2), 167–179 (2008).

18. Patterson, J. & Hubbell, J. A. Enhanced proteolytic degradation of molecularly engineered PEG hydrogels in response to MMP-1 and MMP-2. *Biomaterials*. **31** (30), 7836–7845 (2010).

19. Fairbanks, B. D., Schwartz, M. P., Halevi, A. E., Nuttelman, C. R., Bowman, C. N. & Anseth, K. S. A versatile synthetic extracellular matrix mimic via thiol-norbornene photopolymerization. *Adv Mater*. **21** (48), 5005–5010 (2009).

20. Lutolf, M. P. & Hubbell, J. A. Synthetic biomaterials as instructive extracellular microenvironments for morphogenesis in tissue engineering. *Nat Biotechnol*. **23** (1), 47–55 (2005).

21. Rydholm, A. E., Reddy, S. K., Anseth, K. S. & Bowman, C. N. Development and Characterization of Degradable Thiol-Allyl Ether Photopolymers. *Polymer*. **48** (15), 4589–4600 (2007).

22. Mosiewicz, K. A., Kolb, L., *et al.* In situ cell manipulation through enzymatic

hydrogel photopatterning. *Nat Mater*. **12** (11), 1072–1078 (2013).

23. Yang, T., Long, H., Malkoch, M., Gamstedt, K. E., Berglund, L. & Hult, A. Characterization of well-defined poly(ethylene glycol) hydrogels prepared by thiol-ene chemistry. *J Polym Sci Part A Polym Chem*. **49** (18), 4044–4054 (2011).

24. Burdick, J. A. & Murphy, W. L. Moving from static to dynamic complexity in hydrogel design. *Nat Commun*. **3** 1269 (2012).

25. Rehmann, M. S. & Kloxin, A. M. Tunable and dynamic soft materials for three-dimensional cell culture. *Soft Matter*. **9** (29), 6737–6746 (2013).

26. Lin, C. C., Raza, A. & Shih, H. PEG hydrogels formed by thiol-ene photo-click chemistry and their effect on the formation and recovery of insulin-secreting cell spheroids. *Biomaterials*. **32** (36), 9685–9695 (2011).

27. Salinas, C. N., Cole, B. B., Kasko, A. M. & Anseth, K. S. Chondrogenic Differentiation Potential of Human Mesenchymal Stem Cells Photoencapsulated within Poly(Ethylene Glycol)–Arginine-Glycine-Aspartic Acid-Serine Thiol-Methacrylate Mixed-Mode Networks. *Tissue Eng*. **13** (5), 6–8 (2007).

28. Ifkovits, J. L., Burdick, J. A. & Ph, D. Photopolymerizable and Degradable Biomaterials for Tissue Engineering Applications. *Tissue Eng*. **13** (10), 2369–2385 (2007).

29. Shih, H. & Lin, C. Cross-Linking and Degradation of Step-Growth Hydrogels Formed by Thiol−Ene Photoclick Chemistry. *Biomacromolecules*. **13** 2003–2012 (2012).

30. Shih, H. & Lin, C. Visible-Light-Mediated Thiol-Ene Hydrogelation Using Eosin-Y as the Only Photoinitiator. *Macromol Rapid Commun*. **34** 269–273 (2013).

31. Roberts, J. J. & Bryant, S. J. Comparison of photopolymerizable thiol-ene PEG and acrylate-based PEG hydrogels for cartilage development. *Biomaterials*. **34** (38), 9969–9979 (2013).

32. Sanchez, R., Riddle, M., Woo, J. & Momand, J. Prediction of reversibly oxidized protein cysteine thiols using protein structure properties. *Protein Sci*. **17** 473–481 (2008).

33. Gould, S. T., Darling, N. J. & Anseth, K. S. Small Peptide Functionalized

Thiol-Ene Hydrogels as Culture Substrates for Understanding Valvular Interstitial Cell Activation and de novo Tissue Deposition. *Acta Biomater*. **8** (9), 3201–3209 (2012).

34. Deforest, C. A., Sims, E. A. & Anseth, K. S. Peptide-Functionalized Click Hydrogels with Independently Tunable Mechanics and Chemical Functionality for 3D Cell Culture. *Chem Mater*. **22** (16), 4783–4790 (2010).

35. Kreevoy, M. M., Harper, E. T., Duvall, R. E., Wilgus III, H. S. & Ditsch, L. T. Inductive Effects on the Acid Dissociation Constants of Mercaptans. *J Am Chem Soc*. **82** 4899–4902 (1961).

36. Aimetti, A. A., Shoemaker, R. K., Lin, C. & Anseth, K. S. On-resin peptide macrocyclization using thiol–ene click chemistry. *Chem Commun*. **46** (23), 4061–4063 (2010).

37. DeForest, C. A. & Anseth, K. S. Cytocompatible click-based hydrogels with dynamically tunable properties through orthogonal photoconjugation and photocleavage reactions. *Nat Chem*. **3** (12), 925–931 (2011).

38. Fairbanks, B. D., Schwartz, M. P., Bowman, C. N. & Anseth, K. S. Photoinitiated polymerization of PEG-diacrylate with lithium phenyl-2,4,6-trimethylbenzoylphosphinate: polymerization rate and cytocompatibility. *Biomaterials*. **30** (35), 6702–6707 (2009).

39. Bryant, S. J., Nuttelman, C. R. & Anseth, K. S. Cytocompatibility of UV and visible light photoinitiating systems on cultured NIH/3T3 fibroblasts in vitro. *J Biomater Sci Polym Ed*. **11** (5), 439–457 (2000).

40. Mahmoud, Z. N., Gunnoo, S. B., Thomson, A. R., Fletcher, J. M. & Woolfson, D. N. Bioorthogonal dual functionalization of self-assembling peptide fibers. *Biomaterials*. **32** (15), 3712–3720 (2011).

41. Johnson, J. A., Finn, M. G., Koberstein, J. T. & Turro, N. J. Construction of Linear Polymers, Dendrimers, Networks, and Other Polymeric Architectures by Copper-Catalyzed Azide-Alkyne Cycloaddition "'Click'" Chemistry. *Macromol Rapid Commun*. **29** (12–13), 1052–1072 (2008).

42. Khurana, R., Schaefer, J. L., Archer, L. A. & Coates, Geoffrey, W. Suppression of Lithium Dendrite Growth Using Cross-Linked Polyethylene/Poly(ethylene oxide) Electrolytes: A New Approach for Practical Lithium-Metal Polymer Batteries. *J Am Chem Soc*. **136** (20), 7395–7402 (2014).

43. Fairbanks, B. D., Singh, S. P., Bowman, C. N. & Anseth, K. S.

Photodegradable, photoadaptable hydrogels via radical-mediated disulfide fragmentation reaction. *Macromolecules*. **44** (8), 2444–2450 (2011).

44. Ruoslahti, E. & Pierschbacher, M. D. New Perspectives in Cell Adhesion: RGD and Integrins. *Science*. **238** (4826), 491–497 (1987).

45. Bryant, S. J. & Anseth, K. S. Photopolymerization of Hydrogel Scaffolds. *Scaffolding Tissue Eng*. 71–90 (2005).

46. Anderson, S. B., Lin, C., Kuntzler, D. V & Anseth, K. S. Biomaterials The performance of human mesenchymal stem cells encapsulated in cell-degradable polymer-peptide hydrogels. *Biomaterials*. **32** (14), 3564–3574 (2011).

47. Lowe, A. B. Thiol-ene "click" reactions and recent applications in polymer and materials synthesis. *Polym Chem*. **1** 17–36 (2010).

48. Gerecht, S., Burdick, J. A., Ferreira, L. S., Townsend, S. A., Langer, R. & Vunjak-novakovic, G. Hyaluronic acid hydrogel for controlled self-renewal and differentiation of human embryonic stem cells. *Proc Natl Acad Sci United States Am*. **104** (27), 1–6 (2007).

49. Cramer, N. B., Reddy, S. K., Brien, A. K. O. & Bowman, C. N. Thiol-Ene Photopolymerization Mechanism and Rate Limiting Step Changes for Various Vinyl Functional Group Chemistries. *Macromolecules*. **36** (21), 7964–7969 (2003).

50. Elliott, J. E., Macdonald, M., Nie, J. & Bowman, C. N. Structure and swelling of poly(acrylic acid) hydrogels: effect of pH, ionic strength, and dilution on the crosslinked polymer structure. *Polymer*. **45** 1503–1510 (2004).

51. Zubov, V. P., Kumar, M. V., Masterova, M. N. & Kabanov, V. A. Reactivity of Allyl Monomers in Radical Polymerization. *J Macromol Sci Part A - Chem*. **13** (1), 111–131 (1979).

52. Salinas, C. N. & Anseth, K. S. Mixed Mode Thiol-Acrylate Photopolymerizations for the Synthesis of PEG-Peptide Hydrogels. *Macromolecules*. **41** (16), 6019–6026 (2008).

53. Toepke, M. W., Impellitteri, N. A., Theisen, J. M. & Murphy, W. L. Characterization of Thiol-Ene Crosslinked PEG Hydrogels Dr. *Macromol Mater Eng*. **298** (6), 699–703 (2013).

54. Discher, D. E., Janmey, P. & Wang, Y. Tissue Cells Feel and Respond to the Stiffness of Their Substrate. *Science*. **310** 1139–1143 (2005).

55. Levental, I., Georges, P. C. & Janmey, P. A. Soft biological materials and their impact on cell function. *Soft Matter*. **3** (3), 299–306 (2007).

56. Schwartz, M. P., Fairbanks, B. D., Rogers, R. E., Rangarajan, R., Zaman, H. & Anseth, K. S. A synthetic strategy for mimicking the extracellular matrix provides new insight about tumor cell migration. *Integr Biol*. **2** 32–40 (2010).

57. Raeber, G. P., Lutolf, M. P. & Hubbell, J. A. Molecularly Engineered PEG Hydrogels: A Novel Model System for Proteolytically Mediated Cell Migration. *Biophys J*. **89** (2), 1374–1388 (2005).

58. Kloxin, A. M., Kasko, A. M., Salinas, C. N. & Anseth, K. S. Photodegradable Hydrogels for Dynamic Tuning of Physical and Chemical Properties. *Science*. **324** (5923), 59–63 (2009).

59. Guvendiren, M. & Burdick, J. A. Engineering synthetic hydrogel microenvironments to instruct stem cells. *Curr Opin Biotechnol*. **24** (5), 841–846 (2013).

60. Fejerskov, B., Jensen, B. E. B., Jensen, N. B. S., Chong, S. & Zelikin, A. N. Engineering Surface Adhered Poly(vinyl alcohol) Physical Hydrogels as Enzymatic Microreactors. *Appl Mater Interfaces*. **4** (9), 4981–4990 (2012).

61. Kobel, S., Limacher, M., Gobaa, S., Laroche, T. & Lutolf, M. P. Micropatterning of Hydrogels by Soft Embossing. *Langmuir*. **25** (15), 8774–8779 (2009).

62. Ren, X., Jin, Y., Jae, H. & Kim, I. S. Chemosphere on the levels of cell cycle regulatory protein expression in primary cultured rabbit renal proximal tubule cells. *Chemosphere*. **74** (1), 84–88 (2008).

63. Lee, S. H., Moon, J. J. & West, J. L. Three-dimensional micropatterning of bioactive hydrogels via two-photon laser scanning photolithography for guided 3D cell migration. *Biomaterials*. **29** (20), 2962–2968 (2008).

64. Lin, C. & Anseth, K. S. Cell–cell communication mimicry with poly(ethylene glycol) hydrogels for enhancing β-cell function. *Proc Natl Acad Sci United States Am*. **108** (16), 6380–6385 (2011).

65. Nuttelman, C. R., Tripodi, M. C. & Anseth, K. S. Synthetic hydrogel niches that promote hMSC viability. *Matrix Biol*. **24** (3), 208–218 (2005).

66. Guvendiren, M. & Burdick, J. A. Stiffening hydrogels to probe short- and long-term cellular responses to dynamic mechanics. *Nat Commun*. **3** 792–799 (2012).

67. Weber, L. M., Lopez, C. G. & Anseth, K. S. Effects of PEG hydrogel crosslinking density on protein diffusion and encapsulated islet survival and function. *J Biomed Mater Res - Part A*. **90** (3), 720–729 (2009).

68. Marklein, R. A. & Burdick, J. A. Controlling Stem Cell Fate with Material Design. *Adv Mater*. **22** (2), 175–189 (2010).

69. Lutolf, M. P., Gilbert, P. M. & Blau, H. M. Designing materials to direct stem-cell fate. *Nature*. **462** 433–441 (2009).

Chapter 3

NEW APPROACHES FOR THE ANALYSIS OF CELL-SECRETED PROTEINS WITHIN SYNTHETIC EXTRACELLULAR MATRICES

3.1 Abstract

Cells interact with and remodel their microenvironment by degrading and replacing structural proteins and secreting soluble factors which signal other cells in the microenvironment to respond (e.g., recruitment to wounded or diseased tissue). Synthetic material scaffolds have been developed by researchers to investigate how cells behave within a well-defined *in vitro* culture environment to identify critical factors that drive function and fate. However, it is poorly understood how cells remodel these initially well-defined matrices, which may alter behavior and response. Here we developed techniques to identify large proteins deposited within poly(ethylene glycol) (PEG)-based hydrogel scaffolds and soluble factors secreted into culture medium. Specifically, human mesenchymal stem cells (hMSCs) cultured within PEG hydrogel scaffolds were decellularized, proteins were isolated by degradation of the hydrogel, and PEG macromer was separated from the digested protein sample (peptides) via spin column. Shotgun proteomics via HPLC with MALDI-MS identified large proteins fibronectin and collagen VI, which were confirmed by immunostaining. Luminex® assays performed on medium collected from hMSCs during culture identified secreted soluble factors (VEGF, IL-8). Together, these techniques may be used in future applications to study changes in

secreted proteins in response to different microenvironments or proteins secreted by other cell types within synthetic scaffolds.

3.2 Introduction

The extracellular matrix (ECM) of native tissue is a complex milieu of chemical and physical factors surrounding cells that directs their function and fate *in vivo*.[1] Large insoluble proteins (e.g., collagen, fibronectin, laminin, elastin), proteoglycans (e.g., heparin sulfate) and polysaccharides (e.g., hyaluronic acid) provide structure and binding sites that supports cells and allows their interaction with the ECM.[2–4] Cells remodel the ECM by secretion of enzymes (e.g., matrix metalloproteinases) that degrade existing protein structures, deposit new insoluble proteins to rebuild the structure, and also secrete small soluble proteins that drive additional cellular function and recruit additional cell types that further remodel this environment.[5–7] Toward understanding cell behavior in native tissue ECM, three-dimensional (3D) scaffolds have gained interest in recent years to identify key cell-ECM interactions that drive response and fate.[8,9] In particular, synthetic material scaffolds, often made from polymers (e.g., poly(ethylene glycol) (PEG), poly(ethylene oxide), poly(caprolactone))[10] and modified with chemical factors (e.g., peptides mimicking ECM proteins), offer a higher degree of tunability so that the effects of individual or multiple chemical and physical factors may be de-coupled, allowing enhanced interpretation of response.[11] While synthetic scaffolds are initially well-defined, cells remodel these microenvironments, as in native tissue, by depositing insoluble ECM proteins and secreting soluble chemical factors for network remodeling and cell-cell signaling. These cell-secreted proteins may dynamically alter cell response observed in synthetic scaffolds by adding to or masking binding sites

presented within the initial matrix, thus their identification will help in characterizing cell response *in vitro*. Proteomics-based techniques allow analysis of complex mixtures of proteins and may be used to identify critical factors that cells secrete within their microenvironment in processes like wounding, aging, and disease.[12–16]

Various proteomics techniques have been developed to identify proteins secreted by cells *in vivo* and *in vitro*. Electrophoresis techniques (2D-PAGE, 2D-DIGE) allow the separation of complex mixtures of proteins by mass and charge for subsequent analyses (gel imaging software or mass spectrometry) and protein identification.[17] In particular, 2D-PAGE has been a foundational tool for proteomics research, described in numerous applications including identification of proteins associated with wound healing, cancer, and drug discovery.[18–20] Other separation techniques such as liquid chromatography (HPLC) have been used in tandem with mass spectrometry (ESI, MALDI-TOF) to identify proteins in mixed samples.[19] This technique offers more rapid and inexpensive analysis of a proteome when compared to 2D-PAGE, but some of the complexity of protein structures may be lost if samples are digested prior to separation by LC for shotgun proteomics techniques.[21] More recently, high-throughput techniques have been developed and utilized for the detection of proteins including ELISA microarrays and multiplex microbead assays.[22–25]

Despite the range of tools available to conduct proteomic analyses, analysis of proteins secreted into synthetic 3D microenvironments is largely limited to immunostaining-based techniques or chemical assays that require some initial knowledge of what cells are secreting into their microenvironment. Adelöw, et al. demonstrated the production of the ECM proteins laminin, collagen I, and elastin by human mesenchymal stem cells (hMSCs) and smooth muscle cells (SMCs) via

immunostaining in a degradable PEG hydrogel scaffold for tissue regeneration.[26] Liao, et al, also reported the synthesis of collagen and elastin by vocal fold fibroblasts within a PEG-diacrylate network, observed with immunohistochemical staining and quantified by measurement of hydroxyproline content, ninhydrin assays, and ELISA.[27] Immunostaining and ELISA require the selection of specific antibodies, while ninhydrin and hydroxyproline assays only provide a quantitative measure of the amount of protein in a sample. Thus, the identification of complex mixtures of unknown proteins secreted by cells within synthetic scaffolds remains challenging.

Here, we aimed to develop a set of useful techniques to identify how cells remodel synthetic material scaffolds (Figure 3.1). hMSCs were encapsulated within a well-defined, and tunable PEG-based hydrogel matrix previously described by our group.[28,29] After culture, gels were decellularized to remove some cellular structures and leave behind larger proteins for subsequent analysis. Shotgun proteomics and immunostaining were used to identify and confirm the presence of proteins secreted within networks. Additionally, we investigated soluble factors that are secreted into culture medium, via Luminex® assays. The results of these studies are promising toward understanding cellular remodeling of synthetic microenvironments and identifying secreted factors that may drive additional cell response. These techniques and assays can be adapted to investigate numerous other cell lines cultured within well-defined hydrogel-based models of the ECM. Additionally, information gained from protein analysis may be used in the intelligent design of new scaffolds for cell culture, where proteins secreted by one cell type may be incorporated within another synthetic scaffold used to culture a second cell line and drive response.

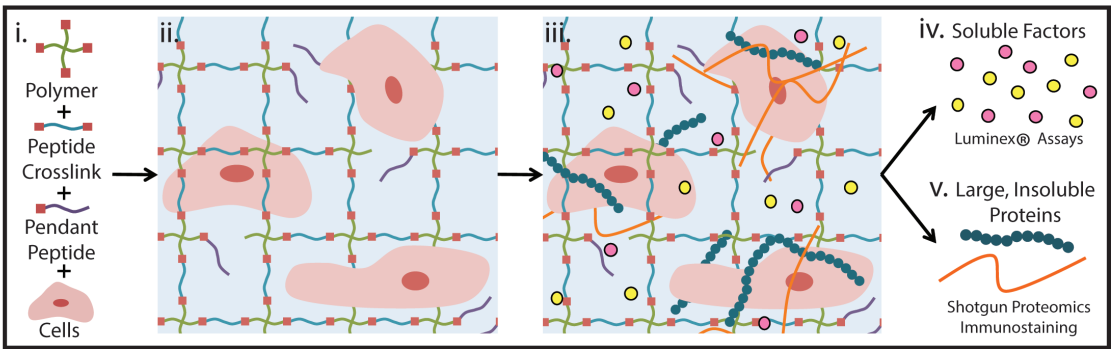

Figure 3.1: **A multi-step approach to identify proteins secreted by cells cultured within synthetic material scaffolds.** Cells (hMSCs) are encapsulated within a well-defined synthetic scaffold made from a crosslinked network of polymer and peptide macromers (i, ii). Cells remodel this environment, secreting large, insoluble proteins and small soluble factors that assist in cell-cell signaling (iii). Here, we describe the use of Luminex® assays to identify soluble factors and a shotgun proteomics technique, coupled with immunostaining, to identify large proteins isolated from hydrogel scaffolds (iv, v).

3.3 Materials and Methods

3.3.1 Preparation of Hydrogels

Macromers to form hydrogels, the inert polymer "backbone" 4-arm poly(ethylene glycol) thiol (PEG4SH, 20 kDa MW), enzymatically-degradable crosslink Ac-K**K(alloc)**G[GPQG↓IWGQ]G**K(alloc)**K (Pep2Alloc), and pendant peptide **K(alloc)**GWGRGDS (fibronectin/vitronectin mimic, RGDS), were synthesized as previously described.[28,29] Macromers were dissolved in Dulbecco's phosphate buffered saline (DPBS) supplemented with 1% penicillin/streptomycin (PS, Invitrogen), and 0.5 µg/mL fungizone (FZ, Invitrogen). Solutions of macromers were mixed at 6 wt% (w/v) PEG4SH, 2 mM RGDS, and stoichiometric ratios of Pep2Alloc (final [SH] = [Alloc]) and polymerized for 1 minute under light at 365 nm and 10 mW/cm^2.

3.3.2 Cell Culture and Encapsulation

hMSCs (Lonza) were maintained in low glucose (1 g/L) Dulbecco's Modified Eagle Medium with sodium pyruvate (DMEM, Invitrogen) supplemented with 10% fetal bovine serum (FBS, Invitrogen), 1% PS, 0.5 μg/mL FZ, and basic fibroblast growth factor (FGF-2, Peprotech). Cells were passaged or collected for encapsulation or Luminex® experiments at 70-80% confluency.

For encapsulation experiments, hMSCs at P6 were collected, counted (hemocytometer), and re-suspended in hydrogel precursor (5000 cells/μL). To make gels for decellularization and shotgun proteomics, 10 μL gels were prepared by pipetting cell/macromer solution into the tip of a sterile, cut syringe and polymerized for 1 minute with collimated light at 365 nM and 10 mW/cm^2 (Exfo Omnicure Series 2000). For immunostaining experiments, gels were prepared by polymerizing 15 μL of hydrogel precursor (cell-free) in the tip of a sterile, cut syringe to form a base. 5 μL cell/macromer solution was polymerized with a second dose of light to form a top layer (final gel volume 20 μL). A live/dead viability/cytotoxicity assay, was also performed on cells encapsulated for 1 and 10 days to confirm viability as previously described for hMSCs cultured within these hydrogels (Supplementary Information, Figure 3.6).[28,29]

3.3.3 Decellularization and Degradation of Protein Samples for Proteomic Analysis

Proteins from hMSCs cultured for 10 days in hydrogels were isolated through adaptation of a decellularization technique (for generating a fibronectin matrix)[30,31] to our 3D hydrogel scaffolds. Washing and lysis buffers were prepared fresh in deionized water: buffer 1(100 mM Na_2HPO_4 at pH 9.6, and 2 mM $MgCl_2$, 2 mM EGTA), lysis buffer (8 mM Na_2HPO_4 at pH 9.6 and 1% NP-40), and buffer 2 (300 mM KCl and 10

mM Na_2HPO_4 at pH 7.5). Hydrogels were rinsed 2 x 15 min with DPBS to remove culture medium. Subsequently, gels were treated 2 x 15 min with buffer 1, 1 x 30 min plus 1 x 60 min with lysis buffer, 2 x 15 min with buffer 2, and 4 x 15 min deionized water to remove cellular structures from the gel. Subsequently, decellularized gels were degraded with collagenase (Thermo Fisher, 50 U/mL in Hank's Balanced Salt Solution HBSS) for 1 hour at 37 °C and lyophilized for subsequent treatments to run proteomic analyses (Figure 3.2 A).

3.3.4 SDS-PAGE to Separate Proteins in Samples Collected from Plates

To determine if proteins from within hydrogels may be isolated via SDS-PAGE for proteomic analysis with an automated in-gel digestion method,[32] a mixture of proteins (Table 3.1) or a molecular weight ladder (10-250 kDa, Bio-Rad) were encapsulated in hydrogels. The following controls and conditions were loaded after treatment: *a)* molecular weight ladder (2-212 kDa, New England Biolabs); *b)* molecular weight ladder (Bio-Rad) *c)* protein mixture, lyophilized *d)* encapsulated molecular weight ladder (2 μL, Bio-Rad), whole gel; *e)* encapsulated protein mixture, whole gel; and *f)* encapsulated protein mixture, gel degraded with collagenase (3 U/mL in HBSS), sample passed through 50 kDa spin column (EMD Millipore), top fraction retained and lyophilized.

Table 3.1: Protein mixture for encapsulation within hydrogels to test protein isolation from PEG hydrogels with SDS-PAGE.

Protein	Molecular Weight (kDa)	Mass in Gel/Lane (µg)
Fibronectin	220	5
Lactoferrin	80	1.25
Bovine Serum Albumin	66.5	0.62
Myoglobin	16.7	10
Aprotinin	6.5	5

For SDS-PAGE, running buffer (57.6 g Glycine, 12 g Tris, 2 g SDS, filled to 2 L in DI water), destain buffer (200 mL Methanol, 140 mL Acetic Acid, filled to 2L in DI water), and sample buffer (50 µL 3x SDS Sample Buffer and 5 µL 30x dithiothreitol [DTT] Reducing Agent) were prepared. Dry protein from sample conditions *c* and *f* was reconstituted in DI water (~0.1 mg in 100 µL) and sample buffer (50 µL) was added to all samples and molecular weight ladders. Samples were heated for 5 min at 95 °C and loaded into lanes of the gel. The gel was placed in an SDS tank and 150 V applied until the blue dye front moved through the gel. After separation, the gel was removed from the SDS tank and rinsed in DI water for 5 minutes. The gel was incubated with SYPRO® Ruby Protein Stain for 3 hours and washed 3x with destain buffer, allowing the last wash to occur overnight. The gel was scanned and imaged to observe separation of the proteins from samples.

3.3.5 Shotgun Proteomics to Identify Proteins Isolated from Hydrogels

Shotgun proteomic analyses were performed as by Valente, et al.[33] with some modifications described below. Briefly, lyophilized gel samples were reconstituted in 25mM ammonium bicarbonate (Fisher Scientific) prior to incubation with 100mM

dithiothreitol (BioRad), 150mM iodoacetamide (Sigma Aldrich), and trypsin (Promega) digestion. Digested samples were acidified with formic acid (Thermo Fisher) and loaded onto 10 kDa MWCO spin columns (EMD Millipore) to separate peptides from PEG. Peptides were desalted using C18 OMIX tips (Agilent) per manufacturer's instructions.

Low pH RP-HPLC was carried out as described[33] on a Tempo LC-MALDI Spotter (ABSciex) with an acetonitrile gradient in 0.1% trifluoroacetic acid (Fisher Scientific) over a 110 minute program. Eluate was deposited onto MALDI target plates every 10 seconds with alpha-cyano-4-hydroxycinnamic acid matrix (HCCA, Sigma Aldrich) spiked with an adrenocorticotropic hormone fragment (Sigma Aldrich) (Figure 3.2 B).

MALDI mass spectrometry was performed with 1000 laser shots per spot over a mass range of 800-4000 m/z with internal calibration. Up to 15 peaks above signal/noise 20 were selected per spot for MSMS. MSMS data were acquired with 2000 laser shots per precursor and submitted to Protein Pilot software (v4.5, ABSciex) for database searches, using the Paragon algorithm (ABSciex), against the homo sapien taxonomy of NCBInr (download date 6/13/14). Accession numbers of hypothetical and unnamed proteins were BLAST searched to identify potential matches.

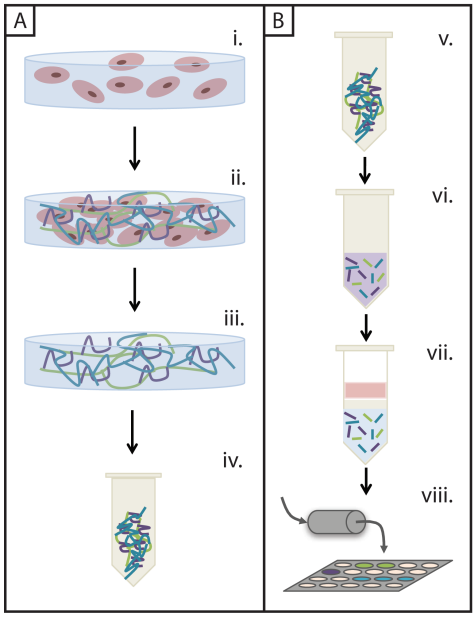

Figure 3.2: **Shotgun proteomics sample preparation workflow. A)** hMSCs are cultured in gels (i) and deposit cells within the network (ii). At selected time points, samples are treated with washing and lysis buffer to remove major cellular compartments, leaving large proteins entrapped within the hydrogel (iii). Gels are degraded with collagenase and samples lyophilized prior to protein digest (iv). **B)** Lyophilized proteins (v) are degraded with seq-grade trypsin (vi) overnight. PEG/peptide fragments from hydrogels were removed via 10 kDa MWCO spin columns (vii, red) and the bottom fraction containing peptide fragments from digested proteins was retained. The sample was desalted, run through RP-HPLC, and deposited every 10 s (mixed with HCCA) onto a MALDI target (viii) for subsequent identification via mass spec analysis and database searches.

3.3.6 Immunostaining for Large Proteins in Hydrogel Scaffolds

Collagen VI (mouse, DSHB Hybridoma Product 5C6; deposited by Engvall, E.S.), fibronectin (mouse, Abcam), and vimentin (rabbit, Abcam) antibodies were selected to confirm the presence of intracellular (vimentin) and extracellular (collagen IV, fibronectin) proteins identified in proteomic analyses. Blocking and permeabilization solutions were prepared fresh: BPSoln1 (3% w/v bovine serum

albumin/BSA + 0.05% v/v Triton-X in DPBS) and BPSoln2 (5% BSA w/v + 0.1% v/v Triton-X in DPBS). hMSCs cultured 10 days in hydrogels (15 μL base + 5 μL cell suspension on top) were rinsed of culture medium for 2 x 5 min with DPBS and fixed in 4% paraformaldehyde in DPBS for 15 minutes. After fixation, samples were washed 1 x 5 min DPBS and 2 x 5 min BPSoln1. Gels were incubated 1 hour at room temperature with BPSoln2 to block and permeabilize prior to incubation overnight at 4 °C with primary antibodies (Collagen VI, 10 μg/mL; Fibronectin, 10 μg/mL; Vimentin, 1 μg/mL) in BPSoln2. After primary antibody incubation, gels were rinsed 3 x 1 hour in BPSoln1 and secondary antibodies incubated overnight at 4 °C in BPSoln2 (Phalloidin, Sigma Aldrich, 1:250 dilution; Goat-anti-mouse AF488, Thermo Fisher, 1:300 dilution; Goat-anti-rabbit AF488, Thermo Fisher, 1:300 dilution). After secondary antibody incubation, samples were rinsed 3 x 45 min in BPSoln1 followed by 1 hour incubation with DAPI (DAPI, Thermo Fisher, 700 nM in DPBS) and 3 x 30 min rinses in DPBS. Samples were stored at 4 °C, protected from light, until imaging on a Zeiss LSM 800 confocal microscope (z-stacks, 100 images per stack, 2 μm spacing).

3.3.7 Collection of Culture Medium for Luminex® Assays

For Luminex® experiments, forty-eight hours prior to seeding, hMSCs at P6 were fed with medium without FGF-2 so that it was not present in the assay. Cells were collected, counted, and seeded at 10000 cells/cm^2 in 6 well plates (n = 3 wells) and fed every 48 hours during culture. After 8 days in culture, media was collected and centrifuged (1000 rpm, 5 min) to remove any cell debris. Samples were aliquotted and stored at -20 °C until assayed (Figure 3.3).

3.3.8 Luminex® Multiplex Analysis of Secreted Cytokines

A Luminex® assay (EMD Millipore) was selected containing vascular endothelial growth factor (VEGF), endothelial growth factor (EGF), basic fibroblast growth factor (FGF-2), interleukin 8 (IL-8), tumor necrosis factor alpha (TNF-α), and platelet-derived growth factor AB/BB (PDGF AB/BB) analytes. Assays were performed following standard instructions provided by EMD Millipore as briefly described below.

On the first day of the Luminex® assay, the human cytokine standard (10000, 2000, 400, 80, 16, and 3.2 pg/mL), media samples from cell culture, and "blank" media samples were incubated in the provided 96-well plate with pre-mixed Luminex® beads. After overnight incubation, allowing the factors present in the standard and samples to bind with analytes on the bead surface, samples were removed and detection antibodies and streptavidin-phycoerythrin were added to the beads (1 hour). The 96-well plate was run through the Luminex® system to detect beads bound with analytes (Figure 3.3).

Data analysis was performed using the xPONENT Software with a 5-parameter logistic. The standard curves for each analyte were qualified by visual inspection, comparison of the net mean fluorescence index (MFI) values, the standard deviation of points, and percent recovery. Specifically, standard curves for each analyte were visually inspected for any abnormal curve fits (e.g., plateauing, bottoming out, duplicate standard separation) and the appropriate standards removed; net MFI values that were too close to those of the background were invalidated; and points with percent recovery outside 75-125% were also invalidated (Supplementary Information, Table 3.4). Analyte concentrations were determined after validating the standard curves for each analyte.

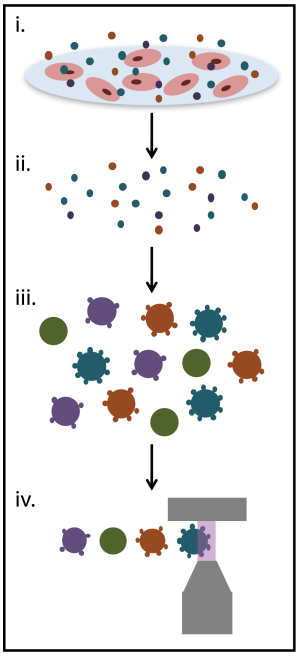

Figure 3.3: **Luminex® Assay workflow.** hMSCs cultured on plates secrete proteins into culture medium (i). Medium is collected at selected time points, centrifuged to remove debris (ii), and stored at -20 °C until assay. Media samples are incubated with Luminex® beads overnight, allowing analyte attachment (iii). After overnight incubation, detection antibodies are added and samples are passed through a Luminex® 200 system to identify analytes and detect their concentrations (iv).

3.4 Results and Discussion

3.4.1 Large Proteins Secreted within the Matrix Isolated and Identified

Identification of large proteins secreted by cells within synthetic scaffolds presents a unique challenge toward understanding cell behavior and response *in vitro*. First, these proteins add to the complexity of the pre-defined synthetic microenvironment and may alter the response of cells as additional binding sites are made present or as binding sites from peptides initially within the matrix are masked. Additionally, identification of these proteins within scaffolds may help with intelligent

design of new scaffolds as peptides mimicking these proteins may be synthesized and incorporated. We have developed a PEG-based hydrogel scaffold with tunable biomechanical and chemical properties for cell culture applications to identify key factors in the ECM that drive cell function and fate;[28,29] however, little is known about how cells remodel this environment.

Toward development of techniques to identify large proteins present within synthetic microenvironments, we adapted three previously-described techniques for proteomics analyses to isolate and identify proteins secreted within our 3D PEG-based hydrogels: *i)* SDS-PAGE for the isolation of proteins for MALDI-MS, *ii)* Shotgun proteomics by HPLC coupled with MADLI-MS, and *iii)* immunostaining select proteins of interest.

3.4.1.1 SDS-PAGE to Isolate Proteins from PEG Hydrogels

SDS-PAGE is a technique that has been previously used to separate proteins secreted by cells during culture for subsequent proteomic analysis. One benefit with the use of SDS-PAGE to isolate proteins is the preservation of the whole protein, which may provide additional information on the protein function. We first aimed to isolate proteins encapsulated within hydrogels with minimally destructive techniques and run SDS-PAGE.

PEG-SDS interactions present a challenge for application of the technique to separate proteins from PEG-based hydrogels. Zheng, et al. demonstrated that the separation of PEGylated proteins with SDS-PAGE smeared and broadened gel bands while native PAGE permitted a clear separation of proteins.[34] However, native PAGE is dependent on both protein mass and charge, thus separation of protein mixtures such as those deposited within hydrogel networks proves difficult. To address the issue

with PEG-SDS interaction, we investigated whole gel loading and removal of PEG from samples prior to loading.

Here, we encapsulated a mixture of proteins of different molecular weight (Table 3.1 and Figure 3.4, iii) and a molecular weight ladder (Figure 3.4, 1) within PEG-based hydrogels to determine if they might be isolated via SDS-PAGE. For our first condition, whole gels loaded with proteins were soaked with SDS and loaded into a lane. We hypothesized that the covalent crosslinks between PEG and peptide macromers would prevent some of the issues with SDS-PEG interactions (micelle formation) and that the mesh/pore size[35] of hydrogels would permit the migration of proteins into the PAGE gel lane. After mixture and heating with SDS sample buffer, gels were loose, indicating that some interactions with SDS had occurred. Whole gels were loaded into single lanes (Figure 3.4, i and ii). We observed spreading and smearing of bands, supporting our observation that SDS-PEG interactions had occurred. The second condition we investigated was the encapsulation of proteins within hydrogels, degradation of the hydrogel with collagenase, and removal of PEG/peptide hydrogel macromers from the protein sample with a spin column (50 kDa). Two drawbacks of this technique are that collagenase will degrade collagen, known to be secreted by hMSCs, and any proteins or collagen peptide fragments below 50 kDa will be removed with PEG/peptide macromers (~20 kDa MW). We still observed spreading and smearing of bands in this condition (Figure 3.4, iv), indicating that PEG remained in samples after removal with spin columns, which we hypothesize may be fragments of hydrogel that were not degraded or were connected with the encapsulated proteins. With this information, we chose to pursue alternate options for the identification of large proteins secreted by cells within hydrogels, namely a

shotgun proteomics technique and immunostaining to confirm protein identification as described in the next two sections.

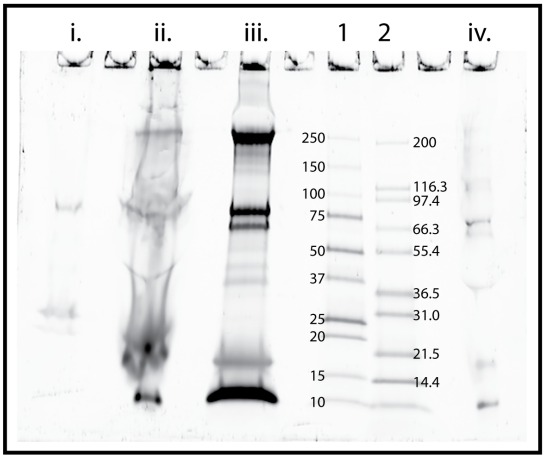

Figure 3.4: **SDS-PAGE on protein samples and molecular weight ladders encapsulated in synthetic hydrogels.** To test if proteins may be separated from gels by electrophoresis, a protein mixture (iii, Table 3.1) and a molecular weight ladder (1) were encapsulated in PEG-based hydrogels. Whole gels containing the molecular weight ladder (i) and proteins (ii) were loaded directly into lanes after treatment with SDS sample buffer. Gels softened with the addition of SDS and bands were smeared indicating interactions with SDS affected the separation. Removal of PEG from protein samples prior to loading was also tested. Specifically, the mixture of proteins was encapsulated in a hydrogel, hydrogels were degraded with collagenase, and PEG/peptide macromer fragments were removed with a spin column (50 kDa MWCO) with the top fraction containing proteins retained. The lane containing degraded sample (iv) was smeared, indicating that some amount of PEG remains after use of a spin column. Note that two molecular weight ladders (1, 2) were loaded in case interference from neighboring lanes due to PEG-SDS interactions occurred. *Data collected by Leila Choe.*

3.4.1.2 Shotgun Proteomics Identifies Proteins Secreted by hMSCs within PEG Hydrogels

Numerous proteomics techniques to identify proteins secreted by cells are available, however, selection of an appropriate method can prove challenging due to sample type and complexity.[18,36] Shotgun proteomics permits the analysis of complex mixtures of proteins with little information about the protein composition prior to analysis. We selected this technique partly because of the challenges associated with isolation of proteins from PEG-based hydrogels.

Whole proteins entrapped within synthetic scaffolds are difficult to isolate due to the high abundance of polymers relative to protein and entanglements of polymers with proteins. Additionally, the removal of the polymer is required to prevent potential interference with mass readings (e.g., increased molecular weight of proteins due to PEG-protein entanglements). We have incorporated a matrix metalloproteinase (MMP)-degradable peptide crosslink to permit cell-driven degradation within our hydrogel networks; however, we can also selectively degrade gels by cleavage of this peptide upon the exogenous application of enzymes. With this, gel degradation and PEG removal may easily be incorporated into the workflow for shotgun proteomics as previously described.[33]

To isolate proteins, we initially degraded gels with collagenase and lyophilized the samples in preparation for tryptic digest. After digest, samples containing PEG/peptide gel macromers and cell-secreted peptides were separated via spin column (10 kDa MWCO) allowing cell-secreted peptide fragments to pass through while removing trypsin (MW ~ 23 kDa), collagenase (MW ~ 68-130 kDa), and PEG/peptide macromer fragments (MW > 20 kDa). The bottom fraction was retained and run through RP-HPLC and spotted with 4-HCCA onto a target for MALDI-MS analysis

and protein identification (Abbreviated Results, Table 3.2; Full Results, Supplementary Information, Tables 3.5 and 3.6). It is important to note that protein identification was performed on sample from two gels and only high confidence matches (>95% confidence, >1.85 contribution) are reported from searches. Thus, only the most highly expressed proteins within samples were identified. In future work, a larger numbers of samples (higher total protein content) or more sensitive methods may permit the identification of additional proteins present in samples.

Collagen VI and fibronectin, which have previously been identified in hMSC culture,[37–40] were found within our synthetic scaffolds, indicating that the techniques described allowed isolation and identification of large ECM proteins at low sample concentration. While we are primarily interested in the identification of large ECM proteins, vimentin and other intracellular proteins also were identified. We hypothesize that due to the relatively small pore size and hMSC spreading within PEG hydrogel networks, not all of the cellular proteins wash out of the gel during and after decellularization. Here, the detergent NP-40 was used to decellularize scaffolds and allow removal of nuclear components,[31] but alternate techniques for decellularization[41] to remove cytoskeletal components (e.g., actin, vimentin) could be investigated in future studies if intracellular protein removal is desired. However, with the relative ease of sample preparation (decellularization and degradation), straightforward incorporation into existing shotgun proteomics workflow, this technique is promising for the identification of proteins secreted by other cell types or in response to extracellular stimulus (e.g., peptides that promote binding to networks, addition of cytokines) within synthetic microenvironments. Additionally, the identification of both large intra- and extracellular proteins permits an additional handle on the analysis

of cell behavior within 3D scaffolds, where proteins associated with a mesenchymal phenotype (vimentin) and several associated with differentiation (collagen VI, actin, fibronectin, tubulin), may indicate that the hMSCs cultured here were undergoing chondrogenesis.[42–44]

Table 3.2: **Abbreviated table of results for proteins identified by shotgun proteomics.** Hypothetical protein (gi|31874109) was determined to be fibronectin via BLAST search (Supplementary Information, Table 3.6). Other unnamed and hypothetical proteins (gi|189053217; gi|21739834) were identified via BLAST search as peroxiredoxin and AP-5 complex subunit beta-1, respectively. Notably, large ECM proteins collagen VI and fibronectin are present within the sample at high confidence levels from sample with low protein concentration. *Data collected by Leila Choe.*

Accession Number	Protein Name	Confidence (%)
gi|4502027	serum albumin preproprotein	99
gi|31874109	hypothetical protein	99
gi|62896523	vimentin variant	99
gi|55743106	collagen alpha-3(VI) chain isoform 5 precursor	99
gi|49457374	HIST1H4F	99
gi|62897625	beta actin variant	99
gi|73909156	Annexin A2	99
gi|62087582	H2A histone family, member V isoform 1 variant	99
gi|73762521	delta-globin Troodos variant	99
gi|87196339	collagen alpha-1(VI) chain precursor	99
gi|49456871	TUBB	99
gi|189053217	unnamed protein product	99
gi|156104889	protein AF-9 isoform a	99
gi|21739834	hypothetical protein	99
gi|258690785	estrogen receptor alpha 3*,4,5,6,7,8*/1068 isoform, partial	99
gi|68533107	MYH10 variant protein	99
gi|2330597	MHC class I antigen	99
gi|74099694	sulfite oxidase, mitochondrial	99

3.4.1.3 Immunostaining Confirms the Presence of Proteins Identified via Shotgun Proteomics

Traditionally, immunostaining has been used to identify large proteins secreted within 3D *in vitro* synthetic culture scaffolds due to challenges associated with the isolation of proteins from within a crosslinked material.[26,27,37,40] However, this technique is limited in that the user must select a panel of antibodies targeting proteins of interest. We used immunostaining here to determine if the isolation and protein analysis techniques described above correctly identified proteins secreted within our PEG-based hydrogels. Specifically, hMSCs cultured for 10 days were stained for vimentin, fibronectin, and collagen VI. Strong signal was observed for each protein (Figure 3.5 A) when compared to negative controls (secondary antibody only, Figure 3.5 B). It is important to note that fibronectin and collagen VI were observed to be localized to the cell membrane surface, which may mask binding to peptides (e.g., RGDS) initially present within synthetic microenvironments at late culture times. Based on these results, the developed shotgun proteomics technique to identify proteins isolated from decellularized scaffolds is promising for broader application to identify proteins secreted by other cell lines or to understand cell response within synthetic microenvironments.

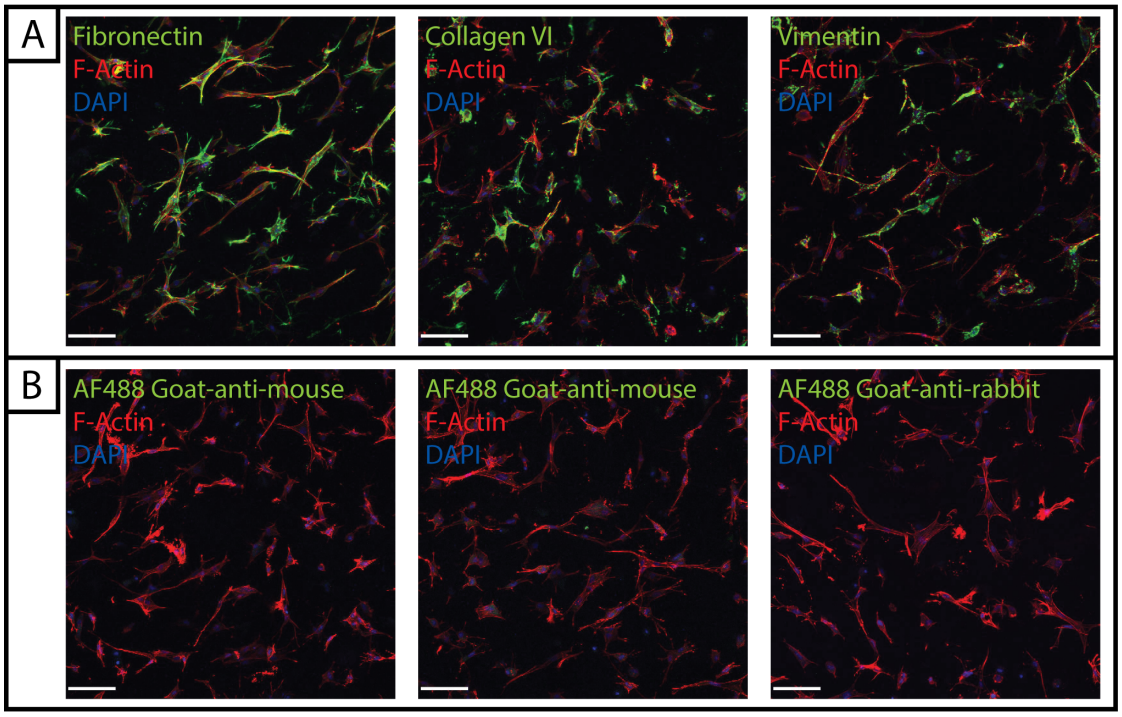

Figure 3.5: **Immunostaining proteins identified by shotgun proteomics. A)** Samples were stained for fibronectin, collagen VI, and vimentin, which had been identified by shotgun proteomics. All proteins were present in the immunostained samples. Note that fibronectin and collagen VI are located on the surface of the cells while vimentin is localized within the cell body. **B)** Negative controls with only secondary antibodies applied were used to confirm positive staining for each protein in (A). Z-stack projections, 100 μm scale bar.

3.4.2 Soluble Factors Secreted into Culture Medium Identified via Luminex® Assays

Soluble factors secreted by hMSCs have been implicated in wound healing and disease processes (e.g., tissue repair and regeneration,[45,46] cancer progression and tumor growth[47]). Here, we used Luminex® multiplex bead assays to identify the presence of soluble factors and their relative concentrations secreted by hMSCs into culture medium. A 6-plex panel targeting VEGF, EGF, FGF-2, IL-8, TNF-α, and

PDGF AB/BB was selected for identification of factors associated with inflammation and wounding healing conditions.[48–50]

Growth medium collected from hMSCs and "blank" culture medium (control) was assayed and concentrations of analytes identified (Table 3.3). No significant concentration of PDGF-AB/BB was detected, and low, but significant levels of EGF, FGF-2, and TNF-α were present in hMSC culture medium ($p << 0.05$). IL-8, a pro-inflammatory cytokine that has been shown to promote cell migration in wounding and cancer metastasis,[51,52] was found at high concentrations in the sample. High levels of VEGF secretion were observed, another factor reported to be secreted by hMSCs, associated with angiogenesis, which promotes tissue regeneration and wound healing.[53–55] These data indicate that hMSCs are secreting soluble factors involved in regulation of wound healing and tissue repair, matching those reported in literature.

Table 3.3: **Concentration of analytes (pg/mL) secreted by hMSCs in 2D culture.** IL-8 and VEGF are secreted at high concentrations relative to the blank concentration. Note that readouts of <3.2 and <16 indicate that negligible concentrations of factors were present in the sample, so the minimum value accepted for the standard curve concentration is reported. Standard error values for each hMSC sample concentration are reported.

Sample	**EGF**	**FGF-2**	**PDGF-AB/BB**	**IL-8**	**TNF-α**	**VEGF**
hMSC	4.44 ± 0.06	13.26 ± 0.15	N/A	420.90 ± 13.26	0.55 ± 0.03	399.01 ± 10.19
Blank	2.99	9.98	<3.2	0.50	0.22	<16

While this data represents preliminary results for the identification of soluble factors secreted in 2D microenvironments, the technique may easily be adapted to 3D by collection of medium from wells containing gels. If needed, analytes may be

concentrated with spin columns to improve signal for the assay. In future studies, hMSCs may be stimulated by the addition of other factors including different peptides tethered to synthetic matrices or soluble factors to drive differentiation to determine how external stimulation affects secretion of soluble factors.

3.5 Conclusions

Herein, we described the development of techniques to identify proteins secreted in synthetic PEG-based hydrogel matrices. A shotgun proteomics approach permitted the identification of several large proteins isolated from decellularized hydrogel samples and was confirmed by immunostaining. Luminex® multiplex bead assays identified the secretion of factors associated with wound healing and disease. Together these techniques represent a new method for global identification of unknown soluble and insoluble proteins secreted by cells within synthetic scaffolds, with proteins identified in samples collected from hMSCs matching those reported in literature. These new methods are promising for future application in identifying proteins secreted by other cell lines during *in vitro* culture, understanding cell response to external stimuli, and the intelligent design of novel scaffolds for tissue engineering and cell culture applications.

3.6 Acknowledgements

The authors thank Dr. Kelvin Lee and Leila Choe for their collaboration on the work, conducting SDS-PAGE and shotgun proteomics experiments and assistance with Luminex® Assays. The authors also thank Dr. Matthew Rehmann for protein mixtures used in SDS-PAGE experiments. We thank the NSF SBE2 IGERT program at the University of Delaware (fellowship awarded to Lisa Sawicki), the Institutional

Development Award from NIH for COBREs (P20GM104316 and P30GM110758-01), and the Susan G. Komen Foundation Career Catalyst Research Grant (CCR16377327) for funding.

3.7 Supplementary Information

Table 3.4: **Net MFI values of standard curve analytes in Luminex® assays.** Net MFI values (shown above) and percent recovery were evaluated to confirm or invalidate points in the standard curve (invalid points highlighted red). Standards 5 and 6 were invalidated for FGF-2 because net MFI values were close to background. Standard 6 for PDGF was invalidated due to large variance in the net MFI. Standard 1 for VEGF was invalidated due to percent recovery out of 80-120% range (86.05 and 126.74 %). Standards 5 and 6 were invalidated for VEGF because net MFI values were close to background.

Standard Curve	Expected Concentration (pg/mL)	EGF	FGF-2	PDGF	IL-8	TNF-α	VEGF
1	10000	21488.75	11023	6274	26766	26010.75	7011.5
1	10000	21654.75	11167.5	6486.5	26856	25893.75	8051.5
2	2000	15479.25	4091.5	1716.5	16891	14237.75	2040.5
2	2000	15490.75	3893	1723.5	16134.5	14330.75	1802.5
3	400	4666.75	490.5	331	5374	4003.75	193.5
3	400	4589.75	547	345.5	5468.5	4225.75	177.5
4	80	611.75	29	67	1356.5	1049.75	13.5
4	80	586.25	32	74.5	1376.5	1080.75	15.5
5	16	42.75	1	12	256.5	195.25	0.5
5	16	45.25	1	14	257.5	206.75	1.5
6	3.2	7.25	0	4	52.5	41.75	-0.5
6	3.2	5.75	0	1.5	53.5	37.75	0.5
Background	0	0.25	-1	0	0.5	-0.25	0.5
Background	0	-0.25	1	0	-0.5	0.25	-0.5

Table 3.5: **Complete list of proteins identified by shotgun proteomics.** Large proteins isolated from decellularized samples were identified, with high confidence (>95%) specified for database searches. Accession numbers of unnamed and hypothetical proteins were BLAST searched and matches were identified (Supplementary Information, Table 3.6). *Data collected by Leila Choe.*

Sample Number	Accession Number	Protein Name
1	gi|4502027	serum albumin preproprotein
1	gi|23307793	serum albumin
1	gi|189054552	unnamed protein product
1	gi|119626071	albumin, isoform CRA_h
2	gi|31874109	hypothetical protein
3	gi|62896523	vimentin variant
3	gi|340219	vimentin
3	gi|21757045	unnamed protein product
3	gi|167887751	vimentin variant 3
3	gi|16552261	unnamed protein product
4	gi|55743106	collagen alpha-3(VI) chain isoform 5 precursor
4	gi|55743098	collagen alpha-3(VI) chain isoform 1 precursor
4	gi|530371361	collagen alpha-3(VI) chain isoform X2
4	gi|530371359	collagen alpha-3(VI) chain isoform X1
4	gi|240255535	collagen alpha-3(VI) chain isoform 4 precursor
4	gi|219841772	COL6A3 protein
4	gi|219521324	COL6A3 protein
4	gi|119591516	collagen, type VI, alpha 3, isoform CRA_h
4	gi|119591513	collagen, type VI, alpha 3, isoform CRA_e
4	gi|119591511	collagen, type VI, alpha 3, isoform CRA_c
5	gi|49457374	HIST1H4F
5	gi|45767731	HIST1H4I protein
5	gi|119575948	histone 1, H4e
5	gi|119575932	histone 1, H4c
6	gi|62897625	beta actin variant
7	gi|73909156	Annexin A2
7	gi|34364597	hypothetical protein
7	gi|18645167	Annexin A2
8	gi|62087582	H2A histone family, member V isoform 1 variant
9	gi|73762521	delta-globin Troodos variant
9	gi|71727231	beta globin
9	gi|6003534	hemoglobin beta subunit variant
9	gi|6003532	hemoglobin beta subunit variant
9	gi|4504349	hemoglobin subunit beta
9	gi|4378804	hemoglobin beta chain
9	gi|40886941	hemoglobin beta
9	gi|29446	unnamed protein product

Table 3.5 continued.

9	gi|26892090	beta globin chain variant
9	gi|256028940	beta-globin
9	gi|187940241	hemoglobin beta chain variant
9	gi|18462105	delta-globin
9	gi|18418633	mutant beta-globin
9	gi|179409	beta-globin
9	gi|13549112	beta globin chain variant
10	gi|87196339	collagen alpha-1(VI) chain precursor
11	gi|49456871	TUBB
11	gi|332246227	tubulin beta-2B chain isoform 2
11	gi|27227551	class II beta tubulin isotype
11	gi|189069169	unnamed protein product
14	gi|189053217	unnamed protein product
15	gi|156104889	protein AF-9 isoform a
16	gi|21739834	hypothetical protein
17	gi|258690785	estrogen receptor alpha 3*,4,5,6,7,8*/1068 isoform, partial
18	gi|68533107	MYH10 variant protein
18	gi|641958	non-muscle myosin B
18	gi|530410345	myosin-10 isoform X3
18	gi|530410343	myosin-10 isoform X2
18	gi|367460090	myosin-10 isoform 3
18	gi|367460087	myosin-10 isoform 2
18	gi|119610456	myosin, heavy polypeptide 10, non-muscle, isoform CRA_c, partial
18	gi|109734611	Myosin, heavy chain 10, non-muscle
19	gi|2330597	MHC class I antigen
20	gi|74099694;	sulfite oxidase, mitochondrial
20	gi|530400755	sulfite oxidase, mitochondrial isoform X1

Table 3.6: **List of unnamed or hypothetical proteins from Table 3.5 identified by BLAST search.** Accession numbers of unnamed and hypothetical proteins were BLAST searched and the top five hits for searches are reported above. Sample numbers 1, 3, 7, 9, 11, which had other top hits identified with shotgun analysis, were confirmed by BLAST search. Samples 2, 14, and 16, which did not have other hits identified with shotgun analysis were identified as fibronectin, peroxiredoxin, and AP-5, respectively.

Sample Number	Accession Number	Accession Number, Protein Name
1	gi|189054552	gi|4502027, serum albumin preproprotein gi|28592, serum albumin gi|23307793, serum albumin gi|6013427, serum albumin precursor gi|28590, unnamed protein product
2	gi|31874109	gi|34364820, hypothetical protein gi|119590949, fibronectin 1, isoform CRA_n gi|16933542, fibronectin isoform 3 preproprotein gi|119590945, fibronectin 1, isoform CRA_j gi|530370043, fibronectin isoform X9
3	gi|21757045	gi|62414289, vimentin gi|62896523, vimentin variant gi|340219, vimentin gi|47115317, VIM gi|167887751, vimentin variant 3
7	gi|34364597	gi|50845388, annexin A2 isoform 1 gi|73909156, Annexin A2 gi|4757756, annexin A2 isoform 2 gi|18645167, Annexin A2 gi|16306978, Annexin A2
9	gi|29446	gi|23268449, hemoglobin beta chain variant Hb S-Wake gi|71727231, beta globin gi|4504349, hemoglobin subunit beta gi|229959, Chain B, Refined Crystal Structure of Deoxyhemoglobin S. I. Restrained Least-Squares Refinement at 3.0-Angstroms Resolution gi|26892090, beta globin chain variant
11	gi|189069169	gi|4507729, tubulin beta-2A chain isoform 1 gi|27227551, class II beta tubulin isotype gi|21746161, tubulin beta-2B chain gi|49456871, TUBB gi|223486, tubulin beta

Table 3.6 continued.

14	gi|189053217	gi|4505591, peroxiredoxin-1 gi|973743966, Chain A, Human Peroxiredoxin-1 C83s Mutant gi|164519504, Chain A, Crystal Structure of Human Peroxiredoxin I In Complex With Sulfiredoxin gi|440306, enhancer protein gi|260656338, Chain A, Crystal Structure of Sulfiredoxin In Complex with Peroxiredoxin I And Atp:mg2+
16	gi|21739834	gi|379317153, AP-5 complex subunit beta-1 gi|119594844, DKFZp761E198 protein, isoform CRA_b gi|10732604, unknown gi|114325483, DKFZp761E198 protein gi|119594843, DKFZp761E198 protein, isoform CRA_a

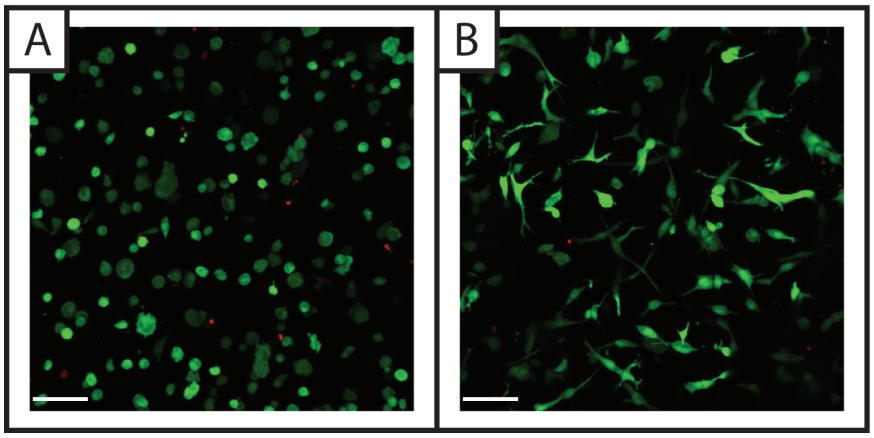

Figure 3.6: **Live/dead viability/cytotoxicity stain.** hMSCs encapsulated at **A)** 1 day and **B)** 10 days remain viable within hydrogels (green = live, red = dead). Notably, cells spread within matrices by day 10, indicating local degradation of the network and binding to RGDS peptide. 100 μm scale bar.

REFERENCES

1. Alberts, B., Johnson, A., Lewis, J., Raff, M., Roberts, K. & Walter, P. Cell junctions, cell adhesion, and the extracellular matrix. *Mol Biol Cell*. 1065–1125 (2002).

2. Hynes, R. O. The Extracellular Matrix: Not Just Pretty Fibrils. *Science*. **326** (5957), 1216–1219 (2009).

3. Bosman, F. T. & Stamenkovic, I. Functional structure and composition of the extracellular matrix. *J Pathol*. **200** 423–428 (2003).

4. Theocharis, A. D., Skandalis, S. S., Gialeli, C. & Karamanos, N. K. Extracellular matrix structure. *Adv Drug Deliv Rev*. **97** 4–27 (2016).

5. Bonnans, C., Chou, J. & Werb, Z. Remodelling the extracellular matrix in development and disease. *Nat Publ Gr*. **15** (12), 786–801 (2014).

6. Birkedal-Hansen, H. Proteolytic remodeling of extracellular matrix. *Curr Opin Cell Biol*. **7** 728–735 (1995).

7. Larsen, M., Artym, V. V, Green, J. A. & Yamada, K. M. The matrix reorganized: extracellular matrix remodeling and integrin signaling. *Curr Opin Cell Biol*. **18** 463–471 (2006).

8. Lee, J., Cuddihy, M. J. & Kotov, N. A. Three-Dimensional Cell Culture Matrices: State of the Art. *Tissue Eng Part B*. **14** (1), 61–86 (2008).

9. Pampaloni, F., Reynaud, E. G. & Stelzer, E. H. K. The third dimension bridges the gap between cell culture and live tissue. *Nat Rev Mol Cell Biol*. **8** 839–845 (2007).

10. Hoffman, A. S. Hydrogels for biomedical applications. *Adv Drug Deliv Rev*. **64** 18–23 (2012).

11. Tibbitt, M. W. & Anseth, K. S. Hydrogels as extracellular matrix mimics for 3D cell culture. *Biotechnol Bioeng*. **103** (4), 655–663 (2009).

12. Didangelos, A., Yin, X., *et al.* Extracellular Matrix Composition and Remodeling in Human Abdominal Aortic Aneurysms: A Proteomics Approach.

Mol Cell Proteomics. **10** (8), 1–15 (2011).

13. Delany, J. P., Floyd, Z. E., *et al.* Proteomic Analysis of Primary Cultures of Human Adipose-derived Stem Cells: Modulation by Adipogenesis. *Mol Cell Proteomics*. **4.6** 731–740 (2005).

14. Eustace, B. K., Sakurai, T., *et al.* Functional proteomic screens reveal an essential extracellular role for hsp90α in cancer cell invasiveness. *Nat Cell Biol*. **6** (6), 507–514 (2004).

15. Kim, W., Park, B., *et al.* Wound healing effect of adipose-derived stem cells: A critical role of secretory factors on human dermal fibroblasts. *J Dermatol Sci*. **48** 15–24 (2007).

16. Lee, M. J., Kim, J., *et al.* Proteomic Analysis of Tumor Necrosis Factor-a-Induced Secretome of Human Adipose Tissue-Derived Mesenchymal Stem Cells. *J Proteome Res*. **9** 1754–1762 (2010).

17. Timms, J. F. & Cramer, R. Difference gel electrophoresis. *Proteomics*. **8** 4886–4897 (2008).

18. Hirsch, J., Hansen, K. C., *et al.* Proteomics: current techniques and potential applications to lung disease. *Am J Physiol - Lung Cell Mol Physiol*. **287** (1), L1–L23 (2004).

19. Issaq, H. J. Review The role of separation science in proteomics. *Electrophoresis*. **22** 3629–3638 (2001).

20. Reymond, M. A. & Schlegel, W. Proteomics in cancer. *Adv Clin Chem*. **44** (7), 103–142 (2007).

21. Baggerman, G., Vierstraete, E., Loof, A. De & Schoofs, L. Gel-Based Versus Gel-Free Proteomics: A Review. *Comb Chem High Throughput Screen*. **8** 669–677 (2006).

22. Gonzalez-Gonzalez, M., Jara-Acevedo, R., *et al.* European Journal of Pharmaceutical Sciences Nanotechniques in proteomics: Protein microarrays and novel detection platforms. **45** 499–506 (2012).

23. Espina, V., Woodhouse, E. C., Wulfkuhle, J., Asmussen, H. D., Petricoin, E. F. & Liotta, L. A. Protein microarray detection strategies: focus on direct detection technologies. *J Immunol Methods*. **290** 121–133 (2004).

24. Macbeath, G. Protein microarrays and proteomics. *Nat Genet*. **32** 526–532

(2002).

25. Krishhan, V. V, Khan, I. H. & Luciw, P. A. Multiplexed microbead immunoassays by flow cytometry for molecular profiling: Basic concepts and proteomics applications. *Crit Rev Biotechnol*. **29** (1), 29–43 (2009).

26. Adelow, C., Segura, T., Hubbell, J. A. & Frey, P. The effect of enzymatically degradable poly(ethylene glycol) hydrogels on smooth muscle cell phenotype. *Biomaterials*. **29** 314–326 (2008).

27. Liao, H., Munoz-pinto, D., Qu, X. & Hou, Y. Influence of hydrogel mechanical properties and mesh size on vocal fold fibroblast extracellular matrix production and phenotype. *Acta Biomater*. **4** 1161–1171 (2008).

28. Sawicki, L. A. & Kloxin, A. M. Light-mediated Formation and Patterning of Hydrogels for Cell Culture Applications. *J Vis Exp*. (115), e54462 (2016).

29. Sawicki, L. A. & Kloxin, A. M. Design of thiol–ene photoclick hydrogels using facile techniques for cell culture applications. *Biomater Sci*. **2** (11), 1612–1626 (2014).

30. Chen, L. B., Segal, R., Chen, L. B., Murray, A., Bushnell, A. & Walsh, M. L. Studies on Intercellular LETS Glycoprotein Matrices Studies on Intercellular Matrices. *Cell*. **14** 377–391 (1978).

31. Mao, Y. & Schwarzbauer, J. E. Stimulatory effects of a three-dimensional microenvironment on cell-mediated fibronectin fibrillogenesis. *J Cell Sci*. **118** (19), 4427–4436 (2005).

32. Finehout, E. J. & Lee, K. H. Comparison of automated in-gel digest methods for femtomole level samples. *Electrophoresis*. **24** 3508–3516 (2003).

33. Valente, K. N., Schaefer, A. K., Kempton, H. R., Lenhoff, A. M. & Lee, K. H. Recovery of Chinese hamster ovary host cell proteins for proteomic analysis. *Biotechnol J*. **9** 87–99 (2014).

34. Zheng, C. Y., Ma, G. & Su, Z. Native PAGE eliminates the problem of PEG–SDS interaction in SDS-PAGE and provides an alternative to HPLC in characterization of protein PEGylation. *Electrophoresis*. **28** 2801–2807 (2007).

35. Zustiak, S. P. & Leach, J. B. Hydrolytically degradable poly(ethylene glycol) hydrogel scaffolds with tunable degradation and mechanical properties. *Biomacromolecules*. **11** (5), 1348–1357 (2010).

36. Domon, B. & Aebersold, R. Options and considerations when selecting a quantitative proteomics strategy. *Nat Publ Gr*. **28** (7), 710–721 (2010).

37. Grayson, W. L., Ma, T. & Bunnell, B. Human Mesenchymal Stem Cells Tissue Development in 3D PET Matrices. *Biotechnol Prog*. **20** 905–912 (2004).

38. Twomey, J. D., Thakore, P. I., Hartman, D. A. & Hsieh, A. H. Roles of type VI collagen and decorin in human mesenchymal stem cell biophysics during chondrogenic differentiation. *Eur Cells Mater*. **27** 237–250 (2014).

39. Hayami, T., Ph, D., Lotz, J. C., Ph, D., Kapila, S. & Ph, D. Chondrogenic Differentiation of Human Mesenchymal Stem Cells in Three-Dimensional Alginate Gels. *Tissue Eng Part A*. **14** (5), 667–680 (2008).

40. Kollmer, M., Keskar, V., Hauk, T. G., Collins, J. M., Russell, B. & Gemeinhart, R. A. Stem Cell-Derived Extracellular Matrix Enables Survival and Multilineage Differentiation within Superporous Hydrogels. *Biomacromolecules*. **13** 963–973 (2012).

41. Keane, T. J., Swinehart, I. T. & Badylak, S. F. Methods of tissue decellularization used for preparation of biologic scaffolds and in vivo relevance. *Methods*. **84** 25–34 (2015).

42. Kloxin, A. M., Kasko, A. M., Salinas, C. N. & Anseth, K. S. Photodegradable Hydrogels for Dynamic Tuning of Physical and Chemical Properties. *Science*. **324** (5923), 59–63 (2009).

43. Bobick, B. E., Chen, F. H., Le, A. M. & Tuan, R. S. Regulation of the Chondrogenic Phenotype in Culture. *Birth Defects Res Part C*. **87** 351–371 (2009).

44. Park, H. W., Shin, J., Kim, C. & Osteoclast, B. Proteome of mesenchymal stem cells. *Proteomics*. **7** 2881–2894 (2007).

45. Discher, D. E., Mooney, D. J. & Zandstra, P. Growth Factors, Matrices, and Forces Combine and Control Stem Cells. *Science*. **324** 1673–1678 (2009).

46. Aggarwal, S. & Pittenger, M. F. Human mesenchymal stem cells modulate allogeneic immune cell responses. *Blood*. **105** (4), 1815–1823 (2005).

47. Derose, Y. S., Wang, G., *et al.* Tumor grafts derived from women with breast cancer authentically reflect tumor pathology, growth, metastasis and disease outcomes. *Nat Med*. **17** (11), 1514–1520 (2011).

48. Motaln, H., Schichor, C. & Lah, T. T. Human Mesenchymal Stem Cells and Their Use in Cell-Based Therapies. *Cancer*. **116** (11), 2519–2530 (2010).

49. Kyurkchiev, D., Bochev, I., *et al.* Secretion of immunoregulatory cytokines by mesenchymal stem cells. *World J Stem Cells*. **6** (5), 552–570 (2014).

50. Ranganath, S. H., Levy, O., Inamdar, M. S. & Karp, J. M. Harnessing the Mesenchymal Stem Cell Secretome for the Treatment of Cardiovascular Disease. *Cell Stem Cell*. **10** (3), 244–258 (2012).

51. Hackenberg, A. S. S., Froelich, A. R. K., Hagen, K. R. R. & Kleinsasser, N. Human Mesenchymal Stem Cells Promote Cancer Motility and Cytokine Secretion in vitro. *Cells tissues organs*. **198** 327–337 (2013).

52. Walter, M. N. M., Wright, K. T., Fuller, H. R., Macneil, S. & Johnson, W. E. B. Mesenchymal stem cell-conditioned medium accelerates skin wound healing: An in vitro study of fibroblast and keratinocyte scratch assays. *Exp Cell Res*. **316** (7), 1271–1281 (2010).

53. Kagiwada, H., Yashiki, T., Ohshima, A., Tadokoro, M. & Nagaya, N. Human mesenchymal stem cells as a stable source of VEGF-producing cells. *J Tissue Eng Regen Med*. **2** 184–189 (2008).

54. Zisa, D., Shabbir, A., Suzuki, G. & Lee, T. Vascular endothelial growth factor (VEGF) as a key therapeutic trophic factor in bone marrow mesenchymal stem cell-mediated cardiac repair. *Biochem Biophys Res Commun*. **390** (3), 834–838 (2009).

55. Wu, Y., Chen, L., Scott, P. G. & Tredget, E. E. Mesenchymal Stem Cells Enhance Wound Healing Through Differentiation and Angiogenesis. *Stem Cells*. **25** 2648–2659 (2007).

Chapter 4

UNDERSTANDING BREAST CANCER CELL CULTURE AND ACTIVATION IN RESPONSE TO EXTRACELLULAR CUES WITHIN BIOMIMETIC HYDROGEL MICROENVIRONMENTS

4.1 Abstract

Breast cancer reoccurs in approximately 20 percent of patients more than 5 years after successful treatment of the primary tumor and almost exclusively within a distant, metastatic tissue site.[1] It is hypothesized that the extracellular matrix (ECM) of these metastatic tissue sites regulates dormancy and recurrence of cancer as the initial microenvironment is remodeled over time upon aging or wounding.[2] *In vitro* culture models have been developed to investigate key factors in the ECM that regulate dormancy and recurrence;[3,4] however, the chemical and mechanical properties of these scaffolds are often difficult to control, so identifying individual or combinations of cues responsible for cell response proves challenging. Here, we have developed a fully synthetic three-dimensional (3D) cell culture scaffold with tunable chemical and mechanical properties to investigate breast cancer *in vitro*. Specifically, poly(ethylene glycol) (PEG)-based hydrogels containing cell-degradable peptide crosslinks and modified with receptor-binding peptides (RGDS, GFOGER, IKVAV) mimicking ECM proteins found within metastatic tissue sites were synthesized. Estrogen receptor negative (ER-, MDA-MB-231) and ER+ (T-47D) breast cancer cells were cultured within these environments to investigate response to individual or multiple mechanical and chemical cues. The size and shape of cell clusters formed within

microenvironments was monitored to assess activation for the different conditions. Additionally, the role of β1 integrin binding was investigated toward identifying interactions that may be responsible for regulation of response. These studies represent a novel approach to investigating breast cancer dormancy and recurrence *in vitro*.

4.2 Introduction

Late recurrence of metastatic breast cancer, more than five years after successful treatment of the primary tumor, is often difficult to detect and treat, resulting in poor prognosis for patients.[1] In order to successfully establish within a metastatic microenvironment, cells must enter the bloodstream, evade immune response during circulation, extravasate from blood vessels, and adhere within the new metastatic tissue microenvironment.[5,6] Cancer cells that metastasize but fail to properly adhere to the extracellular matrix (ECM) of metastatic tissue sites are hypothesized to form dormant tumor cells or micrometastases that recur at late times.[2] Subsequent changes in the composition of physical and chemical factors presented by the native ECM, with aging, wounding, or disease, are thought reactivate these quiescent cells or micrometastases, forming a new, proliferating tumor.[7,8] However, the critical factors in the ECM that regulate dormancy and reactivation remain poorly understood and must be identified to improve treatments to prevent late metastatic recurrence.

Toward understanding metastasis and recurrence, researchers have investigated breast cancer subtypes associated with different patient outcomes. Broadly, luminal and basal subtypes, expressing estrogen (ER), progesterone (PR), or human epidermal growth factor 2 (HER2) receptors, have different potentials for invasion, metastasis, and recurrence.[9,10] Basal, or triple negative subtypes (ER-, PR-, HER2-), tend to

metastasize and form new tumors immediately or at early times (< 5 years) after entering a new tissue site.[10,11] Luminal cancers, often ER+, while less aggressive, have been associated with late recurrence through the formation of dormant cells or micrometastases.[1,10,12] Cell lines derived from these tumor subtypes have been used to investigate behavior and response to treatment in two- and three-dimensional (2D, 3D) *in vitro* culture systems.[9,13,14] While subtype is an important factor to consider in diagnosing and treating disease, additional studies are needed to identify specific cell-ECM interactions that regulate tumor cell activity for the distinct subtypes.

Common sites for metastasis and recurrence, including the bone marrow, liver, and lungs, have distinct properties due to their different function in the body.[15–17] These metastatic niches present a complex milieu of chemical and physical cues that cells sense and respond to. ECM structure provides a 3D mechanical support for cells, made of insoluble proteins (e.g., collagen, laminin, fibronectin, elastin), glycosaminoglycans (e.g., hyaluronic acid), and proteoglycans (e.g., aggrecan) that form a fibrillar network with different mechanical properties based on tissue type and composition.[18,19] Young's modulus (E), which describes the stiffness of a material, has been reported for various metastatic tissue sites and range from soft (bone marrow, E ~ 600 Pa; liver, E ~ 640 Pa)[20,21] to stiff (lungs, E ~ 5,000-6,000 Pa).[21] Stiffness has been shown to play a role in regulating proliferation and growth of clusters and implicated in tumor cell dormancy.[22–24] Beyond structure, insoluble ECM proteins also provide binding sites that allow adhesion to the matrix, which have been shown to drive dormancy and activation through binding cellular integrins (e.g., $\alpha5\beta1$, $\alpha v\beta3$).[25] Additionally, niche cells (e.g., fibroblasts, human mesenchymal stem cells hMSCs), remodel this complex ECM with aging or wounding by degrading existing proteins,

depositing new proteins, and secreting small soluble factors (e.g. fibroblast growth factor FGF-2, transforming growth factor beta TGFβ).[26–29] Identification of critical mechanical and chemical factors present within this complex milieu that regulate cell response is required to understand mechanisms regulating dormancy.

Several *in vitro* models to study dormancy and recurrence in response to the metastatic ECM have been described. In a 2D model of dormancy, fibronectin and FGF-2 were shown to induce dormancy, but also maintain survival, through integrin α5β1.[4,30] Barkan, et al. reported that the addition of fibronectin and collagen to basement membrane extract (BME) for 3D cell culture maintained activation of breast tumor cells through integrin β1 signaling.[3,31] Lack of mechanical property control and differences between biochemical composition of these model systems and the native ECM make it challenging to identify key ECM signals that promote dormancy or activation. Synthetic materials scaffolds have gained increasing interest in recent years for the culture of cancer cells *in vitro*. The formation of tumor spheroids have been reported in several synthetic polymer-based scaffolds[22,32,33] and behavior related to metastasis and response to drug treatments match that observed *in vivo*. These synthetic scaffolds and seminal works on understanding dormancy *in vitro* motivate the need to develop a novel model of the metastatic tissue ECM to study breast cancer dormancy and recurrence.

Herein, we present a well-defined, synthetic 3D scaffold for the culture of breast cancer to investigate response to the presentation of key factors found within metastatic tissue ECM (Figure 4.1). Specifically, a poly(ethylene glycol) (PEG)-based hydrogel system with tunable mechanical properties has been modified with biochemical cues mimicking the ECM proteins collagen (GFOGER),

fibronectin/vitronectin (RGDS), and laminin (IKVAV), found within metastatic tissues. MDA-MB-231 (ER-) and T-47D (ER+) breast cancer cells have been encapsulated within discrete environments, and their response quantified. Toward understanding activation within these microenvironments, we have investigated the effects of matrix density and single or combinations of peptides on activation during culture. Additionally, the role of integrin β1 in regulating activation within select conditions has been studied. This 3D synthetic material system represents a novel approach to investigate breast cancer activity within an *in vitro* model system, and a primary investigation of cancer cell response to different mixtures of chemical signals within soft and stiff synthetic 3D substrates.

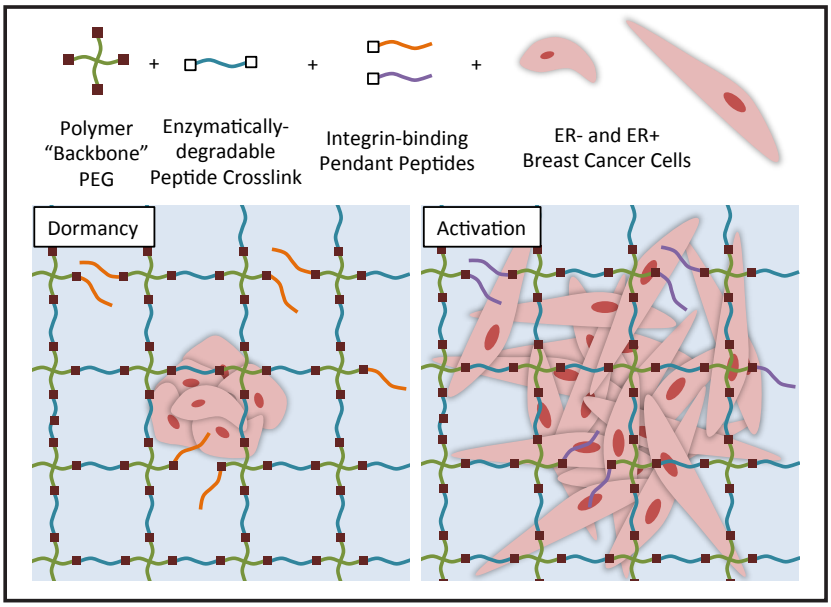

Figure 4.1: **General schematic of breast cancer culture in hydrogels.** Synthetic PEG-based hydrogel scaffolds with well-defined chemical and mechanical properties will be used to probe for key factors present within the microenvironment that regulate dormancy and activation of metastatic breast cancers.

4.3 Materials and Methods

4.3.1 Macromer and Initiator Synthesis

Macromers for hydrogel formation were synthesized using previously-described methods.[34,35] 4-arm poly(ethylene glycol) thiol (PEG4SH, 20 kDa MW), the "backbone" within the hydrogel structure, providing a reactive free thiol, was synthesized via a 3-step reaction. Peptides containing alloxycarbonyl (alloc)-protected lysines, providing a reactive vinyl, were synthesized via solid phase peptide synthesis (MBHA rink amide resin, Novabiochem; Chemmatrix, Protein Technologies) on a Protein Technologies PS3 synthesizer using Fmoc chemistry. Synthesis of the enzymatically-degradable crosslink Ac-K**K(alloc)**G[GPQG↓IWGQ]G**K(alloc)**K (Pep2Alloc) and pendant peptides **K(alloc)**$(PEG_2)_2$W(PEG_2)IKVAV (laminin mimic, IKVAV), **K(alloc)**GWGRGDS (fibronectin/vitronectin mimic, RGDS), **K(alloc)**G$(POG)_4$FOGERG$(POG)_4$G (collagen mimic, GFOGER) were confirmed via mass spectrometry. The photoinitiator, lithium acylphosphinate (LAP), to generate radicals for polymerization, also was synthesized as described.

4.3.2 Hydrogel Synthesis and Characterization

Hydrogels were polymerized for mechanical and biochemical characterization as previously-described.[34,35] Briefly, PEG4SH, Pep2Alloc, and pendant peptides (IKVAV, RGDS, or GFOGER) were dissolved in phosphate buffered saline (PBS) supplemented with 1% penicillin streptomycin (PS, Invitrogen) and 0.5 μg/mL fungizone (FZ, Invitrogen). Gel precursor solution, containing 6, 8, or 10 percent PEG by weight (wt%), was prepared by mixing PEG4SH with 2 mM pendant peptides and stoichiometric ratios of Pep2Alloc (final [SH] = [Alloc]). Precursor was pipetted into the tip of a cut syringe (1 mL) or sandwiched between glass slides, coated with Rain-

X, and spaced with a 0.254 mm gasket. Collimated light at 365 nm and 10 mW/cm^2 (Inpro Technologies collimating adaptor, Exfo Omnicure Series 2000) was applied for 1-5 min to polymerize gels. After polymerization, gels were removed from syringe tips or slides and placed in appropriate buffer (PBS, growth medium, Ellman's reaction buffer) for subsequent analysis.

To evaluate the mechanical properties of gels, modulus measurements were performed on 6, 8, and 10 wt% gels containing 2 mM RGDS, polymerized for 5 minutes, and swollen overnight in culture medium at 37 °C. Gels were placed between parallel plates on a TA AR-G2 rheometer and compressed to 0.25 N normal force to prevent slip. Strain- and frequency-sweeps were performed to determine the linear viscoelastic regime, and 5% strain and 5 rad/s frequency were selected to perform swollen modulus measurements (n = 4 gels).

To evaluate the incorporation of different pendant peptides in gels, Ellman's assay was performed to check free thiol concentration post-polymerization, as previously-described.[34,35] Here, 10 wt% gels polymerized with 2 mM of RGDS, GFOGER, or IKVAV were evaluated (n = 3 gels).

4.3.3 Cell Culture and Collection

MDA-MB-231 and T-47D breast cancer cells were cultured on tissue culture poly(styrene) in DMEM (Corning Cellgro) supplemented with 10 % v/v fetal bovine serum (FBS, Invitrogen) and 1% PS. Growth medium was replaced every 48-72 hours during culture. At 80% confluency, cells were passaged (1:4) or collected for experiments. Specifically, to collect cells for experiments, cells were removed from plates (trypsin/EDTA, 5 minutes, Corning Cellgro), counted via hemocytometer, and aliquotted for the desired number of cells based on the experiment and conditions. The

aliquots were centrifuged (1200 rpm, 3 minutes) and the cell pellet retained for subsequent treatment with blocking antibodies or mixture with hydrogel precursor for encapsulation (described below).

4.3.4 β1 Blocking

Antibody, AIIB2 (rat, DSHB; deposited by C.H. Damsky), was used to block β1 integrin on the surface of T-47D and MDA-MB-231 cells harvested for encapsulation experiments. Prior to encapsulation, cell aliquots were suspended in DMEM containing 100 μg/mL AIIB2 antibody and incubated for 1 hour at 37 °C. Aliquots were centrifuged (1200 rpm, 3 min) and the cell pellet was resuspended in hydrogel precursor for encapsulation (described below). Growth medium supplemented with 100 μg/mL AIIB2 was replaced every 48-72 hours during culture of β1-blocked cells.

4.3.5 Cell Encapsulation

Cell encapsulation was performed as previously described, and with modification to minimize nutrient gradients for long-term culture.[34,35] MDA-MB-231 and T-47D cells were collected, centrifuged, and re-suspended in gel precursor (6 or 10 wt%, 2 mM total pendant peptide) at 5000 cells/μL. For viability experiments, cell suspensions were pipetted into the tips of sterile cut syringes (20 μL) and irradiated with light (365 nm, 10 mW/cm^2) for 1 min. Post-polymerization, gels were placed in a sterile, untreated 48-well plate and rinsed with fresh culture medium. Culture medium was replaced every 48-72 hours.

To prevent potential gradient effects from encapsulation in thick (20 μL) gels during long culture periods, cells were encapsulated with the following method: *i)* 15

μL of cell-free gel precursor was polymerized in a sterile, cut syringe tip mold (1 min, 365 nm, 10 mW/cm^2), and *ii)* 5 μL of cells suspended in gel precursor (5000 cells/μL) was pipetted on top of the 15 μL base and polymerized with a second dose of light (1 min, 365 nm, 10 mW/cm^2). Post-polymerization, gels were placed in sterile, untreated 48-well plates with the cell layer on top and rinsed with fresh culture medium. Culture medium was replaced every 48-72 hours during the course of experiments. This "on-top" encapsulation method was used for immunostaining experiments investigating cell response to matrix density, individual and peptide combinations, a culture time course, and β1 blocking.

4.3.6 Viability Assays

Viability of MDA-MB-231 and T-47D cells encapsulated in hydrogels was determined using a live/dead viability/cytotoxicity kit (Invitrogen). Cells were encapsulated in 6 and 10 wt% gels containing 2 mM RGDS and cultured for 1 and 3 days (n = 3). At day 1 and 3, gels were rinsed of medium (3 x 10 min, PBS), stained (1 x 45 min, 4 μM ethidium homodimer, 2 μM calcein AM in PBS), and rinsed (3 x 10 min, PBS). Samples were immediately imaged on a Zeiss LSM 780 confocal. Three z-stacks (100 images per stack, 2 μm spacing) were taken per gel (n = 3), for a total of 9 images. To quantify percent viability, live (green) and dead (red) cells were counted in each image z-projection.

4.3.7 Immunostaining Experiments

3D immunostaining experiments were conducted to investigate cell response within synthetic microenvironments. Blocking and permeabilization solutions were prepared fresh: BPSoln1 (3% w/v bovine serum albumin/BSA + 0.05% v/v Triton-X

in PBS) and BPSoln2 (5% BSA w/v + 0.1% v/v Triton-X in PBS). At select time points during culture, encapsulated ("on-top") cells were rinsed (2 x 5 min, PBS) and fixed (1 x 15 min) in 4% paraformaldehyde (PFA) in PBS. PFA was removed, gels were washed (1 x 5 min PBS, 2 x 5 min BPSoln1), and the fixed cells were permeabilized and blocked (1 x 60 min, BPSoln2). After blocking, cells were incubated overnight at 4 °C with primary antibodies (Ki-67, Abcam, 1:100 dilution) in BPSoln2. The next day, gels were rinsed (3 x 60 min, BPSoln1) and incubated with secondary antibodies Alexa Fluor 488 goat-anti-mouse (ThermoFisher, 1:300 dilution) and F-actin (Sigma Aldrich, 1:250 dilution) in BPSoln2 overnight at 4 °C, protected from light. On the final day of immunostaining, gels were rinsed (3 x 45 min, BPSoln1) and incubated with DAPI (700 nM in PBS) for 1 hour. Gels were rinsed (3 x 30 min, PBS) and stored at 4 °C in PBS, protected from light, until imaging.

Cells cultured in different environments (Table 4.1, list of conditions) were immunostained to investigate cell response to the following: *A)* Matrix density, cells cultured for 10 days; *B)* single and combinations of peptides, cells cultured for 10 days; *C)* time course, cells cultured for 3, 10, 20, 30, and 40 days; and D) β1 blocking, cells cultured for 10 days. After immunostaining, gels were imaged on a Zeiss LSM 800 confocal. Three z-stack images (100 images per stack, 2 μm spacing) were taken per gel (n = 3), for a total of 9 images. Images were analyzed in Volocity and MATLAB as described in 1.3.8.

Table 4.1: **Conditions examined for immunostaining encapsulation experiments.** For each experiment, 3 gels were formed per condition (n = 3). All gels were polymerized for 1 minute with light at 365 nm and 10 mW/cm^2 and cells were encapsulated at 5000 cells/μL, confined within a 5 μL top gel layer.

Condition Number	GFOGER (mM)	RGDS (mM)	IKVAV (mM)	Weight % PEG	Experiment
1	2	0	0	6	A, B, C, D
2	2	0	0	10	A
3	0	2	0	6	A, B, D
4	0	2	0	10	A
5	0	0	2	6	A, B, C
6	0	0	2	10	A
7	0	0	0	6	B
9	0.25	0.25	1.5	6	B
10	0.1	0	1.9	6	B
11	0	0.1	1.9	6	B
12	0.05	0.05	1.9	6	B

4.3.8 Volocity and MATLAB Imaging Analysis

Z-stack images were initially processed in Volocity 3D imaging analysis software. Specifically, the shape and size of clusters and cells was determined by analysis of the cytoskeleton (stained for F-actin). Clusters and cells were identified by finding objects in the red channel. Filters to close and fill holes in the object were applied to improve the precision of volume measurements. A noise filter (medium) was added to smooth the surface of clusters and cells for more accurate surface area measurements. Additionally, touching objects were separated and objects touching the edges of the image or with volume less than 1000 μm^3 (debris) were excluded. The volume, surface area, and shape factor of each cell or cluster in each image was reported.

MATLAB was used to count and bin the cluster/cell data from Volocity into discrete sub-groups based on shape factor or volume to identify conditions in which cells remain active. To evaluate cell spreading and protrusions within different matrix conditions, the number of cells and cell clusters were counted for the following shape factor (SF) groups: *I)* SF > 0.8; *II)* 0.75 < SF ≤ 0.8; *III)* 0.7 < SF ≤ 0.75; *IV)* 0.65 < SF ≤ 0.7; *V)* 0.6 < SF ≤ 0.65; *VI)* 0.55 < SF ≤ 0.6; *VII)* 0. 5 < SF ≤ 0.55; and *VIII)* 0.5 ≤ SF; where shape factor = 1 is a perfect sphere. To compare cell and cell cluster size within different conditions, the number of cells and clusters were counted for the following volumes (V): *I)* V < 25,000 μm^3, small, 1-5 cell clusters; *II)* 25,000 ≤ V < 50,000 μm^3, medium, 5-10 cell clusters; *III)* 50,000 ≤ V < 75,000 μm^3, large, 10-15 cell clusters; and *IV)* V ≥ 75,000 μm^3, extra large, greater than 15 cell clusters. Volume groups were based on the approximate volume of a single cell, 5,000 μm^3, as determined by analysis of single cell volume from live/dead images taken at Day 1 (T-47D: 4900 ± 100, 5900 ± 200; MDA-MB-231: 5400 ± 100, 4300 ±100 μm^3 in 6 and 10 wt% gels, respectively). The counts for each image per condition were averaged and standard error values calculated.

4.4 Results and Discussion

4.4.1 Hydrogel Mechanical Properties and Composition Controlled to Mimic the Metastatic Tissue ECM

PEG-based hydrogel scaffolds offer users a high level of control over matrix mechanical and chemical properties. Several ways in which mechanical properties may be tuned include adjusting the macromer molecular weight, which alters distance between crosslinks, or changing macromer concentration, which changes matrix density. In both cases, the pore size of the network is altered which corresponds to

different material modulus, or stiffness, where high modulus is associated with small pore size (low macromer molecular weight or high macromer concentration).[36–38] However, it is important to note that small pore size may restrict growth of the cells post-encapsulation, resulting in lower viability during long-term culture. To prevent this, enzymatically-degradable peptide crosslinks are incorporated within networks, which locally degrade with the secretion of various matrix metalloproteinases (MMPs).[39]

The bulk mechanical properties of common metastatic tissue sites range from soft (bone marrow, liver, E ~ 600, 640 Pa) to stiff (lungs, E ~ 5000-6000 Pa).[20,21] To capture these properties, macromer concentration was varied within hydrogels and modulus was characterized after swelling in culture medium. The moduli of swollen 6, 8, and 10 wt% (with respect to PEG) gels crosslinked with an enzymatically-degradable peptide (GPQG↓IWGQ) and containing 2 mM RGDS were measured at 37 °C with parallel-plate rheology. 6 wt% gels had the lowest moduli (E ~ 3G) at 702 ± 85 Pa, and 8 and 10 wt% gels had higher moduli at 2683 ± 508 Pa and 6184 ± 381 Pa, respectively. These moduli are within the range of reported metastatic tissue ECM moduli (Figure 4.2 A). In subsequent studies, we investigate the effects of the 6 wt% and 10 wt% gels, mimetic of the bone marrow, liver, and lung, on cell response during culture.

In addition to control over the mechanical properties, synthetic hydrogels provide a bioinert network that may be modified with chemical cues to impart biological activity. Individual or multiple cues may be added to the network at precise concentrations so the effects of single or multiple factors may be discerned in simple to complex environments. Short amino acid sequences derived from proteins

(peptides) that bind receptors on the surface of cells (e.g., integrins) have been identified and used in hydrogel scaffolds to promote adhesion and control cell fate in 3D. While numerous, we selected three peptide sequences that are widely used to mimic collagen, fibronectin/vitronectin, and laminin, the most prevalent proteins within metastatic tissue ECM that also play a role in wounding/aging.

The collagen mimic, GFOGER, which primarily targets integrins α1β1 and α2β1,[40] was synthesized containing an allyloxycarbonyl-protected lysine (K(alloc)) to allow covalent incorporation within the network and $(POG)_n$ repeat units, which help with assembly into triple helices. The peptide was purified with HPLC and mass spectrometry confirmed the peptide molecular weight, 3152 g/mol. RGDS, a mimic of fibronectin, vitronectin and other proteins, has been broadly used to promote adhesion to bioinert scaffolds through binding integrins αvβ3 (strongest), α5β1, α8β1, αvβ1, αvβ5, αvβ6, αvβ8, and αIIbβ3,[41,42] was synthesized with K(alloc) for pendant incorporation. The molecular weight of 946 g/mol was confirmed after purification. Finally, IKVAV, a mimic of laminin that primarily targets the laminin receptor[43] was built with a K(alloc) for pendant attachment and $(PEG)_2$ repeat units to improve solubility due to the presence of hydrophobic isoleucine, valine, and alanine amino acid residues. The molecular weight, 1363 g/mol, was confirmed after purification.

Differences in hydrophilicity, net charge, assembly, and size (steric hindrance to access alloc groups) of peptides may affect their covalent attachment to PEG-based networks and thus the observed response. To determine if the peptides built here have similar levels of attachment within hydrogels, we quantified free thiol concentration after polymerization of 10 wt% gels containing 2 mM GFGOER, RGDS, or IKVAV. After polymerization (1 min light, 365 nm, 10 mW/cm^2), gels were rinsed and swollen

in Ellman's reaction buffer. Quantitative Ellman's assay was run on whole gels, and the free thiol concentration determined (Figure 4.2 B). No significant difference in the concentration of free thiols ($p > 0.05$) post-polymerization was observed indicating similar levels of attachment for all peptides.

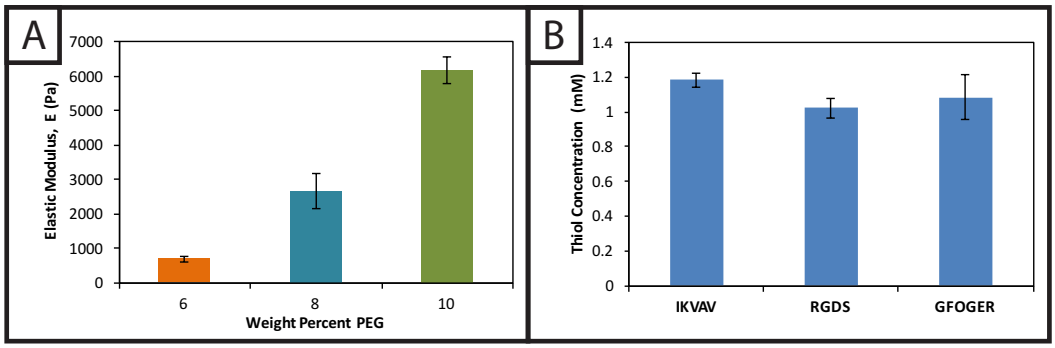

Figure 4.2: **Mechanical and chemical properties of PEG hydrogel scaffolds. A)** The elastic modulus of hydrogels was tuned to mimic the bulk mechanical properties of common metastatic tissue sites (bone marrow ~ 600 Pa; liver ~ 640 Pa; lungs ~ 5000-6000 Pa). Specifically, the concentration of PEG and peptide macromers was varied to achieve soft and stiff substrates. The 6 wt% gel modulus of 702 ± 85 Pa is mimetic of the bone marrow and liver, where the 10 wt% gel modulus of 6184 ± 381 Pa is mimetic of the lung. These two moduli will be investigated in subsequent studies. **B)** Multiple peptides will be investigated to identify cancer response, however, their attachment must be consistent to ensure similar concentrations of binding sites are available to encapsulated cells. Ellman's assay confirmed similar levels of free thiols in gels post-encapsulation ($p > 0.05$) indicating consistent attachment of IKVAV, RGDS, and GFOGER peptides.

4.4.2 T-47D and MDA-MB-231 Breast Cancer Cells Remain Viable Post-Encapsulation in PEG-Based Hydrogels

Cancer subtype has been associated with different behavior post-metastasis, with ER- tumors exhibiting aggressive behavior and early recurrence while ER+

tumors form distant metastases that recur at late times. Previous studies investigating dormancy and recurrence in *in vitro* and *in vivo* models have used a variety of different cell lines belonging to ER+ (e.g., D2.0R, MCF-7, K7M2-AS.46, CK5-, ZR75-1, BT474, T-47D) and ER- (e.g., D2A1, MDA-MB-231, K7M2, EWD8, SUM149, SUM159, MDA-MB-453, T4-2) subtypes.[7,44–46] For our culture experiments, we selected the MDA-MB-231 (ER-) and T-47D (ER+) lines to investigate activation within 3D synthetic matrices.

Light and radical-based polymerizations for cell encapsulations have shown to negatively affect cell viability in some cell lines.[47,48] Thus, light dose (intensity and wavelength), concentration of photoinitiator, and polymerization should be minimized to reduce their effects on cells. Long wavelengths of UV (~365 nm) at low intensity (~6 – 10 mW/cm^2) have been shown cytocompatible, with negligible damage to cells (membrane, p53 expression) for radical polymerizations occurring in under 10 minutes.[47,49] The gel-based system used here forms gels in under 10 minutes and has demonstrated high viability with the encapsulation of hMSCs.[34,35] To determine if T-47D and MDA-MB-231 cells remain viable post-encapsulation, we encapsulated cells in 6 and 10 wt% gels crosslinked with degradable peptides and containing 2 mM RGDS, polymerized for 1 minute. At 1 and 3 days post-encapsulation, cells were stained with a live/dead viability/cytotoxicity kit, imaged, and viable cells counted in each 3D image (Figure 4.3, n = 3 gels, 3 images per gel). At day 1, 98 ± 1 % T-47D and 93 ± 1 % MDA-MB-231 cells were viable in 6 wt% gels and 88 ± 2 % T-47D and 77± 3 % MDA-MB-231 cells were viable in 10 wt% gels, indicating minimal initial impact on viability. We hypothesize that the slightly decreased viability in the 10 wt% conditions at day 1 is due to the higher concentration of macromer, which may result

in more radicals proximate to the cell surface or constriction by the matrix during polymerization. After 3 days, the cells were viable at 99 ± 1 % (T-47D, 6 wt%), 95 ± 1 % (MDA-MB-231, 6 wt%), 98 ± 1 % (T-47D, 10 wt%), and 92 ± 1 % (MDA-MB-231, 10 wt%). The higher viability at day 3 may be attributed to the survival of cells that were viable at day 1 with minimal death due to encapsulation within the gel. These viability data are comparable to similar photoinitiated systems[49] and what was observed for hMSCs.

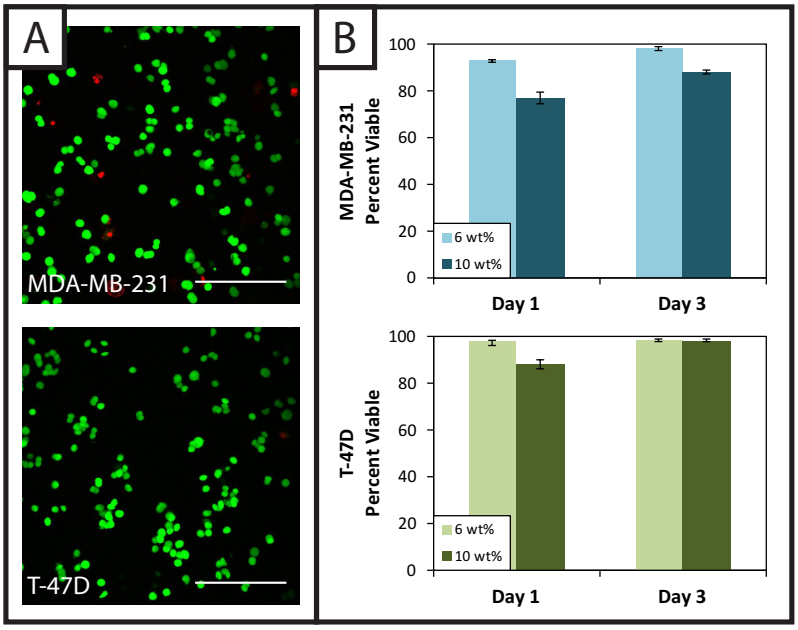

Figure 4.3: **Viability of MDA-MB-231 and T-47D breast cancer cells post-encapsulation. A)** MDA-MB-231 and T-47D breast cancer cells were encapsulated within hydrogels and cultured for 1 and 3 days. Live/dead viability/cytotoxicity stained-cells were imaged and live (green, no membrane damage) and dead (red, nucleus) cells were counted to quantify percent viability. Example images are from 6 wt% gels at D1, 200 μm scale bar. B) Greater than 70% viability was observed for all conditions at D1, with the highest viability in 6 wt% conditions. Cells that survived initial encapsulation remained largely viable within the conditions, corresponding to the increased levels of viability observed at day 3, with all lines greater than 90% viable.

Hypoxia and nutrient-deprivation have been reported in 3D culture systems with thick cell-gel constructs used for long-term cultures, which can affect cell viability and response.[50,51] To determine if this occurs in the described material system, we cultured cells in 20 μL gels or gels with a 15 μL cell-free base and 5 μL top containing cells for 10 days (10 wt%, 2 mM RGDS). At day 10, cells were immunostained and different regions in the gels imaged to determine if any nutrient

gradients or hypoxia may exist. Cells at the base and center of the 20 μL gels exist as single cells or small clusters of cells, especially for T-47D cells, whereas larger clusters and cell spreading is observed at the top of the gels. Cells encapsulated in the "on top" gels exhibit consistent morphologies through the depth of the 5 μL layer (~200 μm), so this technique will be applied in future culture experiments (Supplementary Information, Figure 4.9).

4.4.3 Synthetic Networks with High Matrix Density Restrict Cancer Cell Growth and Activity

While often considered simplified as a culture model when compared to naturally-derived substrates or *in vivo* models, one benefit of synthetic material scaffolds is the ability to independently control their mechanical and chemical properties.[52] Loessner, et al. have described the culture of ovarian cells in a PEG-based hydrogel, which permits the formation of large spheroids in soft environments (G' = 241 ± 19 Pa; comparable to our 6 wt% gels), while stiffer matrices slowed proliferation and smaller spheroids formed.[22] Toward investigating the activity of breast cancer cells within our material system, we first investigated the effects of matrix density on breast cancer cell activation within discrete microenvironments containing GFOGER, RGDS, and IKVAV peptides.

T-47D and MDA-MB231 cells encapsulated in 6 and 10 wt% gels containing 2 mM GFOGER, RGDS, or IKVAV were cultured for 10 days and immunostained (Figure 4.4). Size and morphology of clusters and cells formed during culture were analyzed in Volocity and MATLAB to identify differences in activation within these discrete microenvironments of different modulus. In section 4.4.4, we will discuss the effects of different peptides on activation in depth, but to provide context for results

here, cells exhibit active behavior (large clusters = T-47D, irregular shape = MDA-MB-231) in the RGDS and GFOGER conditions cells when compared to the IKVAV condition (small clusters = T-47D, spherical morphology = MDA-MB-231).

Between the 6 and 10 wt% environments, the ER- MDA-MB-231 cell line remains primarily as small clusters (1-5 cells, Supplementary Information, Figure 4.10 A), with low percent of medium, large, and extra large clusters in each condition. Notably, the shape of cells and clusters in the 6 wt% microenvironment is highly irregular, with ~70-80% of cells having a shape factor less than 0.7 in the RGDS and GFOGER conditions. A more spherical morphology is observed in the 10 wt% environment, with ~50-60% of cells in the GFOGER and RGDS conditions having a shape factor greater than 0.7 (Figure 4.4 A). Although spheroids primarily form within gels containing IKVAV, ~60% of cells have a shape factor less than 0.75 in 6 wt% versus 40% of cells in 10 wt% conditions, indicating decreased activity may occur within the 10 wt% microenvironments. However, for other encapsulations in 6 wt% gels with 2 mM IKVAV (sections 4.4.4, 4.4.5), we have observed ~40 % of cells with a shape factor less than 0.75, indicating that the behavior observed in the IKVAV condition may ultimately depend on different interactions of cells with this biochemical factor as opposed to matrix density effects. T-47D, which are generally less aggressive, exhibit a spherical morphology in both the 6 and 10 wt% conditions (Supplementary Information, Figure 4.10 B), with no specific trend related to matrix density. However, in the 6 wt% gels containing RGDS or GFOGER, ~35-50% of clusters are classified in the medium (5-10 cells), large (10-15 cells), and extra large (>15 cells) clusters groups as opposed to ~25-30% of clusters in the 10 wt% gels (Figure 4.4 B). Taken together, these data would indicate that high matrix density

might restrict cluster growth within 10 wt% microenvironments. In subsequent studies, we focus on the permissive, 6 wt% condition to evaluate the effects of different peptides on activation due to the most distinct cell response and highest levels of activation observed within these networks.

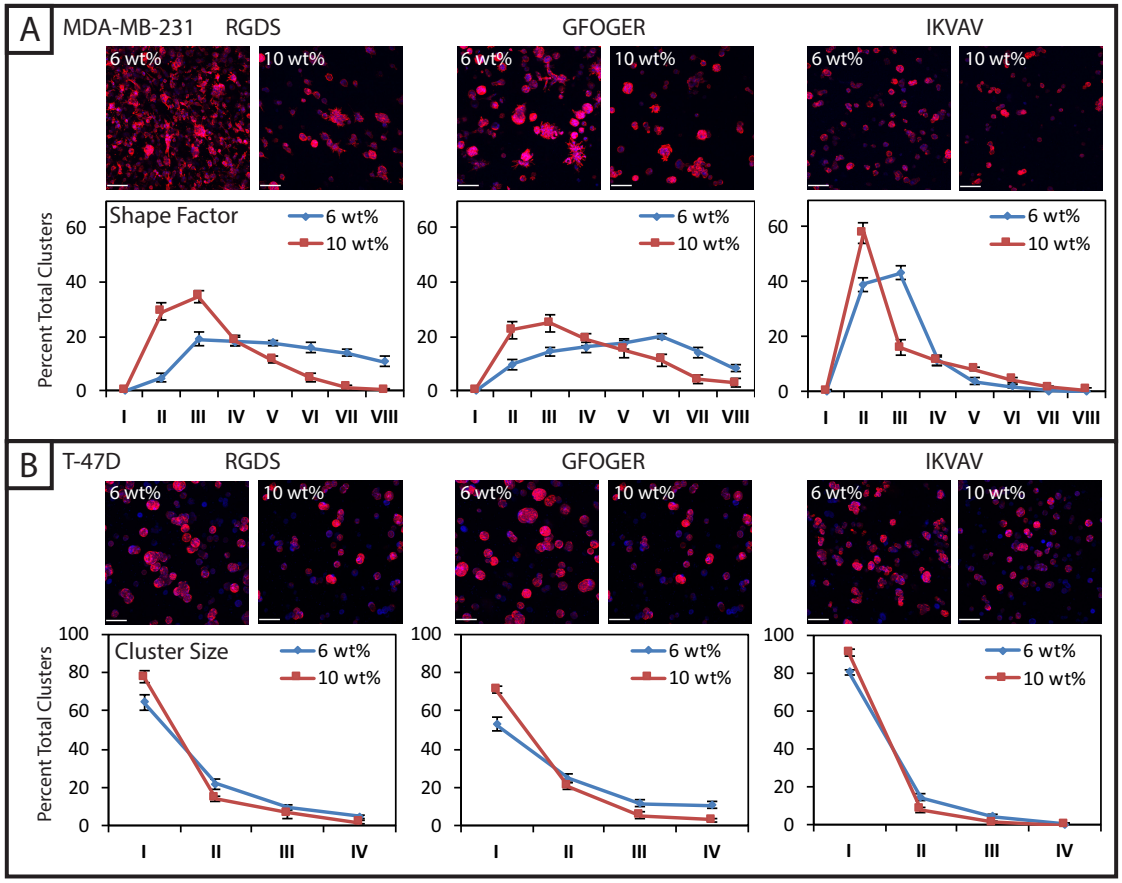

Figure 4.4: **Matrix density effects on cancer cell response during culture. A)** MDA-MB-231 cells spread within 6 wt% gels containing RGDS and GFOGER with high irregularity (low shape factor, toward VIII), while the 10 wt% matrix restricts growth and more spherical clusters form with fewer protrusions (high shape factor, toward I). Generally more spherical in the IKVAV condition, only slight irregularity is observed in the 6 wt% condition compared to the 10 wt% condition. **B)** T-47D cells remain largely spherical during culture in all gel conditions. However, slightly larger clusters form within the 6 wt% gels compared to the 10 wt% gels indicating matrix density may restrict cluster growth. Z-projection images shown with scale bars =100 μm, F-Actin = red, DAPI = blue. **Shape factor** I) SF > 0.8, II) 0.75 < SF ≤ 0.8, III) 0.7 < SF ≤ 0.75, IV) 0.65 < SF ≤ 0.7, V) 0.6 < SF ≤ 0.65, VI) 0.55 < SF ≤ 0.6, VII) 0. 5 < SF ≤ 0.55, and VIII) 0.5 ≤ SF; **Cluster Size** I) V < 25,000 μm^3, II) 25,000 ≤ V < 50,000 μm^3, III) 50,000 ≤ V < 75,000 μm^3, and IV) V ≥ 75,000 μm^3.

4.4.4 Collagen and Fibronectin/Vitronectin Mimetic Peptides Permit Cancer Cell Spreading and Cluster Growth within Synthetic Microenvironments

Proteins and factors to which cells bind within metastatic microenvironments are thought to be key in the process of dormancy and reactivation of breast cancer. Researchers have found that remodeling of the ECM and changes in protein composition due to wounding or aging tissues environment promote the reactivation of dormant tumor cells.[2] Specifically, various studies have shown that increased deposition of fibronectin and collagen I, and secretion of soluble factors like TGFβ, which also stimulates collagen deposition by niche cells,[53] creates a permissive environment for recurrence.[3,31,54] Here, we investigated the response of cancer cells to individual and multiple receptor-binding ligands (RGDS, GFOGER, and IKVAV), mimicking key proteins within metastatic tissue ECM, incorporated within soft matrices (6 wt%).

Focusing first on response to individual peptide sequences, 2 mM of RGDS, GFOGER, or IKVAV, were polymerized with cells in 6 wt% hydrogels and stained after 10 days in culture. Notable differences in the shape of MDA-MB-231 cells in response to the different peptides was observed (Figure 4.5 A). In the IKVAV condition, cells are spherical with the ~80 % of clusters in all images having a shape factor greater than 0.7. In both RGDS and GFOGER conditions, cells are more irregular with ~80-90% of cells having a shape factor less than 0.7. While MDA-MB-231 cells remain primarily as small clusters for all conditions, there are slight increases in the percent of medium, large, and extra large clusters in the RGDS and GFOGER conditions. This indicates that integrin binding and adhesive sites presented by RGDS and GFOGER ligands in matrices provide an activating environment for MDA-MB-231 cells. Little to no difference in the shape and size of T-47D clusters is

observed, with primarily spherical morphology (~80% SF > 0.7) and large clusters (~30-50% medium-extra large) identified in all conditions (Figure 4.5 B). We hypothesize that cluster formation and growth of T-47D cells may result from different interactions of this cell type within synthetic networks, resulting in lower activation (Figure 4.5 B).[13,55] Finally, we also investigated a condition with no peptide and observed similar response to the IKVAV condition with MDA-MB-231 and all conditions with T-47D, indicating that cell-matrix interactions may play a critical role in activation (Supplementary Information, Figure 4.11).

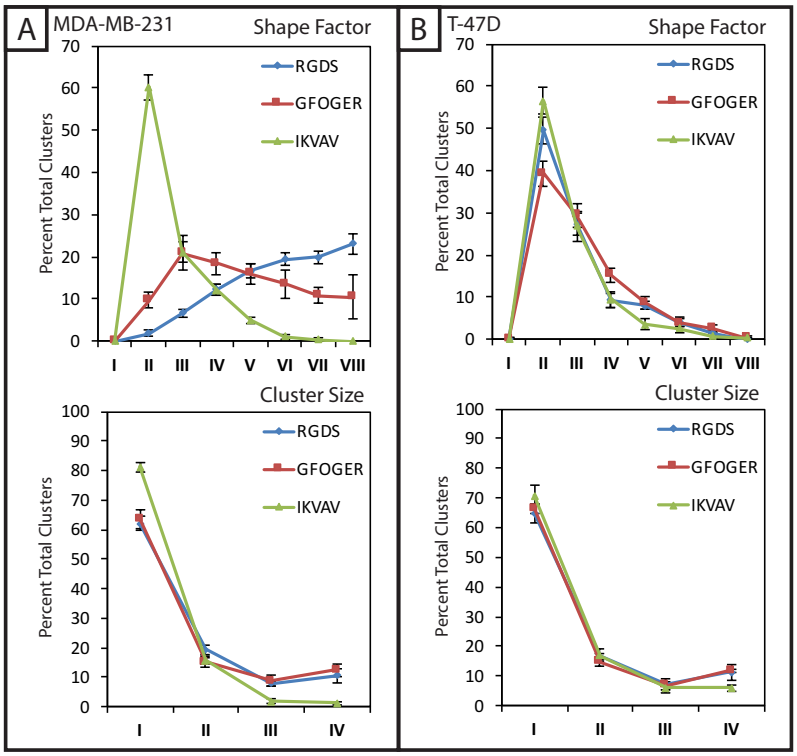

Figure 4.5: **Response of MDA-MB-231 and T-47D to the presentation of individual peptide cues in 6 wt% gels. A)** MDA-MB-231 are highly irregular within the RGDS and GFOGER conditions, but remain primarily spherical within the IKVAV condition. This indicates that binding to the matrix and activity occurs within the RGDS and GFOGER conditions while less activity occurs within the IKVAV condition. Additionally, clusters with high volume (Cluster Size, III and IV) form within the GFOGER and RGDS conditions further supporting that cells are active within these microenvironments. **B)** T-47D clusters remain largely spherical within environments indicating less activity and cellular response to the presentation of different chemical binding groups. No significant difference in cluster size for these conditions is observed, further indicating T-47D survival and cluster growth may depend on different interactions within synthetic microenvironments. **Shape factor** I) $SF > 0.8$, II) $0.75 < SF \leq 0.8$, III) $0.7 < SF \leq 0.75$, IV) $0.65 < SF \leq 0.7$, V) $0.6 < SF \leq 0.65$, VI) $0.55 < SF \leq 0.6$, VII) $0.5 < SF \leq 0.55$, and VIII) $0.5 \leq SF$; **Cluster Size** I) $V < 25{,}000\ \mu m^3$, II) $25{,}000 \leq V < 50{,}000\ \mu m^3$, III) $50{,}000 \leq V < 75{,}000\ \mu m^3$, and IV) $V \geq 75{,}000\ \mu m^3$.

Native tissue is inherently complex, containing mixtures of proteins with which cells interact. RGDS, GFOGER, and IKVAV peptides target specific cellular integrins and receptors, thus combinations of these peptides or other factors may need to be incorporated within environments to observe different responses. To determine whether combinations of multiple receptor-binding peptides within culture might alter cell response, we investigated various conditions inspired by the increased levels of collagen and fibronectin found within wounded and aging tissues. Specifically, conditions rich in IKVAV containing low concentrations of RGDS and GFOGER were examined (Table 4.1, Experiment B). MDA-MB-231 cells responded to the presence of the lowest levels of RGDS and GFOGER in IKVAV (conditions 10-12), with ~50-60% of cells having a shape factor less than 0.7, indicating activation. The most pronounced response was observed in condition 9, where ~85% of cells have a shape factor less than 0.7, comparable to the RGDS-only condition, indicating that response may also depend on ligand concentration (Figure 4.6 A). As previously observed, T-47D cells exhibited little activation within these microenvironments, indicating that the particular mixture of receptor-binding ligands studied here elicits minimal response (Figure 4.6 B). In future studies, other receptor-binding peptides or soluble factors secreted by niche cells (e.g., hMSCs, fibroblasts) may be investigated to identify critical factors that regulate response from T-47D and other ER+ cancer cells.

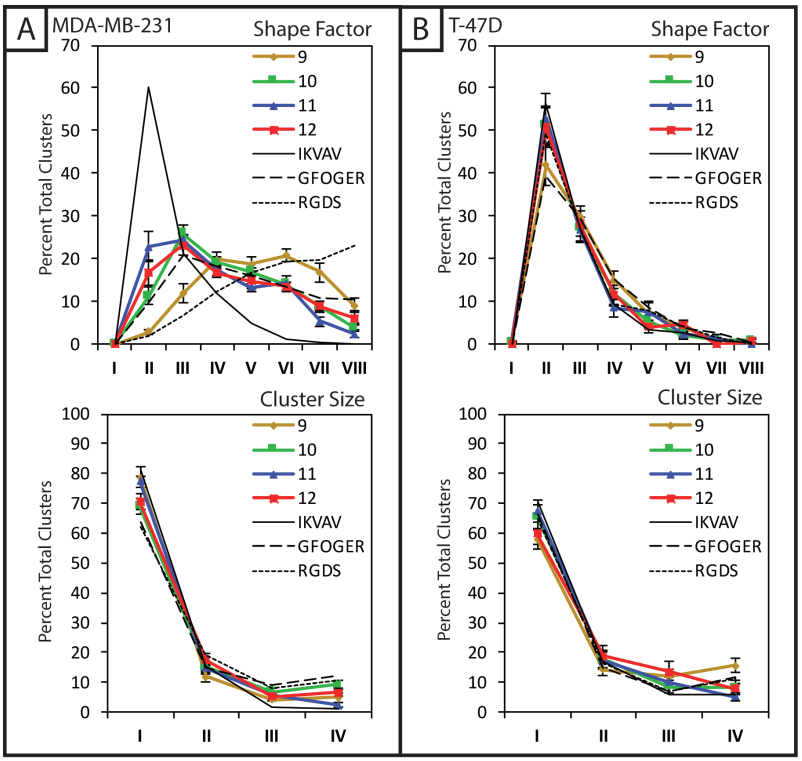

Figure 4.6: **Response of cells to mixtures of receptor-binding peptides. A)** MDA-MB-231 are highly active within microenvironments containing IKVAV supplemented with low levels of RGDS and/or GFOGER. A shift toward irregular shape and increase in cluster size is observed for all conditions containing RGDS and GFOGER. In particular, condition 9 which has the highest concentrations of RGDS and GFOGER trends toward the lowest shape factor, close to that of the RGDS-only condition, indicating that response may be dependent on ligand concentration. **B)** T-47D do not exhibit significant differences in shape factor or cluster size in environments containing different mixtures of peptide ligands, and low levels of activation indicating that response to the selected peptides is minimal. **Shape factor** I) $SF > 0.8$, II) $0.75 < SF \leq 0.8$, III) $0.7 < SF \leq 0.75$, IV) $0.65 < SF \leq 0.7$, V) $0.6 < SF \leq 0.65$, VI) $0.55 < SF \leq 0.6$, VII) $0.5 < SF \leq 0.55$, and VIII) $0.5 \leq SF$; **Cluster Size** I) $V < 25{,}000\ \mu m^3$, II) $25{,}000 \leq V < 50{,}000\ \mu m^3$, III) $50{,}000 \leq V < 75{,}000\ \mu m^3$, and IV) $V \geq 75{,}000\ \mu m^3$. **9)** 0.25 mM RGDS, 0.25 mM GFOGER, 1.5 mM IKVAV; **10)** 0.1 mM GFOGER, 1.9 IKVAV; **11)** 0.1 mM RGDS, 1.9 mM IKVAV; **12)** 0.05 mM RGDS, 0.05 mM GFOGER, 1.9 mM IKVAV.

4.4.5 Low Levels of Proliferation Observed During Long-Term Culture in Environments Containing GFOGER

Monitoring culture in time is critical toward identification of ECMs that permit cancer cell activation. Previous *in vitro* models investigating dormancy and recurrence have studied proliferation via metabolic activity assays or expression of the nuclear proliferation marker, Ki-67.[7,44,54] Here, we studied the of response cells cultured within 6 wt% gels containing either 2 mM IKVAV or GFOGER over 40 days (D3, D10, D20, D30, D40). These conditions were chosen toward investigating response within "dormant" or "remodeled" (high levels of collagen) environments. Here, we monitored Ki-67 expression and the number of clusters (rather than percent) within discrete shape-factor and cluster size groups to investigate proliferation over time in discrete microenvironments.

By D10 in the GFOGER environment, MDA-MB-231 cells exhibit irregular morphology, whereas in the IKVAV condition, spherical morphology dominates during the 40-day culture period (Figure 4.7 A). Notably, changes in the number of cells/clusters occur over time within both conditions (Figure 4.7 A). Between D3 and D10, there is a decrease in cell/cluster number. We hypothesize that cells that have survived initial encapsulation (day 3) have yet to properly adhere within the microenvironment, owing to insufficient or inadequate cell-matrix interactions for survival of the full cell population, which may be confirmed by the spherical morphology observed for MDA-MB-231 at D3. The number of MDA-MB-231 clusters continues to increase between days 20 and 40 for both the conditions. However, the greatest increase is observed in the GFOGER condition, which we attribute to interaction with the peptide. The difference between days 30 and 40 is not significant, and we hypothesize that a maximum density of clusters within 3D culture

may have been reached. MDA-MB-231 clusters in the IKVAV condition also increase between D20 and D40, but at a slower rate due to different cell-matrix interactions. We hypothesize that the mechanism behind proliferation here differs from the GFOGER condition. Specifically, we hypothesize that as MDA-MB-231 cells remodel and deposit proteins into the hydrogel, a more permissive environment may be created that allows low levels of proliferation.

Spherical morphology is observed again for T-47D cultured within both environments during 40 days in culture, indicating only low levels of activation in response to the matrix. However, as with the MDA-MB-231s, changes in the number of cells/clusters over time occur within both conditions (Figure 4.7 B). A more pronounced decrease in cluster number between D3 and D10 is observed for T-47D (~50% versus ~30% for MDA-MB-231), which we believe is due to lower activity as a result of fewer appropriate cell-matrix interactions for promoting the activation of this cell line. Spherical morphology, consistent with cell-cell interactions, persists during 40-day culture and indicates that the behavior of T-47D cells may partly be independent of cell-matrix interaction. Thus, we hypothesize that the increase in cluster number and cluster size over time may be due to deposition of proteins by breast cancer cells into the hydrogel, which provide new cell-matrix interactions and permit low levels of proliferation, as observed in the MDA-MB-231 IKVAV condition. However, more clusters present in the GFOGER condition by D40 versus IKVAV indicate that there may be some minimal cell-matrix interactions that are adequate for promoting slightly higher levels of activation.

Only low levels of Ki-67 expression were observed at D3 and D10 in all conditions, with its disappearance in most images by D20 (Supplementary

Information, Figure 4.12). We attribute this to the fact that Ki-67 is only present during cell division, thus the slow cycling of cells in a 3D microenvironment makes it challenging to capture the exact time a cell is actively dividing with individual time point analyses. Live cell imaging or other markers of cell division/cell cycle (e.g., FUCCI)[56,57] may be investigated in future studies to capture changes in the cell activity and cluster growth over time.

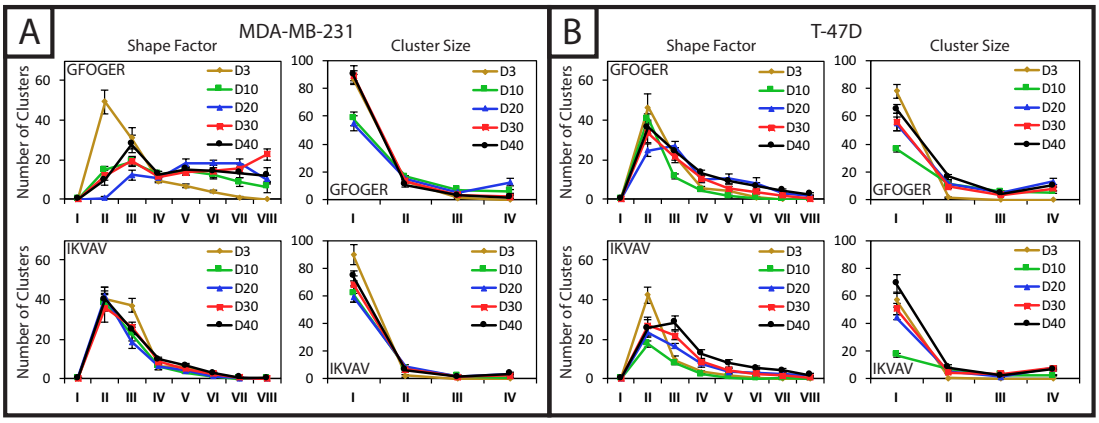

Figure 4.7: **Culture in gels containing GFOGER and IKVAV for 40 days. A)** MDA-MB-231 cultured in 6 wt% gels containing GFOGER and IKVAV exhibit distinct response to the peptides presented. Between D3 and D10, the cells in the GFOGER condition gain irregular morphology that is sustained during the entire 40-day culture. Within the IKVAV condition, cells remain largely spherical over the 40-day culture. A decrease in cluster number is observed between D3 and D10, which we hypothesize results from a percent of cells failing to properly adhere during the first week. Subsequent increase in the number of clusters indicates low levels of proliferation during the remaining culture period. **B)** T-47D cells remain largely as spheroids during the entire 40-day culture. Similar to the MDA-MB-231, a decrease in cluster number is observed between D3 and D10. We hypothesize that the low levels of proliferation observed between D20-D24 could result from the deposition of proteins by T-47D cells within the hydrogel, which may generate a permissive environment for growth. **Shape factor** I) $SF > 0.8$, II) $0.75 < SF \leq 0.8$, III) $0.7 < SF \leq 0.75$, IV) $0.65 < SF \leq 0.7$, V) $0.6 < SF \leq 0.65$, VI) $0.55 < SF \leq 0.6$, VII) $0.5 < SF \leq 0.55$, and VIII) $0.5 \leq SF$; **Cluster Size** I) $V < 25{,}000\ \mu m^3$, II) $25{,}000 \leq V < 50{,}000\ \mu m^3$, III) $50{,}000 \leq V < 75{,}000\ \mu m^3$, and IV) $V \geq 75{,}000\ \mu m^3$.

4.4.6 Binding to Integrin β1 is Critical for Activation within Synthetic Microenvironments

Integrin binding has been implicated in regulating cellular processes associated with dormancy and recurrence. In particular β1 has been a focus of numerous studies investigating cellular pathways that drive proliferation or dormancy. Proliferation of

dormant cells through integrin β1 signaling, which induces phosphorylation of Src and focal adhesion kinase (FAK) and activates extracellular signal-related kinase (ERK), has been reported in 3D.[31,58,59] In 2D, α5β1 up-regulation, mediated by FGF-2 signaling, was associated with the survival of dormant cells on fibronectin. Here, we investigated integrin β1 binding to scaffolds where activation was observed, namely the 6 wt% conditions containing 2 mM GFOGER and RGDS.

β1-blocking antibody (AIIB2) was used to block MDA-MB-231 and T-47D cells prior to encapsulation and supplemented during their culture within gels (100 μg/mL in growth medium, 10 days in culture). β1-blocked MDA-MB-231 exhibited marked differences in behavior for the GFOGER and RGDS conditions (Figure 4.8 A). Specifically, spherical cluster morphology was observed in GFOGER-containing gels (~70-80% SF > 0.7), matching IKVAV behavior previously observed; however, blocked cells in the RGDS condition remained irregular (~80% SF < 0.7). As noted earlier, RGDS binds numerous integrins (αvβ3 (strongest), α5β1, α8β1, αvβ1, αvβ5, αvβ6, αvβ8, and αIIbβ3)[41,42] while GFOGER primarily targets α1β1 and α2β1,[40] thus interaction of MDA-MB-231 with RGDS via other integrins is likely. β1-blocked T-47D exhibited spherical morphology and similar cluster formation behavior (~30-40% medium and large clusters), as seen in non-blocked conditions, further supporting observations that cell-cell interactions may dominate over cell-matrix interactions within the given microenvironment and preferentially drive response of these cells *in vitro* (Figure 4.8 B). Thus, investigation of other integrin-binding peptides or soluble factors secreted by niche cells or in co-culture may be required to see enhanced levels of activation within these synthetic microenvironments.

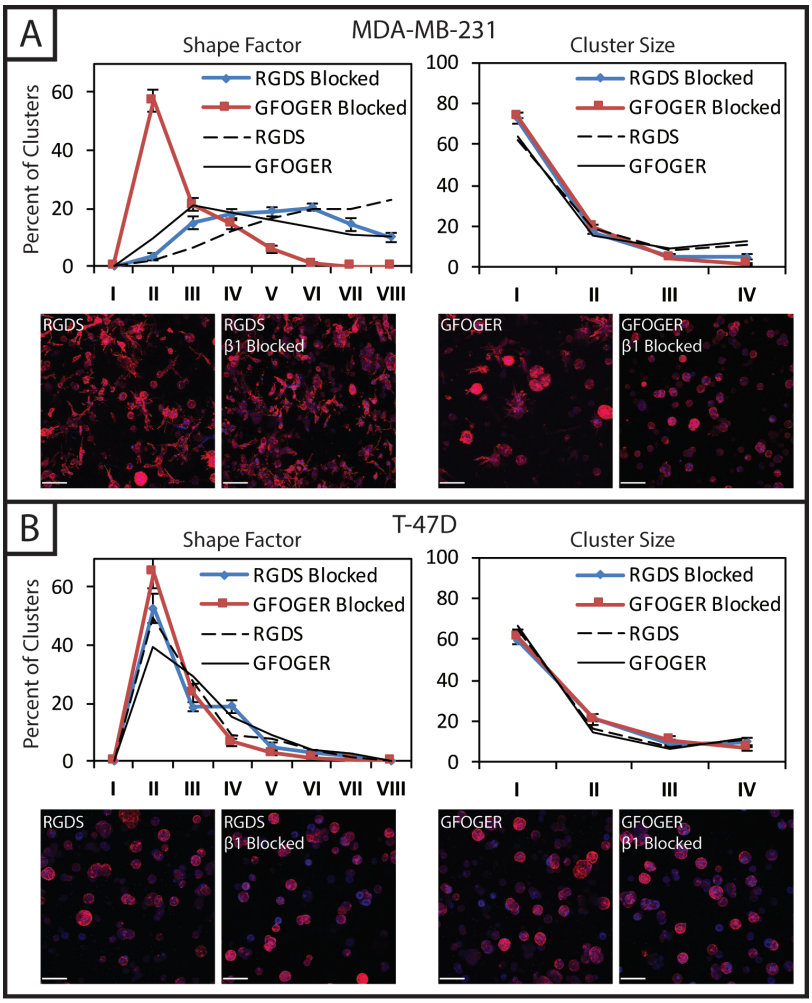

Figure 4.8: **β1 blocking of cells within microenvironments containing RGDS and GFOGER. A)** MDA-MB-231 cells blocked with β1 (AIIB2) exhibit spherical morphology during culture in scaffolds containing GFOGER. However, irregular morphology persists in the RGDS-containing hydrogel indicating cells remain active. We hypothesize that the less specific binding of the RGDS peptide targets other integrins on MDA-MB-231 cells and permits adhesion to and activation within the network. **B)** T-47D response remains the same when β1 is blocked, further supporting minimal levels of activation and binding occur within these networks. Z-projection images shown with scale bars =100 μm, F-Actin = red, DAPI = blue. **Shape factor** I) SF > 0.8, II) 0.75 < SF ≤ 0.8, III) 0.7 < SF ≤ 0.75, IV) 0.65 < SF ≤ 0.7, V) 0.6 < SF ≤ 0.65, VI) 0.55 < SF ≤ 0.6, VII) 0. 5 < SF ≤ 0.55, and VIII) 0.5 ≤ SF; **Cluster Size** I) V < 25,000 μm^3, II) 25,000 ≤ V < 50,000 μm^3, III) 50,000 ≤ V < 75,000 μm^3, and IV) V ≥ 75,000 μm^3.

4.5 Conclusions

The culture of breast cancer cells (MDA-MB-231, T-47D) within a tunable and fully synthetic polymer-based hydrogel scaffold was described for the investigation of factors that may promote dormancy or activation *in vitro*. Precise modulation of both chemical and mechanical properties allowed investigation of individual cues within discrete microenvironments. Matrix density was shown to restrict the activation and outgrowth of both MDA-MB-231 and T-47D cells cultured within stiff, lung-mimetic microenvironments. Response to biochemical cues (peptides) incorporated within networks was also studied, with collagen-mimetic (GFOGER) and fibronectin/vitronectin-mimetic (RGDS) peptides resulting in high levels of activation observed in the MDA-MB-231 cells. Culture of cells over weeks demonstrated low levels of proliferation in both lines, with proliferation of MDA-MB-231 driven by cell-matrix interactions, whereas T-47D cells exhibit less activation in response to the provided microenvironment and appear to rely primarily on cell-cell interactions and matrix remodeling for survival. Finally, β1 was shown to be important in regulating activation of MDA-MB-231 within environments containing GFOGER, whereas RGDS appeared to bind other integrins and cells remained active. These studies represent a novel approach to examine breast cancer response within a fully synthetic, 3D PEG-based scaffold, containing individual or mixtures of biochemical peptide ligands. In future work, this system may be adapted for co-culture with metastatic niche cells to investigate the role of soluble factors in regulating activation, especially related to ER+ T-47D cell response, toward identification of targets for the development of improved treatments for recurrent cancer.

4.6 Acknowledgements

This work was supported by the Institutional Development Award from the National Institutes of Health (P20GM103541), the Pew Charitable Trusts (00026178), a National Science Foundation Career Award (DMR-1253906), the Delaware COBRE program with a grant from the National Institute of Generals Medical Sciences – NIGMS (1 P30 GM110758-01), the Susan G. Komen Foundation Career Catalyst Research Grant (CCR16377327), and the National Science Foundation IGERT SBE2 program at the University of Delaware (fellowship to L. Sawicki). The authors thank Dr. Kenneth van Golen and Dr. Madhura Joglekar for training in breast cancer cell culture. The authors also thank Dr. Wilfred Chen for use of an automated plate reader, Ms. Elisa Ovadia for assistance with sample preparation for timecourse experiments, Mr. Christopher Bresette for assistance with peptide synthesis, and the Delaware Biotechnology Institute Bioimaging Center for access to the Zeiss LSM 780 confocal.

4.7 Supplementary Information

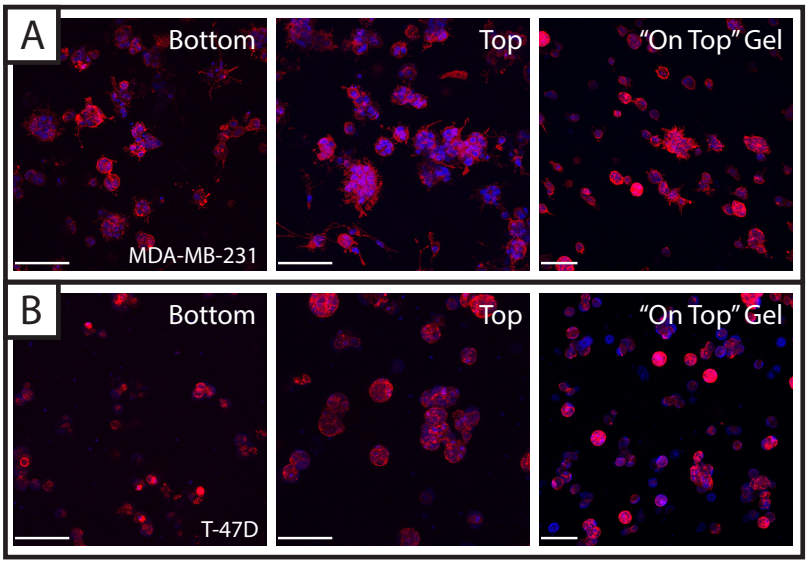

Figure 4.9: **Hypoxia and nutrient deficiency within thick hydrogels. A)** MDA-MB-231 and **B)** T-47D cells cultured within 20 µL discs formed by polymerization in 1 mL syringe tips appear morphologically different at the top and the bottom of the gel after 10 days in culture. Small clusters (esp. in T-47D) found at the bottom of gels, which is directly in contact with a plate during culture, indicate that there may be gradients of nutrients and oxygen through the gel depth. To prevent this, a 15 µL cell-free base was polymerized in the syringe tip followed by a 5 µL layer containing cells. Morphologies are consistent through the depth of these "on top" gels. Note that all of the scale bars are 100 µm. The smaller appearance of the clusters in the "on top" gel is due to imaging on a different microscope with a wider field of view. F-Actin = red, DAPI = blue.

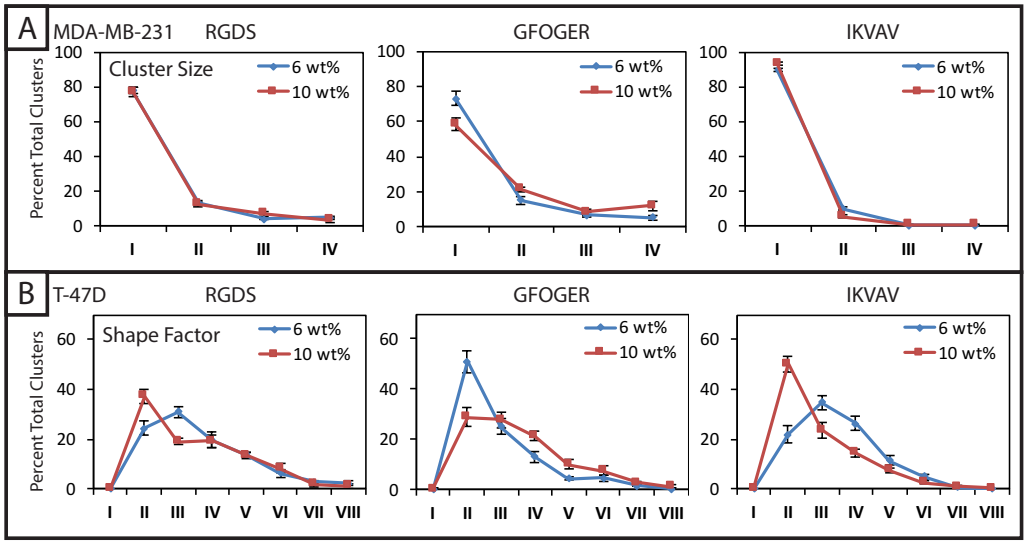

Figure 4.10: **Matrix density effects during culture in synthetic scaffolds. A)** As noted earlier, MDA-MB-231 exhibit highly irregular behavior in 6 wt% hydrogels. However, no significant differences in MDA-MB-231 cluster size are observed between the different matrix densities of 6 and 10 wt% gels. **B)** Cluster size of T-47D changes with matrix density while clusters remain spherical within the different conditions. However, no significant trends in cell shape (shape factor) related to the 6 and 10 wt% conditions are observed. **Shape factor** I) $SF > 0.8$, II) $0.75 < SF \leq 0.8$, III) $0.7 < SF \leq 0.75$, IV) $0.65 < SF \leq 0.7$, V) $0.6 < SF \leq 0.65$, VI) $0.55 < SF \leq 0.6$, VII) $0.5 < SF \leq 0.55$, and VIII) $0.5 \leq SF$; **Cluster Size** I) $V < 25{,}000\ \mu m^3$, II) $25{,}000 \leq V < 50{,}000\ \mu m^3$, III) $50{,}000 \leq V < 75{,}000\ \mu m^3$, and IV) $V \geq 75{,}000\ \mu m^3$.

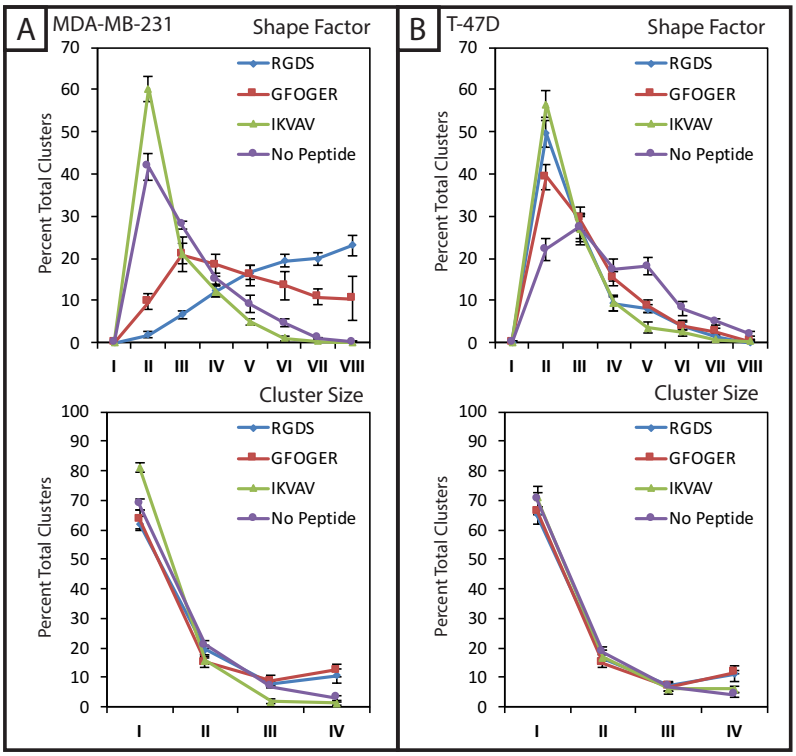

Figure 4.11: **Comparison of binding to RGDS, GFOGER, and IKVAV peptides versus no peptide. A)** MDA-MB-231 and **B)** T-47D exhibit similar response to hydrogels containing no peptide. Specifically, spherical clusters with smaller size (esp. MDA-MB-231) are observed. This behavior is similar to the response within gels containing IKVAV, indicating that binding to IKVAV may not occur or is very weak compared to RGDS and GFOGER. **Shape factor** I) SF > 0.8, II) 0.75 < SF ≤ 0.8, III) 0.7 < SF ≤ 0.75, IV) 0.65 < SF ≤ 0.7, V) 0.6 < SF ≤ 0.65, VI) 0.55 < SF ≤ 0.6, VII) 0. 5 < SF ≤ 0.55, and VIII) 0.5 ≤ SF; **Cluster Size** I) V < 25,000 μm^3, II) 25,000 ≤ V < 50,000 μm^3, III) 50,000 ≤ V < 75,000 μm^3, and IV) V ≥ 75,000 μm^3.

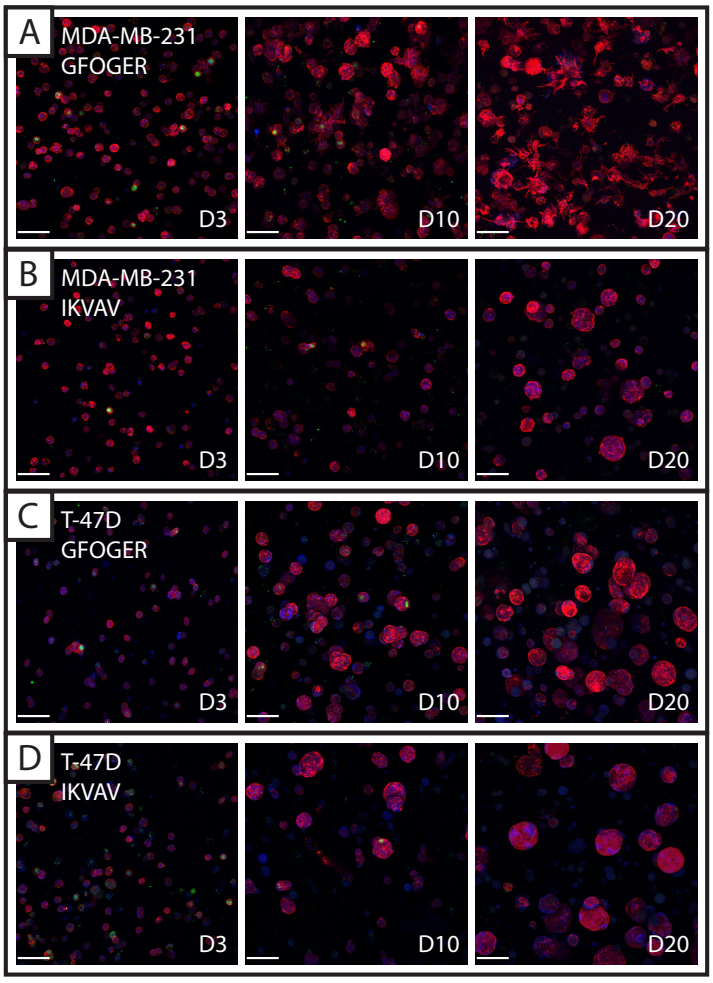

Figure 4.12: **Ki-67 expression during culture. A/B)** MDA-MB-231 and **C/D)** T-47D cells cultured in gels containing GFOGER and IKVAV proliferate slowly over the course of 20 days in culture, with the formation of larger and increased numbers of spheroids as shown above. However, Ki-67, an indicator of if cells are dividing and in the cell cycle (proliferation), is expressed at low levels (only a few cells) at D3 and largely disappears between D10 and D20. Thus Ki-67 is unable to adequately capture the low levels of proliferation observed in the 3D material system described here. Z-projection images with 100 μm scale bars, F-Actin = red, DAPI = blue, Ki-67 = green.

REFERENCES

1. Brewster, A. M., Hortobagyi, G. N., *et al.* Residual Risk of Breast Cancer Recurrence 5 Years After Adjuvant Therapy. *J Natl Cancer Inst*. **100** (16), 1179–1183 (2008).

2. Barkan, D., Green, J. E. & Chambers, A. F. Extracellular matrix: A gatekeeper in the transition from dormancy to metastatic growth. *Eur J Cancer*. **46** (7), 1181–1188 (2010).

3. Barkan, D., Kleinman, H., *et al.* Inhibition of Metastatic Outgrowth From Single Dormant Tumor Cells by Targeting the Cytoskeleton. *Cancer Res*. **68** (15), 6241–6250 (2009).

4. Korah, R., Boots, M. & Wieder, R. Integrin a5B1 Promotes Survival of Growth-Arrested Breast Cancer Cells: An in Vitro Paradigm for Breast Cancer Dormancy in Bone Marrow. *Cancer Res*. **64** 4514–4522 (2004).

5. Joyce, J. A. & Pollard, J. W. Microenvironmental regulation of metastasis. *Nat Rev Cancer*. **9** 239–252 (2009).

6. Miles, F. L., Pruitt, F. L., Golen, K. L. Van & Cooper, C. R. Stepping out of the flow : capillary extravasation in cancer metastasis. *Clin Exp Metastasis*. **25** 305–324 (2008).

7. Ghajar, C. M., Peinado, H., *et al.* The perivascular niche regulates breast tumour dormancy. *Nat Cell Biol*. **15** (7), 807–17 (2013).

8. Sosnoski, D. M., Norgard, R. J., Grove, C. D., Foster, S. J. & Mastro, A. M. Dormancy and growth of metastatic breast cancer cells in a bone-like microenvironment. *Clin Exp Metastasis*. **32** (4), 335–344 (2015).

9. Neve, R. M., Chin, K., *et al.* A collection of breast cancer cell lines for the study of functionally distinct cancer subtypes. *Cancer Cell*. **10** (6), 515–527 (2006).

10. Kennecke, H., Yerushalmi, R., *et al.* Metastatic Behavior of Breast Cancer Subtypes. *J Clin Oncol*. **28** (20), 3271–3277 (2010).

11. Lehmann, B. D., Bauer, J. A., *et al.* Identification of human triple-negative

breast cancer subtypes and preclinical models for selection of targeted therapies. *J Clin Invest*. **121** (7), 2750–2767 (2011).

12. Zhang, X. H.-F., Giuliano, M., Trivedi, M. V., Schiff, R. & Osborne, C. K. Metastasis Dormancy in Estrogen Receptor–Positive Breast Cancer. *Clin Cancer Res*. **19** (23), 6389–6397 (2013).

13. Kenny, P. A., Lee, G. Y., *et al.* The morphologies of breast cancer cell lines in three-dimensional assays correlate with their profiles of gene expression. *Mol Oncol*. **1** (1), 84–96 (2007).

14. Fillmore, C. M. & Kuperwasser, C. Human breast cancer cell lines contain stem-like cells that self-renew, give rise to phenotypically diverse progeny and survive chemotherapy. *Breast Cancer Res*. **10** (2), R25 (2008).

15. Weigelt, B., Peterse, J. L. & van't Veer, L. J. Breast Cancer Metastasis: Markers and Models. *Nat Rev Cancer*. **5** 591–602 (2005).

16. Nguyen, D. X., Bos, P. D. & Massagué, J. Metastasis: from dissemination to organ-specific colonization. *Nat Rev Cancer*. **9** 274–284 (2009).

17. Scully, O. J., Bay, B., Yip, G. & Yu, Y. Breast Cancer Metastasis. *Cancer Genomics and Proteomics*. **9** 311–320 (2012).

18. Alberts, B., Johnson, A., Lewis, J., Raff, M., Roberts, K. & Walter, P. Cell junctions, cell adhesion, and the extracellular matrix. *Mol Biol Cell*. 1065–1125 (2002).

19. Hynes, R. O. The Extracellular Matrix: Not Just Pretty Fibrils. *Science*. **326** (5957), 1216–1219 (2009).

20. Winer, J. P., Janmey, P. A., Mccormick, M. E. & Funaki, M. Bone Marrow-Derived Human Mesenchymal Stem Cells Become Quiescent on Soft Substrates but Remain Responsive to Chemical or Mechanical Stimuli. *Tissue Eng Part A*. **15** (1), 147–154 (2009).

21. Levental, I., Georges, P. C. & Janmey, P. A. Soft biological materials and their impact on cell function. *Soft Matter*. **3** (3), 299–306 (2007).

22. Loessner, D., Stok, K. S., Lutolf, M. P., Hutmacher, D. W., Clements, J. A. & Rizzi, S. C. Biomaterials Bioengineered 3D platform to explore cell-ECM interactions and drug resistance of epithelial ovarian cancer cells. *Biomaterials*. **31** (32), 8494–8506 (2010).

23. Cheng, G., Tse, J., Jain, R. K. & Munn, L. L. Micro-Environmental Mechanical Stress Controls Tumor Spheroid Size and Morphology by Suppressing Proliferation and Inducing Apoptosis in Cancer Cells. *PLoS One*. **4** (2), e4632 (2009).

24. Schrader, J., Gordon-Walker, T. T., *et al.* Matrix Stiffness Modulates Proliferation, Chemotherapeutic Response, and Dormancy in Hepatocellular Carcinoma Cells. *Hepatology*. **53** (4), 1192–1205 (2011).

25. Pontier, S. M. & Muller, W. J. Integrins in breast cancer dormancy. *APMIS*. **116** 677–684 (2008).

26. Bonnans, C., Chou, J. & Werb, Z. Remodelling the extracellular matrix in development and disease. *Nat Publ Gr*. **15** (12), 786–801 (2014).

27. Chang, C., Werb, Z. & Werb, Z. The many faces of metalloproteases: cell growth, invasion, angiogenesis and metastasis. *Trends Cell Biol*. **11** (11), 37–43 (2001).

28. Schultz, G. S. & Wysocki, A. Interactions between extracellular matrix and growth factors in wound healing. *Wound Repair Regen*. **17** 153–162 (2009).

29. Raman, D., Baugher, P. J., Mon, Y. & Richmond, A. Role of chemokines in tumor growth. *Cancer Lett*. **256** 137–165 (2007).

30. Barrios, J. & Wieder, R. Dual FGF-2 and Intergrin α5β1 Signaling Mediate GRAF-Induced RhoA Inactivation in a Model of Breast Cancer Dormancy. *Cancer Microenviron*. **2** 33–47 (2009).

31. Barkan, D., Touny, L. H. El, *et al.* Metastatic Growth from Dormant Cells Induced by a Col-I–Enriched Fibrotic Environment. *Cancer Res*. **70** (19), 5706–5716 (2010).

32. Gill, B. J., Gibbons, D. L., *et al.* A synthetic matrix with independently tunable biochemistry and mechanical properties to study epithelial morphogenesis and EMT in a lung adenocarcinoma model. *Cancer Res*. **72** (22), 6013–6023 (2012).

33. Girard, Y. K., Wang, C., *et al.* A 3D Fibrous Scaffold Inducing Tumoroids: A Platform for Anticancer Drug Development. *PLoS One*. **8** (10), e75345 (2013).

34. Sawicki, L. A. & Kloxin, A. M. Light-mediated Formation and Patterning of Hydrogels for Cell Culture Applications. *J Vis Exp*. (115), e54462 (2016).

35. Sawicki, L. A. & Kloxin, A. M. Design of thiol–ene photoclick hydrogels using

facile techniques for cell culture applications. *Biomater Sci*. **2** (11), 1612–1626 (2014).

36. Shih, H. & Lin, C. Cross-Linking and Degradation of Step-Growth Hydrogels Formed by Thiol−Ene Photoclick Chemistry. *Biomacromolecules*. **13** 2003–2012 (2012).

37. Anseth, K. S., Bowman, C. N. & Brannon-peppas, L. Mechanical properties of hydrogels and their experimental determination. *Biomaterials*. **17** 1647–1657 (1996).

38. Kloxin, B. A. M., Kloxin, C. J., Bowman, C. N. & Anseth, K. S. Mechanical Properties of Cellularly Responsive Hydrogels and Their Experimental Determination. *Adv Mater*. **22** 3484–3494 (2010).

39. Patterson, J. & Hubbell, J. A. Enhanced proteolytic degradation of molecularly engineered PEG hydrogels in response to MMP-1 and MMP-2. *Biomaterials*. **31** (30), 7836–7845 (2010).

40. Knight, C. G., Morton, L. F., *et al.* Recognize the Same Specific Amino Acid Sequence, GFOGER, in Native (Triple-helical) Collagens. *J Biol Chem*. **275** (1), 35–40 (2000).

41. Rice, J. J., Martino, M. M., Laporte, L. De, Tortelli, F., Briquez, P. S. & Hubbell, J. A. Engineering the Regenerative Microenvironment with Biomaterials. *Adv Healthc Mater*. **2** 57–71 (2013).

42. Ruoslahti, E. RGD and other recognition sequences for integrins. *Annu Rev Cell Dev Biol*. **12** 697–715 (1996).

43. Yamada, Y., Hozumi, K. & Nomizu, M. Construction and Activity of a Synthetic Basement Membrane with Active Laminin Peptides and Polysaccharides. *Chem A Eur J*. **17** 10500–10508 (2011).

44. Barkan, D. & Green, J. E. An In Vitro System to Study Tumor Dormancy and the Switch to Metastatic Growth. *J Vis Exp*. **54** e2914 (2011).

45. Guiro, K., Patel, S. A., Greco, S. J. & Rameshwar, P. Investigating Breast Cancer Cell Behavior Using Tissue Engineering Scaffolds. *PLoS One*. **10** (4), e0118724 (2015).

46. Ogba, N., Manning, N. G., *et al.* Luminal breast cancer metastases and tumor arousal from dormancy are promoted by direct actions of estradiol and progesterone on the malignant cells. *Breast Cancer Res*. **16** (6), 1–14 (2014).

47. Bryant, S. J., Nuttelman, C. R. & Anseth, K. S. Cytocompatibility of UV and visible light photoinitiating systems on cultured NIH/3T3 fibroblasts in vitro. *J Biomater Sci Polym Ed*. **11** (5), 439–457 (2000).

48. Williams, C. G., Malik, A. N., Kim, T. K., Manson, P. N. & Elisseeff, J. H. Variable cytocompatibility of six cell lines with photoinitiators used for polymerizing hydrogels and cell encapsulation. *Biomaterials*. **26** (11), 1211–1218 (2005).

49. Guvendiren, M. & Burdick, J. A. Stiffening hydrogels to probe short- and long-term cellular responses to dynamic mechanics. *Nat Commun*. **3** 792–799 (2012).

50. Volkmer, E., Otto, S., *et al.* Overcoming hypoxia in 3D culture systems for tissue engineering of bone in vitro using an automated , oxygen-triggered feedback loop. *J Mater Sci Mater Med*. **23** (11), 2793–2801 (2012).

51. Nillesen, S. T. M., Geutjes, P. J., Wismans, R., Schalkwijk, J., Daamen, W. F. & Kuppevelt, T. H. Van Increased angiogenesis and blood vessel maturation in acellular collagen – heparin scaffolds containing both FGF2 and VEGF. *Biomaterials*. **28** 1123–1131 (2007).

52. Lutolf, M. P., Gilbert, P. M. & Blau, H. M. Designing materials to direct stem-cell fate. *Nature*. **462** 433–441 (2009).

53. Leask, A. & Abraham, D. J. TGF-B signaling and the fibrotic response. *FAESB J*. **18** (7), 816–827 (2004).

54. Chatterjee, M. & Golen, K. L. Van Farnesyl transferase inhibitor treatment of breast cancer cells leads to altered RhoA and RhoC GTPase activity and induces a dormant phenotype. *Int J Cancer*. **129** 61–69 (2011).

55. Holliday, D. L. & Speirs, V. Choosing the right cell line for breast cancer research. *Breast Cancer Res*. **13** (4), (2011).

56. Zielke, N. & Edgar, B. A. FUCCI sensors: powerful new tools for analysis of cell proliferation. *WIREs Dev Biol*. **4** 469–487 (2015).

57. Sakaue-sawano, A., Kurokawa, H., *et al.* Resource Visualizing Spatiotemporal Dynamics of Multicellular Cell-Cycle Progression. *Cell*. **132** 487–498 (2008).

58. Touny, L. H. El, Vieira, A., Mendoza, A., Khanna, C., Hoenerhoff, M. J. & Green, J. E. Combined SFK / MEK inhibition prevents metastatic outgrowth of dormant tumor cells. *J Clin Invest*. **124** (1), 156–168 (2014).

59. Shibue, T. & Weinberg, R. A. Integrin B1-focal adhesion kinase signaling directs the proliferation of metastatic cancer cells disseminated in the lungs. *Proc Natl Acad Sci United States Am*. **106** (25), 10290–10295 (2009).

Chapter 5

CONCLUSIONS AND FUTURE DIRECTIONS

In this chapter, key conclusions from Chapters 2-4 are presented with recommendations for future studies toward understanding breast cancer activation within synthetic microenvironments.

5.1 Design of Well-Defined PEG-Based Hydrogels for Cell Culture Applications

In chapter 2, we described the creation of a novel poly(ethylene glycol) (PEG)-based hydrogel for cell culture applications generated via facile synthetic techniques. Specifically, thiol-modified PEG, peptides containing alloxycarbonyl-protected lysines (providing reactive vinyls), and lithium acylphosphinate (LAP) photoinitiator were synthesized using simple protocols, established in literature.[1,2] These materials are also commercially available, which will permit broader use of the material scaffold in 3D cell culture and tissue engineering applications. Hydrogels polymerized rapidly, within 5 minutes, after the application of light (365 nm and 10 mW/cm^2) and in the presence of LAP, which minimized the effects of light and radicals on cell viability. Specifically, greater than 70% viability was observed for all cell types encapsulated (hMSC, T-47D, MDA-MB-231), with some cell lines and conditions having high viability at greater than 90%. The modulus of the material was tuned to mimic the bulk mechanical properties of soft tissue sites (~600-6000 Pa).[3,4] Additionally, biochemical cues, providing adhesion sites to promote cell-matrix interactions, were

initially added or patterned within the microenvironments with high levels of efficiency as determined via Ellman's assay.

While this system represents a relatively simple approach to generating 3D culture scaffolds, control over properties in time is limited. Specifically, biochemical cues cannot be added after samples are incubated in culture medium as accessible thiol groups for reaction are consumed by species within the medium. Follow-up studies to develop techniques to dynamically alter this scaffold's biochemical and biomechanical properties would allow enhanced investigation of response to temporal property changes. A relatively simple method to address this would be to polymerize gels off-stoichiometry with excess peptide, providing reactive vinyls for later reaction with thiol-containing peptides and polymers. However, this method could disrupt polymerization and would require large amounts of peptides, which is significantly more expensive to synthesize, so other techniques for dynamic modulation should be investigated. Cambria, et al. described the incorporation of LPRTG peptides within PEG-based hydrogel networks and subsequent ligation and cleavage of GGG-EGF (epidermal growth factor fused to a tri-glycine peptide) mediated via sortase A.[5] A similar scheme could be used to add and remove peptides coupled within our hydrogel network by covalent incorporation of LPXTG peptides (modified with K(alloc) for reaction with PEG-thiol) within the initial hydrogel substrate and subsequent addition or cleavage of GGG-Peptides mediated by sortase A.

Beyond investigation of hMSC, MDA-MB-231, and T-47D cell response within synthetic 3D scaffolds, we are also interested in studying the behavior of other tumorigenic and non-tumorigenic cells *in vitro*. To date, we have also encapsulated the MCF-12A, MCF-10A, and MCF-7 lines within our hydrogel scaffolds. MCF-10A and

MCF-12A both exhibit viability (> 70%) post-encapsulation, however low and variable viability was observed for MCF-7 (30-60%) one day after encapsulation (Figure 5.1). We hypothesize that as described in literature, sensitivity to light and radicals during polymerization resulted in the lower viability observed.[6] Probing whether the decreased viability was due to light and radicals, MCF-7s were also encapsulated in PEG-cyclooctyne and PEG-azide networks (SPAAC chemistry), which form a gel without initiation by light or other catalysts. Viability of MCF-7s was preserved post-encapsulation within these materials (> 80%) indicating that damage to light and radicals occurred in the presented material system. For broader use of the developed synthetic hydrogel, cell lines must individually be tested to confirm viability. However, if low viability is observed, other light- and radical-free chemistries (e.g. thiol-maleimide, SPAAC) should be considered for hydrogel formation and cell encapsulation.

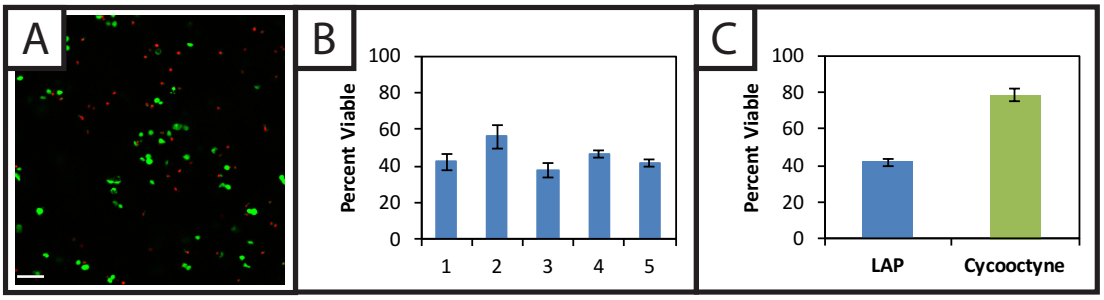

Figure 5.1: **Viability of MCF-7 cells within PEG-based hydrogels. A)** Live/dead viability/cytotoxicity stain was used to quantify survival of MCF-7 cells post-encapsulation. A large number of dead cells (red nuclei) are observed, indicating that the encapsulation is not hospitable to cells. Scale bar, 100 μm. **B)** Low levels (30-60%) of viability was observed across 5 encapsulation experiments. **C)** Encapsulation within gels formed by radical- and light-free polymerization (Cyclooctyne) demonstrated increased levels of viability (79 ± 3%), supporting observations that radicals and light may damage MCF-7 cells during encapsulation.

Finally, toward improving the design of materials scaffolds to study cell binding and response, we are interested in the synthesis of novel peptides with enhanced and specific binding to target integrins (Appendix B). Briefly, the one-bead-one-compound technique developed by Lam, et al., which has been used broadly for drug discovery and screening applications,[7] was used here to generate a library of peptides to identify sequences with enhanced binding to α1β1 and α2β1. In collaboration with Dr. Kit Lam and Dr. Emanual Maverakis, we have synthesized and screened a library based on the collagen-mimetic peptide, GFOGER. Several linear peptide sequences have been identified as potential targets and additional studies are ongoing to characterize their binding to cells and specificity for the α1β1 and α2β1 integrins. Additionally, we are working on the design of cyclic peptide sequences identified in other library screens to enhance binding to αvβ3. Specifically, techniques to make the cyclic LXW7 sequence,[8] which is based on perturbations of the RGDS peptide, are being investigated for covalent incorporation within hydrogel scaffolds and for targeted cancer therapy.

5.2 Development of Proteomics Techniques to Identify Proteins Secreted within Synthetic Scaffolds

In chapter 3, we described the development of a technique to isolate and identify proteins secreted by cells cultured within synthetic material scaffolds. Specifically, hMSCs were cultured in PEG-based hydrogels, allowing cellular remodeling and deposition of proteins within the scaffold. Scaffolds were decellularized to remove some cellular compartments and proteins were collected from the decellularized gels via degradation of an MMP-degradable peptide crosslink with collagenase. The protein/polymer mixture was subsequently digested with trypsin

and large PEG/peptide fragments from the gel were separated from the small peptide fragments of cell-secreted proteins with low MWCO spin columns (10 kDa). Shotgun proteomics via HPLC with MALDI-MS identified the presence of large proteins collagen VI and fibronectin, secreted by hMSCs cultured within gels, and immunostaining confirmed their presence. Luminex® multiplex bead assays also identified soluble factors (VEGF, IL-8) secreted by hMSCs within the microenvironment, which may drive additional cell response. This technique is promising toward future application in identifying proteins secreted by other cell lines or investigating proteins secreted by a single cell type in response to presentation of different hydrogel chemical and physical properties.

In particular, relating to the differences in response and proliferation observed for MDA-MB-231 and T-47D cells cultured within hydrogels (Chapter 4), future work investigating the protein profiles secreted by these cells may help explain observations about their response *in vitro*. Finally, Luminex® bead assays, which were used to analyze samples collected from cells cultured in 2D, can be adapted to 3D cultures and for a broader panel of analytes in future studies.

5.3 Examination of Breast Cancer Behavior and Response within Synthetic 3D Microenvironments

The response of breast cancer cells cultured within synthetic PEG-based hydrogel scaffolds was identified and characterized in chapter 4. With the ability to independently investigate response to mechanical and chemical properties, we were able to identify various microenvironmental factors that may regulate their dormancy and activation. In particular, scaffolds with high matrix density (high modulus, stiff) were found to decrease activity of cells cultured within hydrogels by restricting cluster

growth and spreading within the network. Peptides mimicking fibronectin/vitronectin (RGDS, targets αvβ3, α5β1, and other integrins) and collagen (GFOGER, targets α1β1, α2β1) were found to promote activation within microenvironments as compared to a laminin mimic (IKVAV, targets laminin receptor). Studies blocking β1 demonstrated the loss of activation within hydrogels containing GFOGER while activation was maintained in the RGDS microenvironment, indicating that other integrins may be involved in the activation observed for the RGDS condition. Taken together, these results are promising toward the identification of critical factors that regulate cancer dormancy and recurrence within a synthetic, *in vitro* scaffold.

Motivated by the response observed in hydrogels containing RGDS, where MDA-MB-231 cells remained active after blocking β1, future work can be performed to identify other integrins or receptors associated with active behavior observed *in vitro*. Specifically, it has been demonstrated that different integrins are expressed at different levels by various breast cancer cell lines,[9] which may affect the cell's ability to bind and respond to peptides within a synthetic scaffold. Individual or combinations of integrins can be blocked in future studies to identify additional cell-ECM interactions that may be responsible for cell activation within discrete microenvironments. For example, MDA-MB-231 remained active after blocking β1 in gels containing RGDS (targets α5β1, αvβ3, others), thus blocking β1 and β3 individually and in combination can be performed to investigate the effects of both integrins on activation within hydrogels. Further, blocking the laminin receptor may help elucidate the different response observed in environments containing IKVAV. Other integrin binding peptide sequences can synthesized with enhanced binding to various integrins (e.g., $RGDG_{13}PHSRN$ which strongly binds α5β1)[10] to study

additional biochemical factors that may support activation during 3D culture. Beyond the presentation of factors tethered to synthetic matrices, various soluble factors (e.g., TGF-β1, FGF-2)[11,12] have also been implicated in dormancy and recurrence. These factors, secreted by metastatic niche cells, motivate future work toward the co-culture of breast cancer cells with niche cells (e.g., fibroblasts, hMSCs). This may be achieved through various techniques including the application of conditioned medium to samples (least complex to execute), transwell assays, or direct culture within the same microenvironment (most complex to evaluate).

The assays described here provide information to evaluate cell activation within synthetic microenvironments at discrete time points; however, additional techniques need to be developed to understand cell behavior and response in time as well as on a genomic level. The current techniques used to evaluate response are destructive, end-point analyses (fixed cells for immunostaining), thus the behavior of cells in a single sample microenvironment cannot be monitored over time. As a result, large numbers of samples are required to execute time course experiments, which make it challenging to evaluate multiple conditions at a time. The development of live imaging techniques and the use of dynamic markers of the cell cycle (e.g. FUCCI)[13] or partial labeling of cells with GFP can be explored to monitor cell behavior and provide additional information on proliferation and activation within microenvironments. Finally, toward model validation and identification of critical markers of dormancy and recurrence, RNA sequencing can be used to compare gene expression of cancer cells cultured within our synthetic scaffolds to human and animal data sets.[14–17]

5.4 Summary

In this thesis, a novel approach to investigate the response of breast cancer recurrence was presented. A synthetic hydrogel scaffold with well-defined mechanical and chemical properties was generated for the culture of cells within a 3D microenvironment. Techniques to analyze cellular remodeling of these environments, which alters the properties of these initially well-defined scaffolds, were also developed. Activation in response to the presentation of individual or multiple chemical and physical cues found within metastatic tissue sites was investigated and several conditions promoting activation were identified. Beyond investigation of cancer recurrence, the system presented here may be used in diverse biological applications for the culture of additional cell lines or primary cells to explore critical factors in the ECM that regulate cellular response and fate *in vitro*.

REFERENCES

1. Fairbanks, B. D., Schwartz, M. P., Bowman, C. N. & Anseth, K. S. Photoinitiated polymerization of PEG-diacrylate with lithium phenyl-2,4,6-trimethylbenzoylphosphinate: polymerization rate and cytocompatibility. *Biomaterials*. **30** (35), 6702–6707 (2009).

2. Fairbanks, B. D., Singh, S. P., Bowman, C. N. & Anseth, K. S. Photodegradable, photoadaptable hydrogels via radical-mediated disulfide fragmentation reaction. *Macromolecules*. **44** (8), 2444–2450 (2011).

3. Levental, I., Georges, C. & Janmey, P. A. Soft biological materials and their impact on cell function. *Soft Matter*. **3** 299–306 (2007).

4. Winer, J. P., Janmey, P. A., Mccormick, M. E. & Funaki, M. Bone Marrow-Derived Human Mesenchymal Stem Cells Become Quiescent on Soft Substrates but Remain Responsive to Chemical or Mechanical Stimuli. *Tissue Eng Part A*. **15** (1), 147–154 (2009).

5. Cambria, E., Renggli, K., *et al.* Covalent Modification of Synthetic Hydrogels with Bioactive Proteins via Sortase-Mediated Ligation. *Biomacromolecules*. **16** 2316–2326 (2015).

6. Williams, C. G., Malik, A. N., Kim, T. K., Manson, P. N. & Elisseeff, J. H. Variable cytocompatibility of six cell lines with photoinitiators used for polymerizing hydrogels and cell encapsulation. *Biomaterials*. **26** (11), 1211–1218 (2005).

7. Lam, K. S., Salmon, S. E., Hersh, E. M., Hruby, V. J., Kazmierski, W. M. & Knapp, R. J. A new type of synthetic peptide library for identifying ligand-binding activity. *Nature*. **354** 82–84 (1991).

8. Xiao, W., Wang, Y., *et al.* The use of one-bead one-compound combinatorial library technology to discover high-affinity αvβ3 integrin and cancer targeting RGD ligands with a build-in handle. *Mol Cancer Ther*. **9** (10), 2714–2723 (2010).

9. Taherian, A., Li, X., Liu, Y. & Haas, T. A. Differences in integrin expression and signaling within human breast cancer cells. *BMC Cancer*. **11** (293), (2011).

10. Benoit, D. S. W. & Anseth, K. S. The effect on osteoblast function of colocalized RGD and PHSRN epitopes on PEG surfaces. *Biomaterials*. **26** 5209–5220 (2005).

11. Ghajar, C. M., Peinado, H., *et al.* The perivascular niche regulates breast tumour dormancy. *Nat Cell Biol*. **15** (7), 807–17 (2013).

12. Barrios, J. & Wieder, R. Dual FGF-2 and Intergrin α5β1 Signaling Mediate GRAF-Induced RhoA Inactivation in a Model of Breast Cancer Dormancy. *Cancer Microenviron*. **2** 33–47 (2009).

13. Zielke, N. & Edgar, B. A. FUCCI sensors: powerful new tools for analysis of cell proliferation. *WIREs Dev Biol*. **4** 469–487 (2015).

14. Kim, R. S., Avivar-valderas, A., *et al.* Dormancy Signatures and Metastasis in Estrogen Receptor Positive and Negative Breast Cancer. *PLoS One*. **7** (4), e35569 (2012).

15. Cheng, Q., Chang, J. T., *et al.* A signature of epithelial-mesenchymal plasticity and stromal activation in primary tumor modulates late recurrence in breast cancer independent of disease subtype. *Breast Cancer Res*. **16** (4), 407 (2014).

16. Chen, C., Mcgarvey, P. B., Huang, H. & Wu, C. H. Protein Bioinformatics Infrastructure for the Integration and Analysis of Multiple High-Throughput "omics" Data. *Adv Bioinformatics*. **2010** Article ID 423589 (2010).

17. Huang, H., Hu, Z., Arighi, C. N. & Wu, C. H. Integration of bioinformatics resources for functional analysis of gene expression and proteomic data. *Front Biosci*. **12** 5071–5088 (2007).

Appendix A

REPRINT PERMISSIONS

Chapter 1 was adapted, in part, from *Biomaterials: Controlling Properties Over Time to Mimic the Dynamic Extracellular Matrix* by L. A. Sawicki and A. M. Kloxin, published in *Mimicking the Extracellular Matrix: The Intersection of Matrix Biology and Biomaterials*, Editors: G. A. Hudalla and W. L. Murphy, Chapter 9, 2015, with permission from the Royal Society of Chemistry.

Chapter 2 was adapted, with permission from the Royal Society of Chemistry, from *Design of thiol−ene photoclick hydrogels using facile techniques for cell culture applications* by L. A. Sawicki and A. M. Kloxin, published in *Biomaterials Science*, Volume 2, Number 11, pages 1612-1626, November 2014.

Note from RSC regarding reuse of work:

"Author reusing their own work published by the Royal Society of Chemistry

You do not need to request permission to reuse your own figures, diagrams, etc, that were originally published in a Royal Society of Chemistry publication. However, permission should be requested for use of the whole article or chapter except if reusing it in a thesis. If you are including an article or book chapter published by us in your thesis please ensure that your co-authors are aware of this.

Reuse of material that was published originally by the Royal Society of Chemistry must be accompanied by the appropriate acknowledgement of the publication. The form of the acknowledgement is dependent on the journal in which it was published originally, as detailed in 'Acknowledgements'."

Appendix B

DESIGN OF NOVEL PEPTIDES WITH ENHANCED BINDING TO INTEGRINS

B.1 ONE-BEAD-ONE-COMPOUND COMBINATORIAL LIBRARY

In collaboration with Dr. Kit Lam and Dr. Emanual Maverakis, a one-bead-one-compound (OBOC) peptide library, with perturbations on the collagen-based peptide mimic GFOGER, was built. Specifically, linear and cyclic peptides were synthesized on resin (Table B.1.1) with amino acid substitutions as shown in Tables B.1.2 – B.1.6.

Library synthesis was performed via manual peptide synthesis techniques. TentaGel S NH_2 Resin (Rapp Polymere, 0.32 mmol/g loading, 15 g) was swollen in *N,N*-dimethylformamide (DMF) overnight. Fmoc-protected cysteine (c), *N,N'*-diisopropylcarbodiimide (DIC), and *N*-hydroxybenzotriazole (HOBt) were dissolved in DMF at 5x excess and added to the resin beads. The coupling reaction was allowed to proceed for 2 hours (shaken), and coupling of the cysteine was confirmed via Kaiser test. Resin was rinsed 3x in DMF, 3x in methanol (MeOH), and 3x in DMF. Fmoc deprotection was performed by treatment with 25% piperidine in DMF for 2x 15 min. After deprotection, resin was rinsed with 3x DMF, 3x MeOH, and 3x DMF and Fmoc removal confirmed via Kaiser test. For coupling X_1, resin was split into 30 tubes and individual amino acids (5x excess, Table B.1.2) were coupled to the resin in each tube (activated by 5x excess HOBt/DIC in DMF) for 2 hours. Coupling was confirmed by Kaiser test and the beads were re-combined for washing, deprotection, and washing

post-deprotection. Coupling, deprotection, and washing was performed for the remainder of the amino acids, splitting the resin at positions X_2-X_7 for coupling amino acids in Tables B.1.2-B.1.6. Note that at the positions GX_5, X_6, and X_7, resin was taken to make linear or cyclic peptides of different lengths.

For linear peptides, protecting groups were removed with trifluoroacetic acid (82.5 mL), phenol (7.5 g), thioanisole (5 mL), DI water (5 mL), and triisopropylsilane (2.5 mL) for 3-5 hours. After deprotection, resin was rinsed 1x MeOH, 1x DMF, 1x 5% diisopropylethylamine/DMF, 1x DMF, 3x MeOH, 3x dichloromethane, 1x MeOH, 3x DMF, 1x 50/50 DMF/water, 3x water, 3x ethanol, and 3x 70% ethanol. Peptides were stored at 4 °C in 70% ethanol prior to screening. For cyclic peptide formation, cysteine was coupled to the N'-terminus prior to protecting group deprotection (described above). After side chain deprotection, cyclization buffer (75:5:20 v/v/v water: acetic acid: dimethylsulfoxide, pH 6.0 with ammonium hydroxide) was added to the resin and reacted for 24 hours. Fresh cyclization buffer was added and cyclization was allowed to proceed for an additional 24 hours. Disulfide bond formation was confirmed via Ellman's assay and resin beads were rinsed and stored at 4 °C in 70% ethanol as described above.

Table B.1.1: List of linear and cyclic peptide sequences generated for the OBOC peptide library. Amino acid residues (X_1-X_7) were varied as shown in Tables B.1.2-B.1.6. L = Linear, C = Cyclic.

Name	**Sequence**
L1	$GX_5X_4GX_3X_2X_1c$
L2	$X_6GX_5X_4GX_3X_2X_1c$
L3	$X_7X_6GX_5X_4GX_3X_2X_1c$
C1	$cGX_5X_4GX_3X_2X_1c$
C2	$cX_6GX_5X_4GX_3X_2X_1c$
C3	$cX_7X_6GX_5X_4GX_3X_2X_1c$

Table B.1.2: Thirty amino acid substitutions for the X_1, X_6, and X_7 positions.

#1 Fmoc-Phe(3,4-diCl)-OH MW: 456.4 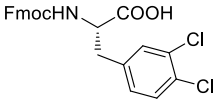	#2 Fmoc-D-Chg-OH MW: 379.4 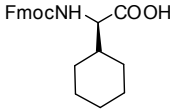	#3 Fmoc-L-HoCit MW: 411.4 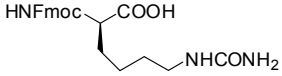	#4 Fmoc-Hyp(tBu)-OH MW: 409.0 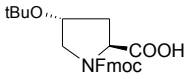
#5 Fmoc-D-Phe(3-Cl)-OH MW: 421.9 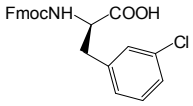	#6 Fmoc-D-3-Pal-OH MW: 388.4 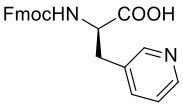	#7 Fmoc- Aib-OH MW: 325.5 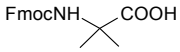	#8 Fmoc-L-1-Nal-OH M MW: 437.47 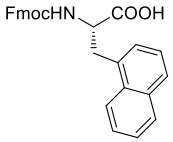
#9 Fmoc-Dpr(Boc)-OH MW: 426.4 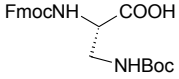	#10 Fmoc-D-Tyr(Me)-OH MW: 417.47 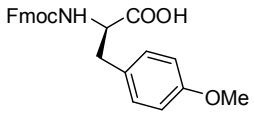	#11 Fmoc-L-Phg-OH MW: 373.4 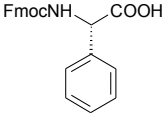	#12 Fmoc-Nle-OH MW: 353.4 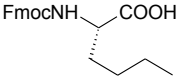
#13 Fmoc-D-Ala-OH MW: 311.3 a 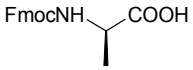	#14 Fmoc-D-Glu(OtBu)-OH MW: 425.5 e 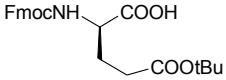	#15 Fmoc-D-Asn(Trt)-OH MW: 596.7 n 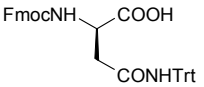	#16 Fmoc-Ile-OH MW: 353.4 I 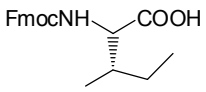
#17 Fmoc-D-Leu-OH MW: 353.4 l 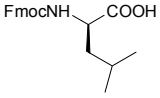	#18 Fmoc-D-Lys(Boc)-OH MW: 468.6 k 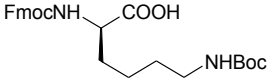	#19 Fmoc-D-Ser(tBu)-OH MW: 383.4 s 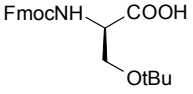	#20 Fmoc-D-Met-OH MW: 371.5 m 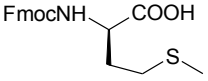
#21 Fmoc-D-Phe-OH MW: 387.4 f 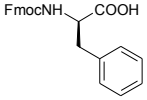	#22 Fmoc-D-Pro-OH MW: 337.4 p 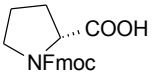	#23 Fmoc-L-Thr(tBu)-OH MW: 397.5 T 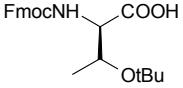	#24 Fmoc-L-Val-OH MW: 339.4 V 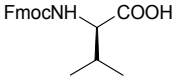

Table B.1.2 continued.

#25 Fmoc-D-Trp(Boc)-OH MW: 526.6 w 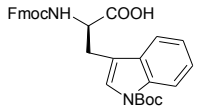	#26 Fmoc-D-His(Trt)-OH MW: 619.7 h 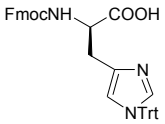	#27 Fmoc-Asp(OtBu)-OH MW: 411.5 D 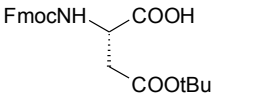	#28 Fmoc-Gln(Trt)-OH MW: 610.7 Q 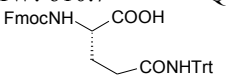
#29 Fmoc-Tyr(tBu)-OH MW: 459.6 Y 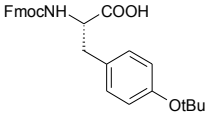	#30 Fmoc-Arg(Pmc)-OH MW: 662.8 R 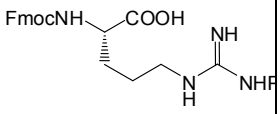		

Table B.1.3: Eighteen amino acid substitutions for the X_2 position.

#1 Fmoc-Arg(Pmc)-OH MW: 662.8 R 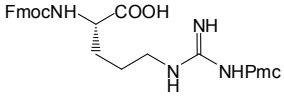	#2 N-Fmoc-amino-(4-N-Boc-piperidinyl) carboxylic acid MW: 466.53 (4-Apc) 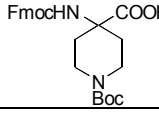	#3 Fmoc-L-HoCit MW: 411.4 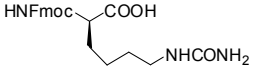	#4 Fmoc-Hyp(tBu)-OH MW: 409.0 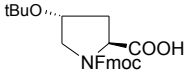
#5 Fmoc-Dpr(Boc)-OH MW: 426.4 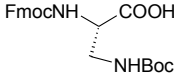	#6 Fmoc-D-3-Pal-OH MW: 388.4 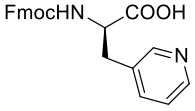	#7 Fmoc- Nva-OH MW: 339.4 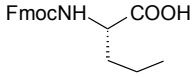	#8 Fmoc-Asp(OtBu)-OH MW: 411.5 D 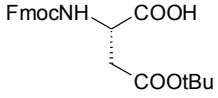
#9 Fmoc-D-Gln(Trt)-OH MW: 610.7 q 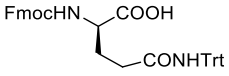	#10 Fmoc- Orn(Boc)-OH MW: 454.5 (132.12) 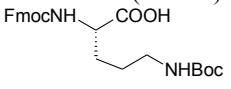	#11 Fmoc-D-Thr(tBu)-OH MW: 397.5 t 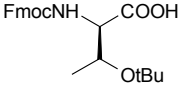	#12 Fmoc-L-Ser(tBu)-OH MW: 383.4 S 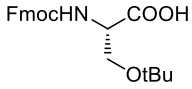

Table B.1.3 continued.

#13 Fmoc-D-Ala-OH MW: 311.3 a 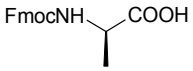	#14 Fmoc-D-Glu(OtBu)-OH MW: 425.5 e 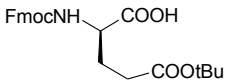	#15 Fmoc-L-Asn(Trt)-OH MW: 596.7 N 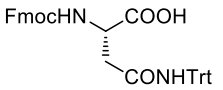	#16 Fmoc-D-Lys(Boc)-OH MW: 468.6 k 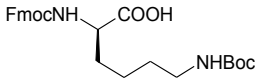
#17 Fmoc-Tyr(tBu)-OH MW: 459.6 Y 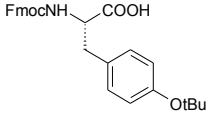	#18 Fmoc-D-His(Trt)-OH MW: 619.7 h 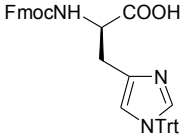		

Table B.1.4: Four amino acid substitutions for the X_3 position.

No.	X	Structure	No.	X	Structure
1	Asp (D)	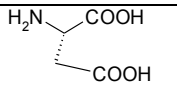	3	Aad	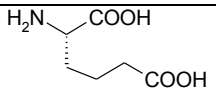
2	Glu (E)	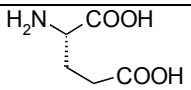	4	Bmc	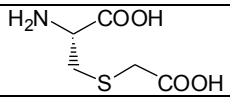

Table B.1.5: Fifteen amino acid substitutions for the X_4 position.

#1 Fmoc-Hyp(tBu)-OH MW: 409.0 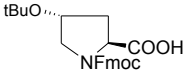	#2 Fmoc-D-Chg-OH MW: 379.4 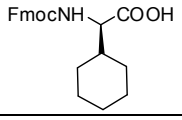	#3 Fmoc-D-Pro-OH MW: 337.4 p 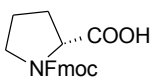	#4 Fmoc-Thz-OH MW: 355.2 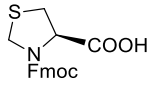
#5 Fmoc- Aib-OH MW: 325.5 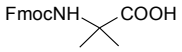	#6 Fmoc-Ach-OH MW: 365.4 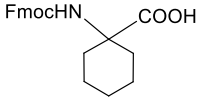	#7 Fmoc-Acpc-OH MW: 323.35 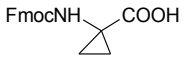	#8 Fmoc-Arg(Pmc)-OH MW: 662.8 R 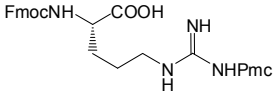

Table B.1.5 continued.

#9 Fmoc-D-Thr(tBu) MW: 397.5 t 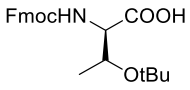	#10 Fmoc-Asp(OtBu)-OH MW: 411.5 D 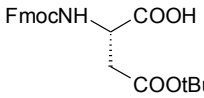	#11 Fmoc-Gln(Trt)-OH MW: 610.7 Q 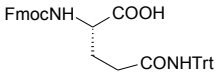	#12 Fmoc-Ser(tBu)-OH MW: 383.4 S 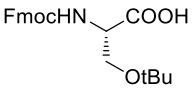
#13 Fmoc-Ala-OH MW: 311.3 A 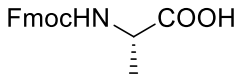	#14 Fmoc-D-Glu(OtBu)-OH MW: 425.5 e 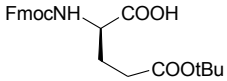	#15 Fmoc-D-Asn(Trt)-OH MW: 596.7 n 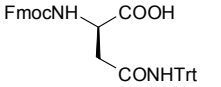	

Table B.1.6: Twenty-eight amino acid substitutions for the X_5 position.

#1 Fmoc-Phe(3,4-diCl)-OH MW: 456.4 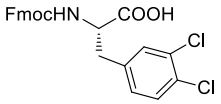	#2 Fmoc-D-Chg-OH MW: 379.4 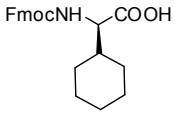	#3 Fmoc-Bpa-OH MW: 491.5 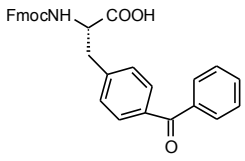	#4 Fmoc-Phe(4-Me)-OH MW: 401.46 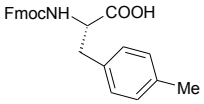
#5 Fmoc-D-Phe(3-Cl)-OH MW: 421.9 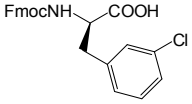	#6 Fmoc-D-3-Pal-OH MW: 388.4 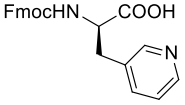	#7 Fmpc-Cha-OH MW: 393.48 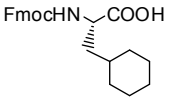	#8 Fmoc-D-Phe(4-CN)-OH MW: 412.4 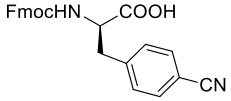
#9 Fmoc-D-HoPhe-OH MW: 401.5 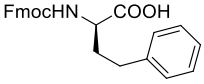	#10 Fmoc-D-Tyr(Me)-OH MW: 417.47 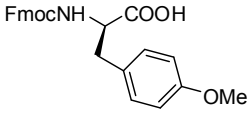	#11 Fmoc-Phg-OH MW: 373.4 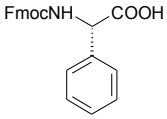	#12 Fmoc-Nle-OH MW: 353.4 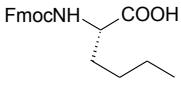

Table B.1.6 continued.

#13 Fmoc-Phe(4-CF_3)-OH MW: 455.4 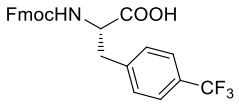	#14 Fmoc-L-1-Nal-OH M MW: 437.47 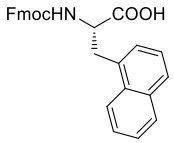	#15 Fmoc-Phe(3,5-diF)-OH MW: 423.4 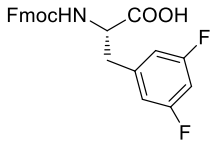	#16 Fmoc-Phe(3,4-diF)-OH MW: 423.4 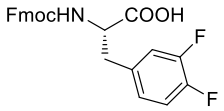
#17 Fmoc-Phe(4-F)-OH MW: 405.4 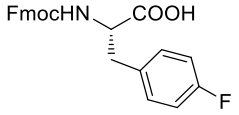	#18 Fmoc-Tyr(tBu)-OH MW: 459.6 Y 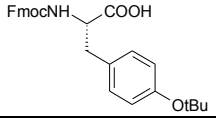	#19 Fmoc-Ser(tBu)-OH MW: 383.4 S 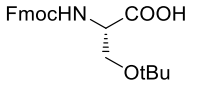	#20 Fmoc-D-Met-OH MW: 371.5 m 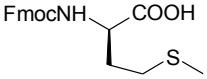
#21 Fmoc-Phe-OH MW: 387.4 F 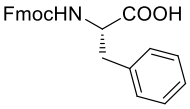	#22 Fmoc-Pro-OH MW: 337.4 P 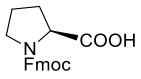	#23 Fmoc-D-Thr(tBu)-OH MW: 397.5 t 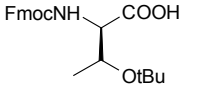	#24 Fmoc-Hyp(tBu)-OH MW: 409.0 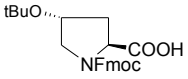
#25 Fmoc-D-Trp(Boc)-OH MW: 526.6 w 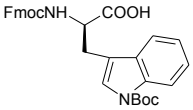	#26 Fmoc-Ach-OH MW: 365.4 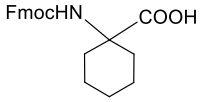	#27 Fmoc-Arg(Pmc)-OH MW: 662.8 R 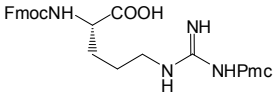	#28 Fmoc-Ala-OH MW: 311.3 A 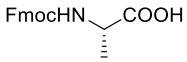

Screening of libraries was performed with hMSCs and K562 cells expressing alpha 1 to investigate binding specificity for α1β1. Sterile beads were rinsed 5x with phosphate buffered saline (PBS) and placed into a nontreated culture dish. Approximately 1 x 10^6 cells in 10 mL culture medium (cell concentration may be tuned depending on study) were added to the beads. Plates with cells and beads were incubated at 37 °C overnight or to time points of interest to allow cell interaction with peptides on the bead surface. Samples were inspected under a Zeiss stereomicroscope and beads with cells bound to the surface were picked out of the plate (Figure B.1.1). Cells were removed from the bead surface by 8 M guanidine chloride prior to

sequence identification. Three peptides from L3 were identified in initial library screens (Table B.1.7) and were built as a "focused" library. These sequences are undergoing additional analysis for binding specificity to α1β1.

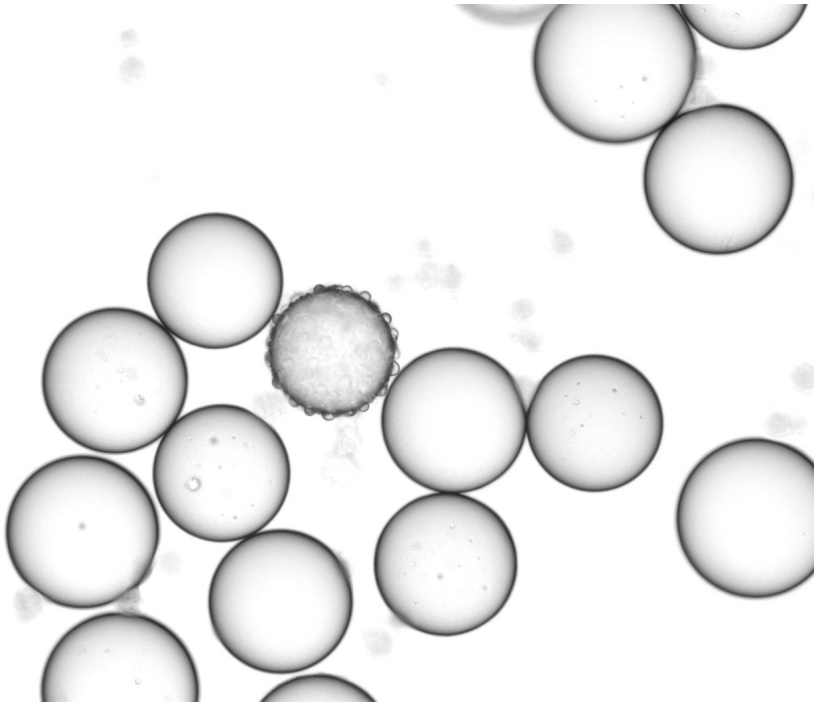

Figure B.1.1: Example of cells bound to the surface of a bead during library screens. These beads were selected for sequence identification.

Table B.1.7: Three linear peptide sequences (L3) were identified in initial peptide library screens. These sequences were synthesized for additional studies on specificity for binding to α1β1.

Peptide	**X_7**	**X_6**	**G**	**X_5**	**X_4**	**G**	**X_3**	**X_2**	**X_1**	**c**
A1	D-His	Nal-1	G	D-Tyr(Me)	Hyp	G	Glu	Arg	D-Lys	c
A2	D-Lys	Nle	G	Pro	Hyp	G	Asp	D-Ala	Arg	c
A3	Nle	Tyr	G	Nal-1	D-Pro	G	Bmc	Arg	Arg	c

B.2 SYNTHESIS OF CYCLIC PEPTIDES IDENTIFIED IN OBOC SCREENING

In addition to the identification of novel peptide sequences using the OBOC technique, we are also developing techniques to covalently attach cyclic peptides identified in other OBOC libraries within hydrogel networks. Specifically, the LXW7 sequence (c-RGDdv-c, cyclized by disulfide bridge between c-c), based on perturbations of RGDS, was shown to have enhanced binding to αvβ3. For cyclization and covalent attachment of this sequence to hydrogel networks formed by thiol-ene click chemistry, we made several modifications to the sequence. To permit cyclization through thiol−ene 'click' chemistry, an alloxycarbonyl-modified lysine (reactive vinyl) and monomethoxytrityl (Mmt)-protected cysteine (reactive thiol) were incorporated at opposite ends of the base peptide sequence. The Mmt-protecting group may be selectively removed in dilute acid conditions to permit cyclization. PEG_2 spacers were added to improve solubility and a trityl (Trt)-protected cysteine was incorporated to allow covalent attachment to thiol−ene hydrogel networks. The Trt-protecting group is deprotected with high concentrations of acid and is removed upon cleavage of the peptide from resin. The final sequence is c(Mmt)-G-RGDdv-K(alloc)-$(PEG_2)_2$-c(Trt). The linear peptide sequence was built on a Protein Technologies PS3 peptide synthesizer and cyclization was performed as follows:

1. After peptide synthesis on the PS3, if desired, split beads into manual peptide synthesis vessels (glass frit) to make linear or cyclic peptides. Cleave the linear peptide as described in step 14 below.

2. Prepare Ellman's reaction buffer (2.4g sodium phosphate, 74.4mg EDTA, 200ml DI H_20; pH 7.5-8 with sodium hydroxide or phosphoric acid) and Ellman's reagent (4 mg in 2 mL Ellman's reaction buffer) to monitor the cyclization reaction via the presence of free thiols.

3. Swell the peptide on resin in dichloromethane (DCM) for 30 minutes and place a few resin beads into a microcentrifuge tube. Apply Ellman's reagent to the beads to check for free thiols. If the solution turns yellow, free thiols are present. At this stage, there should be no free thiols.

4. Mix .54 mL of trifluoroacetic acid (TFA) with 29.46 mL of DCM to make 30 mL of 1.8% TFA solution.

5. Prepare lithium acylphosphinate (LAP) photoinitiator solution by dissolving 110.3 mg LAP in 30 mL of DI water.

6. Remove the Mmt protecting group by applying 1.8% TFA 10 times for 30-60 seconds each while stirring. Place a few resin beads into a microcentrifuge tube and apply Ellman's reagent to check for free thiols. If the solution turns yellow the test indicates free thiols are present and proceed to step 7. If no free thiols are detected, repeat this step.

7. Wash 5x with DCM for 30-60 seconds to remove any remaining TFA.

8. Gently apply air to dry the resin and re-swell in DCM.

9. Add 3 mL of the LAP solution to the beads and allow diffusion into the beads for 10 min while stirring.

10. Apply UV light at ~20mW/cm^2 and 356 nm (while stirring) to initiate reaction between the alloc and free thiol groups.

11. Drain and add fresh LAP solution every 10 minutes to compensate for initiator consumption during reaction. Allow the reaction to proceed for 90 minutes.

12. After 90 minutes, wash the resin with DCM 3 times for 30-60 seconds and blow air through the synthesis vessel to dry.

13. Place several beads into a microcentrifuge tube and apply Ellman's reagent to check for free thiols. If solution doesn't change colors (no free thiols remain), proceed with step 14. If solution is turns yellow repeat steps 8-11.

14. After drying, cleave the peptide from resin (95% v/v TFA, 2.5% v/v water, 2.5% v/v triisopropylsilane, 5% w/v dithiothreitol, 2.5% w/v phenol) for four hours and precipitate in ice cold diethyl ether. Wash 3

times with diethyl ether and dry (desiccator). Store at -20 °C until purification (HPLC) and/or mass spec analysis. Note that the Trt protecting group will be removed with cleavage from resin.

In an initial test of the cyclization procedure, the mass of crude cyclic and linear products was analyzed via ESI (Figure B.2.1). The mass of the linear product was confirmed, indicating that synthesis of peptide on the PS3 was successful. However, noise in the ESI spectrum of the cyclized peptide indicates that the crude cyclic product was not pure. We hypothesize that the reaction between neighboring peptides on a single resin bead may result in the formation of multiple connected peptides, making the product mass difficult to identify.

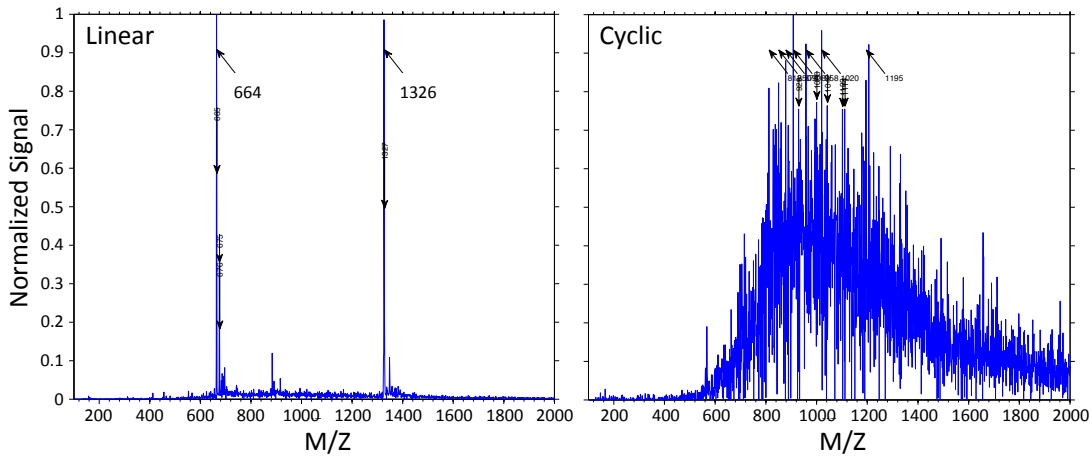

Figure B.2.1: ESI-MS data for crude linear and cyclic peptides. Linear peptides were successfully created via solid phase peptide synthesis on a Protein Technologies PS3 (MW = 1326 g/mol, ½ peak = 664 g/mol). The initial test of the cyclization procedure did not generate a pure cyclic peptide product.

Toward improvement of the cyclization technique, we aimed to generate low loading resin to increase spacing between neighboring peptides on a single resin bead:

1. Deprotect Resin
    - Weigh out ChemMatrix Resin for a 0.25 mmol scale peptide.
    - Swell resin in DMF for 30 minutes and drain after swelling.
    - Add 20% piperidine in DMF to resin and shake/stir for 10 min. Drain and add fresh piperidine/DMF solution for a total of 3 rinses.
    - Rinse deprotected resin 3x DMF, 3x Methanol, 3x DMF, and 3x DCM.
    - If not used immediately, dry resin and store at -20 °C.
2. React with Amino Acid to Establish Reaction Curve
    - Dissolve c(Trt) (4x excess to 0.25 mmol loading) and DIC/HOBt (3.95x excess) in DMF and immediately add to the resin.
    - To establish a reaction curve, let coupling proceed for 2.5, 5, 10, 20, and 30 minutes (Figure B.2.1). Collect beads from each of these time points for analysis.
    - Rinse resin 3x DMF, 3x Methanol, 3x DMF, and 3x DCM then dry.
3. Remove Fmoc with Piperidine and Measure on Nanodrop
    - Accurately weigh 10 mg of resin into an eppendorf tube.
    - Add 800 mL of DMF and allow the resin to swell for 15 minutes.
    - Add 200 mL of piperidine.
    - Vortex to ensure good mixing and let stand at room temperature for 15 minutes.
    - Measure the absorbance at 301 nm versus a 20% piperidine in DMF blank on the NanoDrop.

4. Generate Large Batch of Low-loading Resin Based on Reaction Curve and Synthesize Peptides

   - Repeat steps 1-3, selecting the 5 minute coupling time to attach c(Trt) in step 2, generating a single loading density resin.
   - Confirm loading in step 3 by taking only a small portion of the resin beads.
   - Place resin in a reaction vessel on the PS3 peptide synthesizer and cap remaining free amine sites (acetic anhydride) prior to Fmoc deprotection of the c(Trt) and coupling of the second amino acid residue (PEG_2). Proceed with standard peptide synthesis and cyclization procedures.

Based on the reaction curve, low loading resin was generated for reactions occurring in under 10 minutes (Figure B.2.2). We selected the 5 min coupling time to generate low loading resin, which yielded resin with loading of ~0.01-0.07 mmol/g in subsequent reactions.

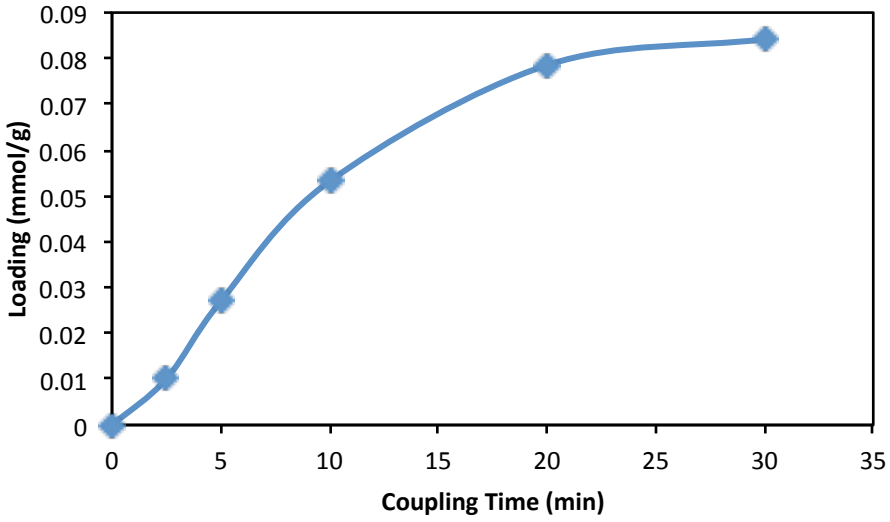

Figure B.2.2: Reaction curve for generating low loading resin. The 5 minute coupling time was selected to generate low loading resin for subsequent cyclic peptide synthesis.

Toward improving the characterization of cyclic peptides post-synthesis, we used an ACQUITY UPLC H-Class/SQD2 mass spectrometer that permits LC-MS analysis of the peptide product. Comparing chromatograms of the linear and cyclic peptides built on low loading resin, the linear product was present within a distinguishable large peak while spreading and multiple peaks were observed in the cyclized product. This further indicates that impurities may present after cyclization (Figure B.2.3).

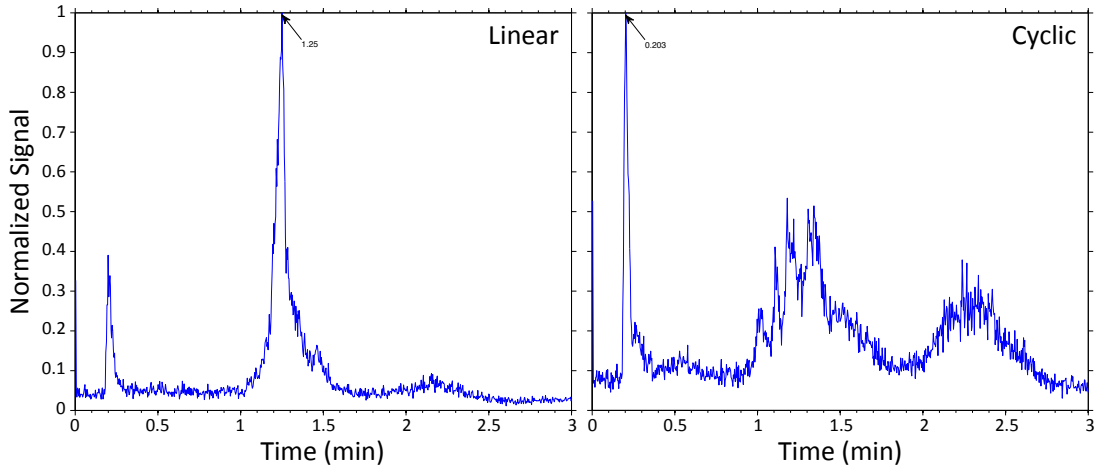

Figure B.2.3: Chromatograms (SQD2) of crude linear and cyclic peptide products built on low loading resin. Linear product was identified in the major peak; however, spreading and multiple peaks present within the cyclic peptide product indicate the presence of impurities.

To attempt purification of the crude cyclic product built on low loading resin, we ran a slow HPLC gradient (5-55% acetonitrile in water, 1-43 minutes) and collected the two largest product peaks observed (Figure B.2.4 A). P1 contained the correct product molecular weight and may contain cyclized peptide (Figure B.2.4 B,

red arrows). Unfortunately, due to impurities and low initial loading, product yield is minimal; so other techniques to perform cyclization (e.g., solution-based cyclization) will be pursued in future work. Additionally, we will investigate techniques to confirm that the generated peptide is cyclic (e.g., 2D NMR).

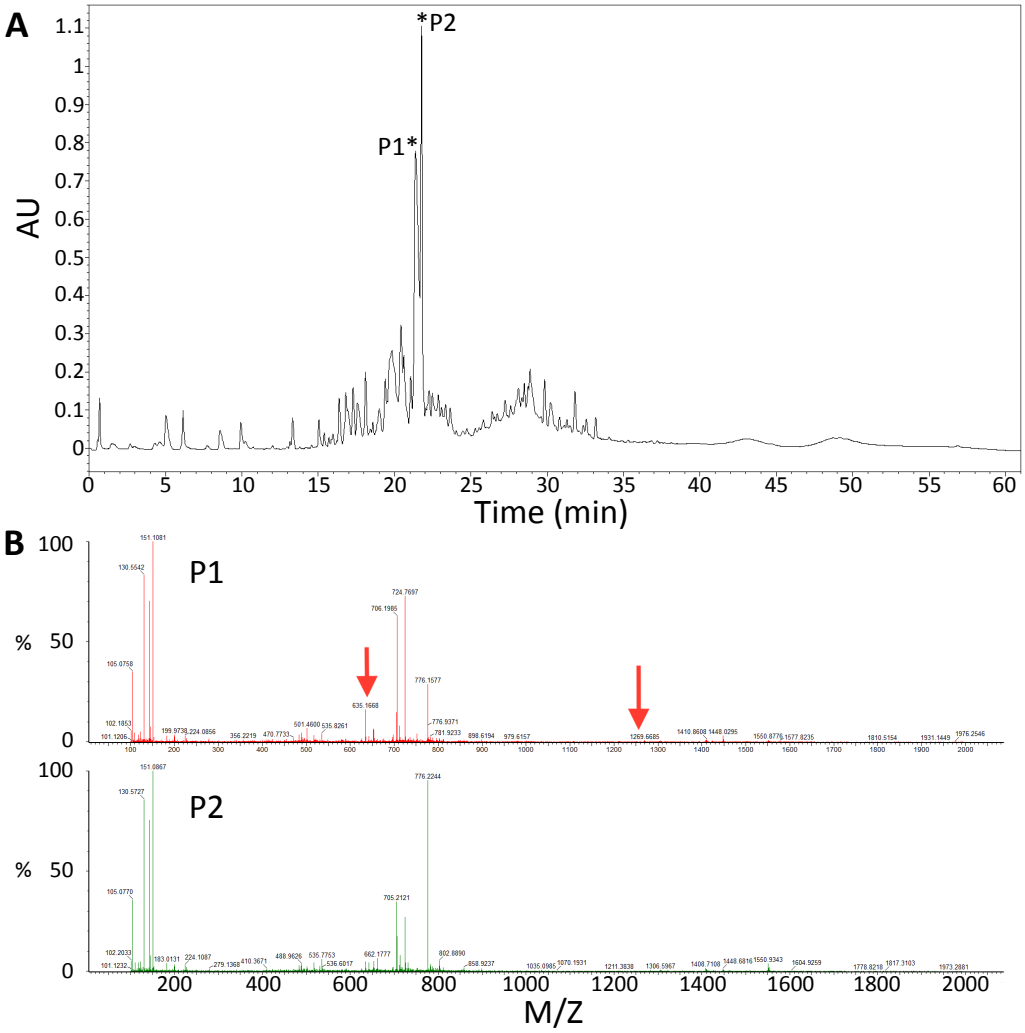

Figure B.2.4: **Purification (HPLC) and mass spec (SQD2) analysis of cyclic peptide built on low loading resin. A)** Cyclic peptide was separated over a slow gradient and major peaks (P1 and P2) were collected for analysis. **B)** The molecular weight of the cyclic peptide was identified (red arrows); however impurities in the sample are present, resulting in low yield.